Forschungszentrum Karlsruhe

Technik und Umwelt

Institut für Reaktorsicherheit

Validation of Calculation Tools for the Estimation of Reaction Products in the Target of Accelerator Driven Systems

Diplomarbeit zum Erwerb des akademischen Grades „Diplom Ingenieur"
Fakultät für Maschinenbau der Universität Karlsruhe (TH)

Projet de fin d'études présenté pour obtenir le diplôme d'ingénieur ENSAM
Ecole Nationale Supérieure d'Arts et Métiers

Pauline Rousseau

Forschungszentrum Karlsruhe GmbH, Karlsruhe

May 2004

Acknowledgements

I would like to thank sincerely all people who contributed to this project:

- All in front I would like to thank Dr. C. Broeders for the interesting subject and the constant availability for answering of my questions, and who introduced me with much patience and helpfulness into this new topic area. He learned to me much as well on the theory as on the working methods in the research sector.

- I make a point of thanking the director of the IRS Prof. Dr. D. G. Cacuci to have welcomed me within this service and Dr. V. Heinzel to refer this work.

- Many thanks to L. Sharp, M. Zimmermann, D. Stephany for their kindness, their help and their good mood.

- I also thank all people who allowed me to advance in my work when there was a dead end namely J. C. David and A. Boudard from CEA, L. Waters from LANL, and I. Broeders from the FZK.

- I especially thank Carmen Villagrassa-Cantón-Roussel who helped and learned me a lot during the last straight line of the project.

- In addition I would like to thank all co-workers for the various assistances and the good work atmosphere.

Contents

List of Figures

List of Tables

Introduction

Since the mid of the nineties, thanks to the broad interest for accelerator driven systems for energy production and nuclear waste incineration, the spallation reactions interest again the scientific world. Indeed, the industrial exploitation of the spallation reaction would be possible. One of the characteristics of the spallation reaction is to "generate" a lot of neutrons. During the reaction, the emitted nucleon has again enough energy to create new reactions with the near nucleus. In a thick target, the number of neutrons is also multiplicated and, as an example, 25 to 30 neutrons can be produced per incoming proton at 1 GeV in a thick lead target. This characteristic allows the application of the spallation reaction model in high intense neutron sources. One of the applications of this reaction is the accelerator driven sub-critical reactor system. They are called hybrid system and are expected to be a solution to transmute the nuclear waste with long-lived actinides or fission products.

In a hybrid system or ADS (Accelerator Driven System), for an Energy Amplifier proposed by C. Rubbia shown in the figure 0-1, an accelerator (linac or cyclotron) creates a proton beam with high energy (between 0,5 MeV and 2 GeV) which goes on a target constituted of a heavy material (Lead, Lead-Bismuth, etc) [1, 2]. This ensemble produces neutrons. This contribution allows maintaining the chain reaction in the sub-critical system. The neutrons produced go on the reactor blanket which is made of fuel for the multiplication of the reaction and of long-lived actinides or fission products for the transmutation to obtain short-lived radioisotopes and stable nuclei. The use of an external neutron source makes the sub-critical reactor more secure.

In figure 0-2 a closed fuel cycle system is shown as proposed in the Accelerator Transmutation of Waste project (ATW) [3, 4]. The transmuter is integrated in the fuel cycle system. Indeed, a spent fuel recycling is required before the transmutation. It is a chemical separation to isolate transuranics and long-lived radioisotopes. Then, the transmutation produces power and a small part (~10%) is used to feed the accelerator and the great majority (~90%) is provided to the grid.

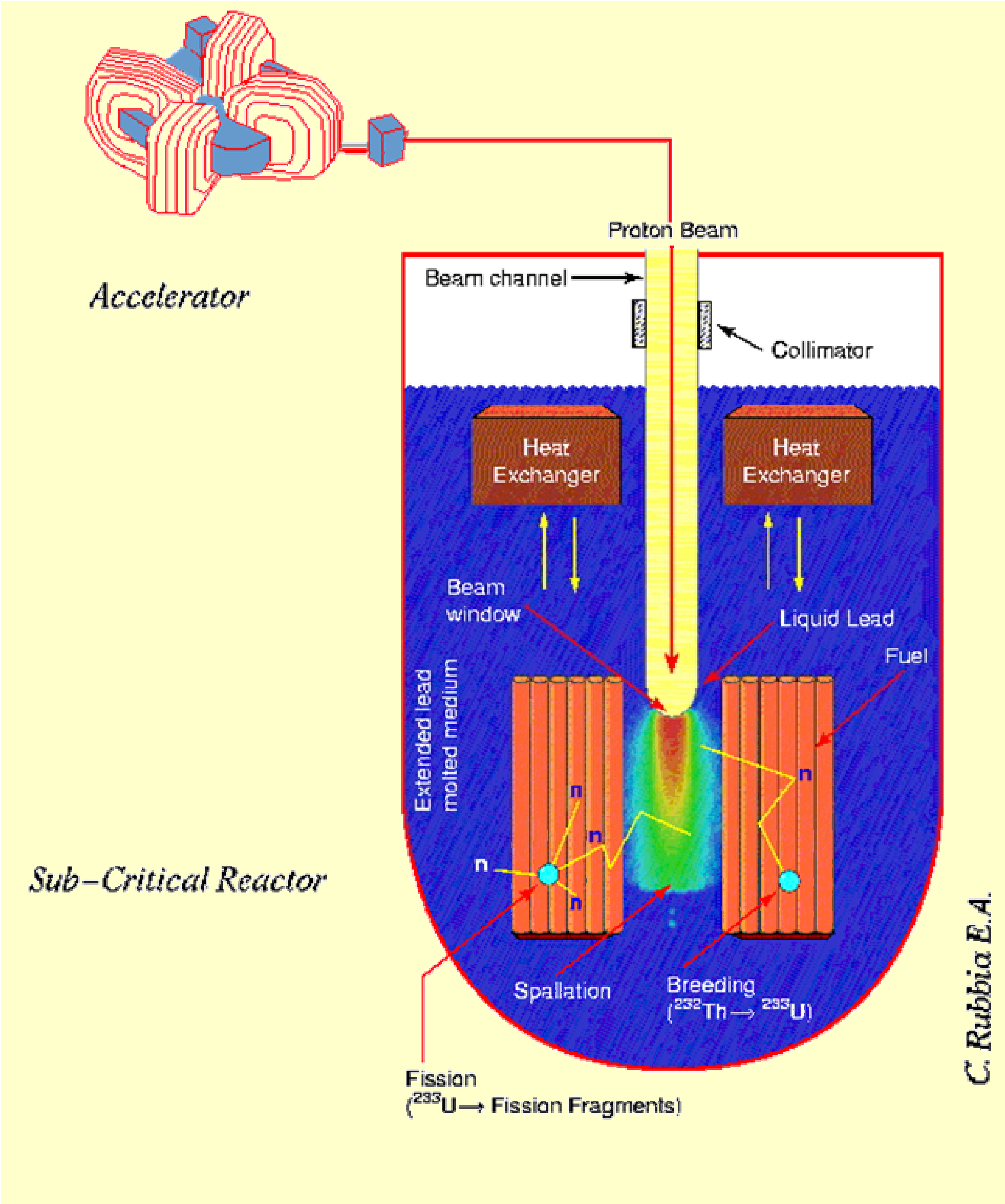

Figure 0-1: *Schematic principle of the Energy Amplifier taken from [5].*

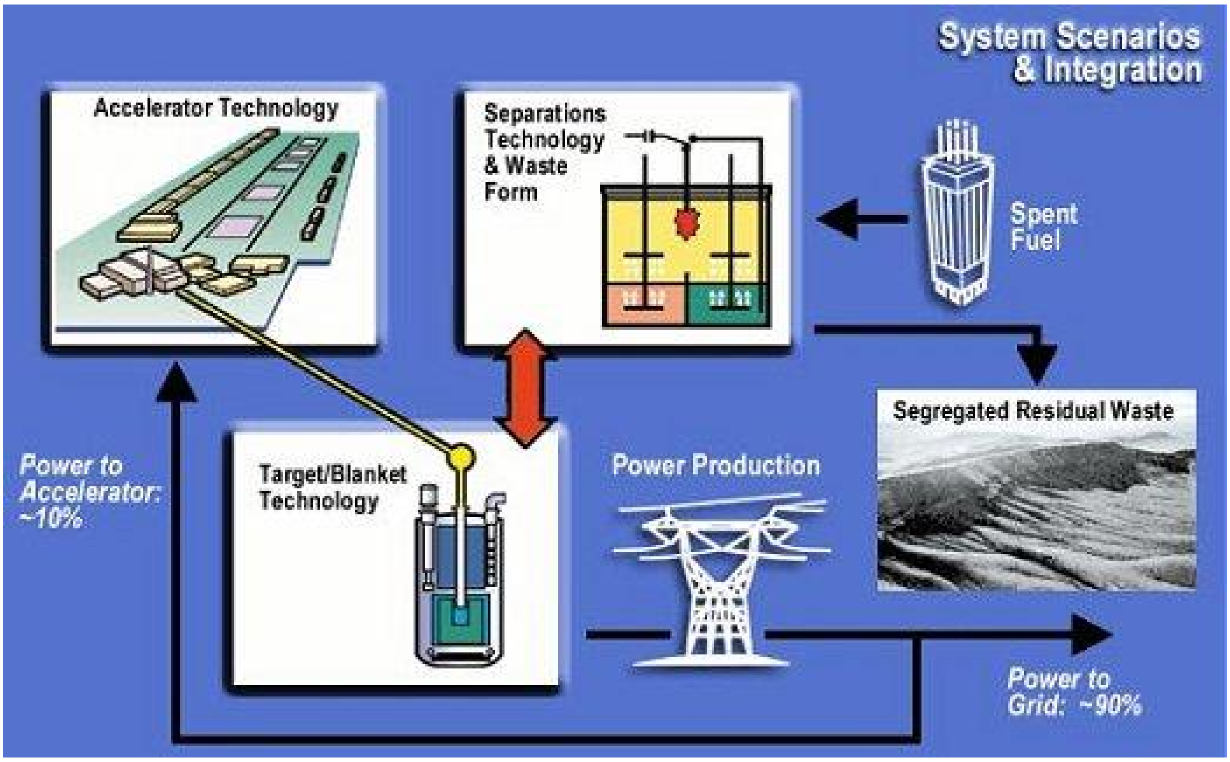

Figure 0-2: *Technical working groups of the ATW taken from [4].*

This work will include various points:

In chapter 1, we recall quickly the general basis of the spallation reaction as well as the various approaches used in the codes. We will study more particularly the physical models applied in the code INCL4 [6] for the intranuclear cascade and in the code ABLA [7, 8] for the evaporation model. The main programs and how they are connected in practice will be described in chapter 2. The main program for performing the simulation of the spallation reaction and the following transport calculations is MCNPX. The main objective of this study is the validation of the implementation of the codes of Cugnon and Schmidt in the new beta version 2.5e of MCNPX and it is developed in chapter 3. The spallation cross sections obtained for different proton energies compared to experimental data will be presented in chapter 3 too. Then, the chapter 4 is dedicated to the LiSoR experiment [9] which is a supporting experiment of the MEGAPIE project [1, 10]. Finally chapter 5 contains a comparison between two codes KAPROS [11] with the modul BURNUP[12] and ORIHET3 [13], which calculate the decay of isotopes. The physical basis of each program and the method to use them in practice is explained.

Chapter 1.

Physicals Models

E. O. Lawrence [14] had observed the spallation reaction for the first time in 1947. In 1952 the idea to use the spallation reaction as external source of a system of energy production is developped. This sources of spallation neutron are important not only for the transmutation of waste, but can be used for irradiation studies or material structure analyses and for tritium production units [15].

This chapter will describe with more details the general features of the spallation reaction and its two stages. At the same time, we will give the charasteristics of a few modelisation codes which will be used in this work.

1.1. The spallation reaction

1.1.1. Mechanism and features

The spallation reaction can be described as an interaction between a high energy light nucleus (neutron, proton…) and a target heavy nucleus [16, 17]. The range of energy of the incoming particles varies from a few hundreds of MeV to a few GeV per nucleon. At these energies, the mechanism can be modeled following the idea of R. Serber [18]. He considers that the reaction can be separated in two different steps: in the first, the wavelength associated with a projectile of a few hundreds of MeV is about 10^{-14} cm. This length is smaller than the typical inter-nucleonic distances in the target core (~ 1 fm=10^{-13} cm). The projectile sees also the nucleons in the nucleus as individual particles and the reaction is a series of nucleon-nucleon collisions. This stage is called intranuclear cascade. These successive collisions involve the ejection of a few nucleons and the repartition of a part of the incoming energy on a big number of nucleons and that leads to the excitation of the target nucleus which is yet called pre-fragment. The second stage is the de-excitation of this pre-fragment via a process of evaporation which may include the fission. If the particles (see figure 1-3) ejected during the two stages have enough energy, they can involve other spallation reaction with near nucleus of the target as the figure 1-1 shows it.

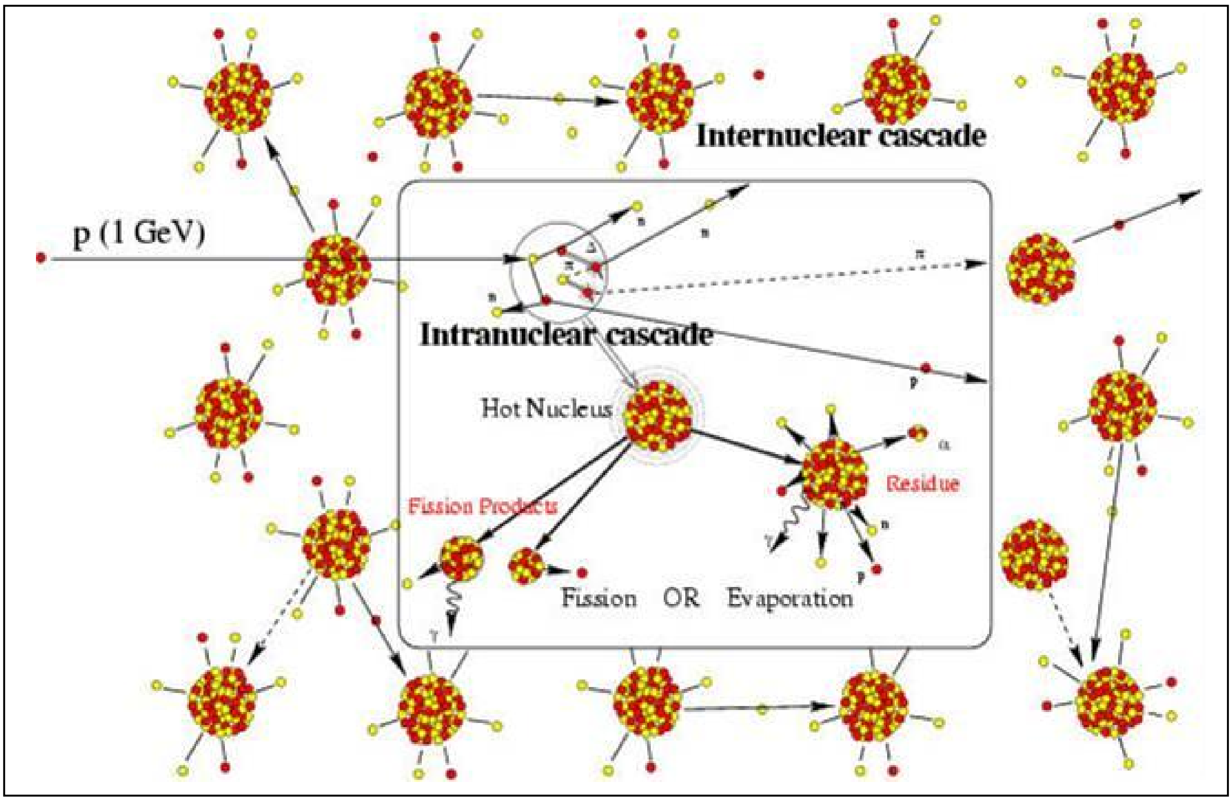

Figure 1-1: *The spallation reaction integrated in a thick target.*

The figure 1-2 describes the different stages and their durations: The intranuclear cascade is a very quick reaction and for the total cascade (propagation time of the incoming nucleon and a few collisions) the time is approximately 10^{-22} s. The second stage is the de-excitation of the nucleus (pre-fragment) via slower processes: the evaporation of particles ($\tau=10^{-19}$ s), possibly the fission and γ and β radiations when the excitation energy is lower than the emission threshold of particles ($\tau=10^{-12}$ s until a second).

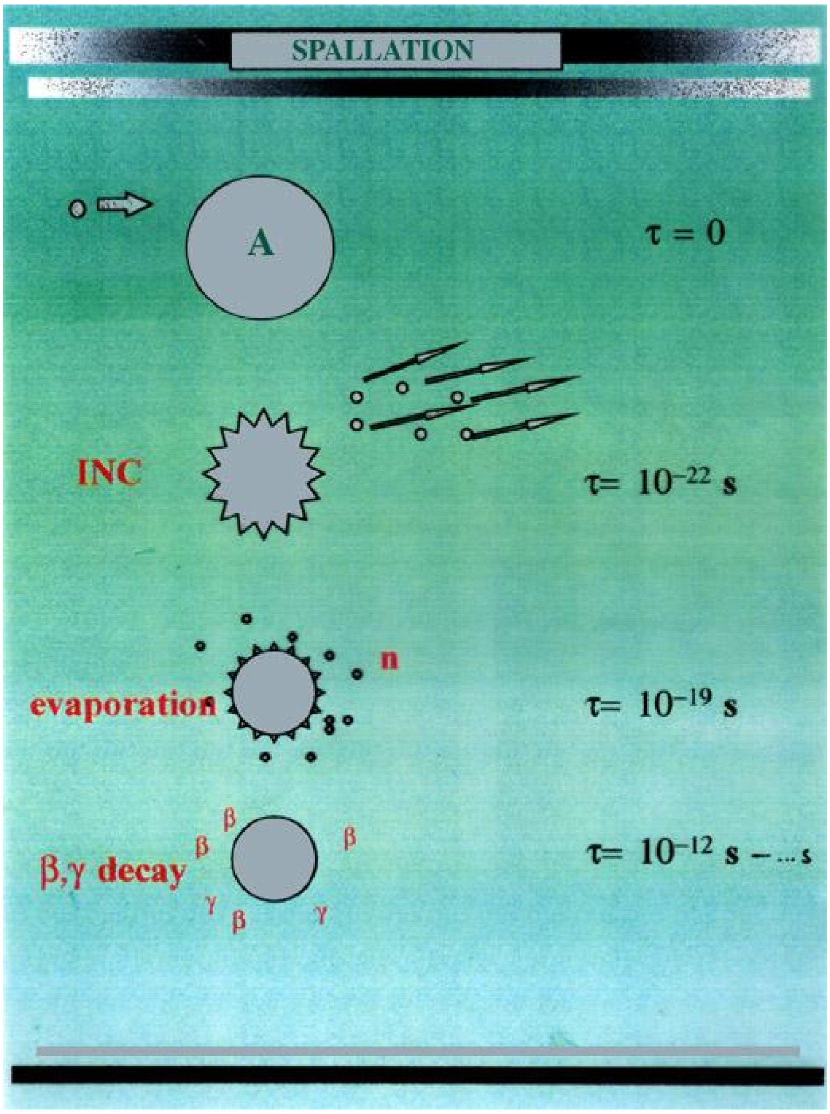

Figure 1-2: *The different stages and their durations of the spallation reaction [19].*

1.1.2. The Intra Nuclear Cascade INC

As mentioned before, the mechanism of a spallation reaction can be divided in two stages (see figure 1-3). The first is the one of nucleon-nucleon collisions, called Intra Nuclear Cascade. The nucleon undergoes a succession of collisions with other nucleons. There are different ways for the modeling of these processes. Indeed different cascade models have been developed for MCNPX as Bertini, ISABEL, CEM and INCL4, based on the Cugnon codes. The code developed by Bertini is one of the first codes of intranuclear cascade [20, 21]. ISABEL is more recent and utilizes similar principles as the Bertini code but with improvements in the definition of the nuclear density. Bertini considers the nucleus as three concentric spheres with different densities whereas ISABEL considers 16 areas. CEM is an improvement of the Dubna intranuclear cascade code [22]. INCL4 was developed by J. Cugnon [6] and we study the characteristics in the section 1.2.

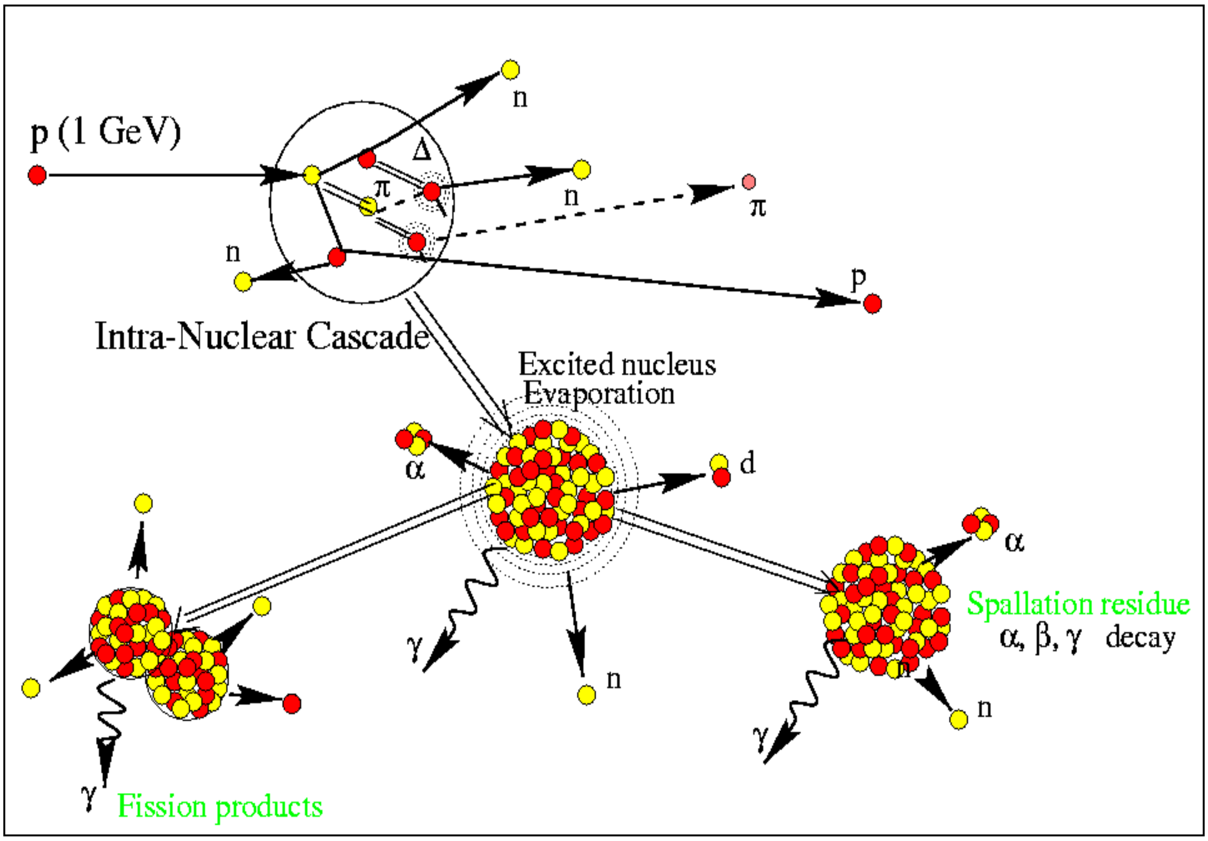

Figure 1-3: *The spallation mechanism.*

In the Bertini and ISABEL models, the cascade may be followed by a pre-equilibrium stage, which is shortly described in the next section.

1.1.3. The pre-equilibrium

Between the cascade and the de-excitation, there is an intermediate state called pre-equilibrium. This stage is characterized by the emission of particles as n, p, d, t, ^{3}He, ^{4}He with high energy. These particles of pre-equilibrium have kinetic energy higher than those of the particles emitted during the de-excitation.
The goal of the insertion of a pre-equilibrium code between the cascade and the evaporation is to decrease the energy of the pre-fragment with the emission of rapid particles. It allows increasing the production of residues near the projectile and decreasing the residues more distant of the projectile at the end of the evaporation.
This effect improves the results of the Bertini-Dressner code with the experimental data. The Bertini and ISABEL options can be coupled with a pre-equilibrium intermediate stage. In contrary, INCL4 makes by itself the transition from the cascade to the thermalisation of the pre-fragment thanks to its stop criterion (described in section 1.2.1).

1.1.4. The de-excitation

The first step of the spallation reaction produces an excited nucleus, called pre-fragment, which must decrease its energy level. Thus, the second step is the evaporation of light particles and/or fission.

There exist 3 different ways for the de-excitation namely the multifragmentation, the fission and the evaporation. The probabilities of these possibilities depend on the nature of the nucleus and on the considered energy.

The multifragmentation:

With sufficient energy, near the energy of separation of the nucleus, mechanical instabilities break the nucleus in several fragments (more than two). The higher the energy is, the larger the number of fragments will be and their size will be small. This mode of de-excitation is principally present when there is a nucleus-nucleus collision. We will neglect this mode in our study proton on lead with 600-1000 MeV.

The fission:

Even in the case of a not very fissile nucleus, the available energy can lead to the fission of the nuclei in two fragments. We speak of “hot” fission for energy higher than 50 MeV. But, this phenomenon is remarkable only for nuclei of charge number higher than 75.

The evaporation:

The pre-fragment de-excites emitting principally nucleons, particles (d, t, ^{3}He α) or light fragments (Isotopes of Lithium or Beryllium). The name evaporation comes from the similarity with the emission of molecules by a liquid in equilibrium with his gaseous form.

We obtain also residual nucleus whose difference in mass compared to the pre-fragment depends directly on the energy deposited at the time of the first reaction. That is the mode we will observe in our study.

1.2. The Cugnon-Schmidt Model

1.2.1. The Cugnon cascade: INCL4

The Cugnon cascade is recent and relatively different of the earlier approach (Bertini, ISABEL and CEM models). The Cugnon cascade [6] was already described in references [15, 17, 23] and the main characteristics are recalled in this section. All the features of the INCL4 cascade are discussed in [24].

The medium

The type of medium is the main criterion to differentiate the different codes. The Bertini and ISABEL codes were based on a nuclear model in which the nucleon density within the nucleus was supposed constant within certain areas (see section 1.1.2) and where the nucleons are not considered individually except the cascade particles. The INCL4 code doesn't consider the nucleus as a continuous medium but as a bundle of individual nucleons moving in a given potential.

The criterion of collision

To determinate the moment where the interaction proton-nucleon has to take place two approaches are often used. In the beginning, the particles are propagating freely until the distance between two of them is lower than a preset minimal distance $d_{ij}^{\min}$ (INCL4 code).

$$d_{ij}^{\min} = \sqrt{\frac{s_{ij}(s_{ij})}{p}} \tag{1.1}$$

where $s_{ij}(s_{ij})$ is the total interaction cross section at the available energy s_{ij} in the centre of mass system.

A radically different approach considers the nucleus as a continuous medium in which the particles have a mean free path. After this path, they collide with a nucleon which takes itself a free course and so on (Bertini and ISABEL codes). The time interval is given by the minimal value of:

$$\Delta t = \min\left(\frac{\langle l_i \rangle}{n b_i}\right) \tag{1.2}$$

where $\langle l_i \rangle$ is the mean free path of each cascade particles, b_i is their velocity and n is a parameter fixed to $n = 20$.

The stopping time

The cascade is considered as finished when the nucleus reached a balanced thermal state. Here too, two approaches exist. One is based on time: the equilibrium state is supposed to be reached with the end of one given time (INCL4 code). The new version integrates a dependence of the stopping time with the target nucleus given by:

$$t_{stop} = f_{stop} t_0 \left(\frac{A_T}{208}\right)^{0.16} \tag{1.3}$$

where f_{stop} is an adjustable parameter and the default value is equal to 1, $t_0 = 70\ fm/c$, and A_T is the atom mass of the target nucleus.

The other is based on the energy: the cascade is considered finished when all the nucleons have an energy lower than a definite threshold called cut-off energy E_{cut} (Bertini and ISABEL codes).

The nuclear surface

The treatment of the nuclear surface parameter is an important feature of the INCL4 code. In the earlier options of MCNPX (Bertini, ISABEL codes) the collisions of the nucleons take place in a mean field described by a potential well with an abrupt surface:

$$R = 1.2A^{1/3} \tag{1.4}$$

In the INCL4 code the density is given by a Wood-Saxon function:

$$r = \begin{cases} \dfrac{r_0}{1+\exp(\frac{r-R_0}{a})} & for \quad r < R_{\max} \\ 0 & for \quad r > R_{\max} \end{cases} \tag{1.5}$$

Where

$$R_0 = \left(2.745\,.10^{-4} A_T + 1.063\right) A_T^{1/3}\ fm \tag{1.6}$$

$$a = 0.510 + 1.63\,.10^{-4}\ A_T\ fm \tag{1.7}$$

$$R_{\max} = R_0 + 8a \tag{1.8}$$

The Pauli blocking

The Pauli principle means that there cannot be, in an atomic nucleus, two nucleons which have the same characterizing features. These characteristics are the type of nucleon (neutron or proton), the energy state, the angular momentum (spin) and the z-component of the spin.

In the Fermi gas model for the atomic nucleus, which is put in the computations for the intranuclear cascade, all possible nucleon states are occupied. The Fermi energy is the highest energy, which a nucleon can have in the nucleus in this Fermi gas model [25]. If during the intranuclear cascade a nucleon comes out, whose energy is smaller than the Fermi energy, and if there is already a nucleon in the nucleus with the same quantum numbers, thus the state is already occupied. With the "strict" application of the Pauli principle therefore later all processes are excluded, in which a nucleon occurs with an energy, which is smaller than Fermi energy. However too many processes are excluded. In the course of the intranuclear cascade nucleons from the atomic nucleus can be pushed out, so that their place becomes free and could be again occupied. This is considered in the Cugnon model with the “statistic” application of the Pauli principle. In this case, statistic considerations are employed. References [26, 27] give more details on the “statistic” application of the Pauli principle

There are in Bertini and ISABEL models no input options, in order to control the application of the Pauli of principle. In both models the “strict” Pauli principle is used. In contrary to the INCL4 model which allows choosing between Pauli “strict” and Pauli “statistic”.

The following table 1-1 recapitulates the main differences between the intranuclear cascades.

Physics process	Bertini	ISABEL	INCL4
Intranuclear cascade Model	Bertini INC	ISABEL INC	improved Cugnon INC
Medium	continuous	continuous	discret
Method	*INC+EQ* or *INC+EQ+PE*	*INC+EQ* or *INC+EQ+PE*	*INC+EQ*
Nuclear density distribution	Density in 3 areas	Density in 16 areas	Wood-Saxon density
Collision criterion	Mean free path	Mean free path	Minimum approach distance
Stop criterion	Energy	Energy	Time
Pauli blocking	Strict	Strict	Statistic

Table 1-1: *Main differences between the intranuclear cascades.*

1.2.2. The evaporation model of Schmidt: ABLA

There are several evaporation models and they are all based on the Weisskopf-Ewing formalism [28, 29]. This statistic model considers two inverse processes: The emission of a particle b ($X \rightarrow Y + b$) and its capture ($Y + b \rightarrow X$). The emission probability per energy unit of the particle b with the energy e is written:

$$P_b(e)\, de \;=\; \frac{r_f\,(E_Y^*)}{r_i\,(E_X^*)} \cdot (2s_b + 1) \cdot (4p\ p^2\ dp / h^3) \cdot s_c(e) \qquad (1.9)$$

Where

$$E_Y^* = E_X^* - Q - e \qquad (1.10)$$

Where

s_b : Spin of particle *b*

r_i : The level density of the nucleus X

r_f : The level density of the nucleus Y

Q : The difference of mass excess

$4p\; p^2\, dp / h^3$: The number of states with a momentum between p and $p + dp$

$s_c(e)$: The capture cross section for the particle *b* by the nucleus Y

E_Y^* : The energy of the nucleus Y

E_X^* : The energy of the nucleus X

The emission probability depends on state density r and capture cross-section s_c.

The code ABLA was developed at the GSI at the beginning of the eighties by K.H Schmidt and his collaborators [7, 8] and reference [26] presents the basis. In this code, the particles which can be evaporated are only n, p, and alpha particles in contrary to the Dresner code which allows the evaporation of p, n, d, ^{3}H, ^{3}He, ^{4}He.

The most recent parameterizations of the density level and of the parameter of the density levels are in the article of Junghans *et al.* [30].

$$r(E) = \frac{p^{1/2}}{12} \frac{e^S}{a'^{1/4} E^{5/4}} \tag{1.11}$$

with

$$S = 2\left[a'\left(E + dU'.f(E) + dP'.h(E)\right)\right]^{1/2} \tag{1.12}$$

The functions $f(E)/E$ and $h(E)/E$ tend toward 0 at high energy and toward 1 at low energy.

dU' accounts for the shell effect and dP' for the pairing.

The parameter a' is another parameterization by Ignatyuk:

$$a' = a_v A + a_S A^{2/3} B_s + a_k A^{1/3} B_K \tag{1.13}$$

with $a_v = 0.073\, MeV^{-1}$ the volume coefficient, $a_S = 0.095\, MeV^{-1}$ the surface coefficient and $a_k = 0\, MeV^{-1}$ the coefficient of bending. B_S represents the surface of the nucleus

normalized to a spherical configuration, and B_k the integrated curve of the nucleus normalized to a spherical configuration.
The capture cross sections are not used in the code ABLA. It has one consequence: the particles spectrum must be imposed. In the code ABLA, this spectrum is Maxwellian.

The following table 1-2 summarized the main differences between the two codes of Dresner and Schmidt.

DRESNER	ABLA
Evaporation of n, p, d, t, ^{3}He, ^{4}He	Evaporation of n, p and ^{4}He
State density parameter ***a* à** A/8 (Ignatyuk)	State density parameter ***a* à** A/12
Decrease of the coulomb barrier with E* Where E* is the excitation energy of the pre-fragment	Coulomb barriers more realistic

Table 1-2: *Main differences between the evaporation models.*

Chapter 2.

Simulation codes

To study this complex reaction, it is necessary to use simulations which describe the spallation reaction and the transport of particles in a thick target. In a thick target the interaction between a particle and the material is very complex because several reactions at different energy levels can take place.

The simulation of the mechanism of the spallation reaction is very complicated and no analytic solution could be found. That's why the statistic treatment with the Monte Carlo method is the applied option. All the existing codes are based on this Monte Carlo method.

The Monte Carlo methods consist of experimental or data-processing simulations of mathematical or physical problems, based on the pulling of random numbers. Generally one uses in fact a series of pseudo-random numbers generated by specialized algorithms. The properties of these series are very close to those of a true random walk. To obtain statistically reliable results, it is necessary to evaluate a lot of histories.

2.1. The Cugnon code in the Stand-alone version

This program has been developed by J. Cugnon at the University of Liege. He uses his model of the intra nuclear cascade. The input file for Cugnon Stand-alone code, shown in table 2-1 allows running a job. The main input parameters are the nuclear potential, f_{stop} which controls the stopping time, *NOSURF* which controls the nuclear surface, *XFOISA* which controlls the parameter of maximum impact and the Pauli blocking. Their meanings are described below.

<u>The nuclear potential</u>

The nuclear potential or potential depth is coded in the Cugnon code in Stand-alone version by V_0 and the default value is fixed to 45 MeV. It is the value generally used for heavy nucleus. Reference [31] gives a parameterization of the potential depth in the valley of stability as a function of the mass number. The equation system (2.1) shows this parametrization. The result for the lead ($V_0 = 45.33 MeV$) is in very good agreement with the default value applied in the Cugnon code in Stand-alone version and in MCNPX.

$$\left.\begin{array}{r} V_0 = 50\, MeV \quad A < 40 \\ V_0 = (53.47 - 0.08667 A)\, MeV \quad 40 < A > 70 \\ V_0 = (48.45 - 0.015 A)\, MeV \quad 70 < A > 210 \end{array}\right\} \qquad (2.1)$$

<u>The stopping time</u>

The stopping time is the time at which the cascade is stopped to proceed with evaporation. This parameter is already described in section 1.2.1. The stopping time is controlled by the parameter f_{stop} and the default value is 1.

<u>The nuclear surface</u>

This nuclear surface specification is a new parameter which introduces a diffuse nuclear surface, corresponding to a Saxon-Woods density distribution as explained in section 1.2.1 (see formula (1.5)).

The input parameter in the code is $NOSURF$ and allows controlling the type of surface. The different possibilities are:

$NOSURF = 1$: Sharp density (hard sphere).

$NOSURF = 0$: Wood-Saxon density and stopping time without impact dependence.

$NOSURF = -1$: Wood-Saxon density and stopping time with impact dependence.

$NOSURF = -2$: Wood-Saxon density and INCL4 stopping time.

<u>The parameter of maximum impact</u>

In the code, the parameter $XFOISA$ allows defining the parameter of maximum impact $B_{\max}$ to sprinkle by particles all the diffuse surface of the nucleus. We have also:

$$B_{\max} = R_0 + XFOISA \times a \qquad (2.2)$$

where a is the diffuseness.

R_0 is the average radius of the nucleus.

The geometrical cross section is then:

$$s_{geo} = 10p\ B_{\max}^2 \quad [mb] \qquad (2.3)$$

The factor 10 is due to the unit conversion. Indeed, $[fm]^2 = 10[mb]$

The Pauli Blocking

The input parameter which controls the Pauli blocking in the code is *NPAULSTR*

$NPAULSTR = 1$: Pauli “strict”.

$NPAULSTR = 0$: Pauli “statistic”.

$NPAULSTR = -1$: No Pauli.

Input value	Meaning
38035	First random number
150000 0 1	Number of shoots Initialization of common hazard when =1 Print number of shoots in the output file
1 1000	Type of shot (1:proton, 2:neutron, 6:deuton) Total kinetic energy (MeV)
208 82	Atomic mass A Atomic number Z
45 1.0 -2 8 0	Nuclear potential (MeV) Stopping time *NOSURF* *XFOISA* *NPAULSTR* (See the explanations below)
1871562739 1882631241 1508947907 1446782547 403824905 1754250443 375560615 1613533623 1015852965 522662927 1673861985 1477557897 44631827 340601027 910049051 62345 72345 1472555179 452820949 335151537	There are 20 different seeds collected at the time of spurious shutdown. There are tests in the program (conservation of A, Z, of energy and impulse) which stopp the job and record the state of seeds. Then one can launch the program directly on this event to avoid the problem by putting Initialization of common hazard =1.

Table 2-1: *Cugnon Stand-alone input file and meaning of the different terms [32].*

2.2. MCNPX

MCNPX means Monte Carlo with N Particles eXtended [33]. MCNPX comes from coupling of two previous codes: LAHET (Los Alamos High Energy Transport Code [34]) which treats the high energy processes and MCNP which allows taking into account the transport of the particles. Further details about the history, the capabilities of the codes and the implementation of the different codes are explained in reference [23].

The new beta-version 2.5e of MCNPX offers new possible physics models:

- The intranuclear cascade of Cugnon: INCL4. It is an adaptation of the code of Cugnon to MCNPX.
- The evaporation model of K. H. Schmidt ABLA.

The calculations are performed with MCNPX version 2.5.e. Its new capabilities and extensions are described in [35].

The parameters described in section 1.2.1 and 2.1 namely the nuclear potential, the stopping factor which controls the stopping time by the equation (1.3) of section 1.2.1, the nuclear surface, the parameter of maximum impact and the Pauli blocking can be controlled in MCNPX 2.5e by the LCC card (see figure 2-1)

The default values for the different parameters described in [36] are:

The nuclear potential is set to 45V, the stopping factor to 1, the nuclear surface to -2, the parameter of maximum impact to 8 and the Pauli blocking to 0 what corresponds to Pauli "statistic".

```
MCNPX test problem
c ----------------------------------------------------------------
c 1000 MeV pencil beam of protons on the axis of a spherical
c Pb208 target of 50cm radius.
c Production Cross Sections calculation.
c ----------------------------------------------------------------
c Cells
c ----------------------------------------------------------------
 1  1  -11.34  -1
 2  0         1

c ----------------------------------------------------------------
c Surfaces
c ----------------------------------------------------------------
 1  so  50.0

c ----------------------------------------------------------------
c Materials
c ----------------------------------------------------------------
 m1   82208.60c 1
c ----------------------------------------------------------------
c Source
c ----------------------------------------------------------------
 sdef erg=1000 par=9 pos=0 0 0 vec=0 0 1 dir=1
 ssw 1 CEL 1
c ----------------------------------------------------------------
c Options
c ----------------------------------------------------------------
 imp:n 1 0
 imp:h 1 0
 phys:n 1088
 phys:h 1088
 mode h
 histp 1
 lca 1 1 0 0023 1 1 0 -2 2
 lea 1 4 1 0 1 0 2 1
 lcc 1 45 8 0 -2
c ----------------------------------------------------------------
c Tallies
c ----------------------------------------------------------------
c ----------------------------------------------------------------
 print
 nps 150000
```

Figure 2-1: *Example of an MCNPX input file for calculating the production cross section on ^{208}Pb irradiated by a 1 GeV proton beam.*

2.3. Structure and sequences of the programs

An explanation is useful to clearly understand the organization of the programs and their sequence. Indeed, it is necessary to specify the input files and the output files of each program, the files used during the calculation, and to see how the various programs follow one another.

2.3.1. MCNPX

After running MCNPX, we use HTAPE3X to obtain the residual nuclei production per source proton. HTAPE3X is an auxillary program in the MCNPX package. And then, the program RORIHET creates the input tables as a function of the mass number or of the charge number for the public domain plotting program XMGRACE.

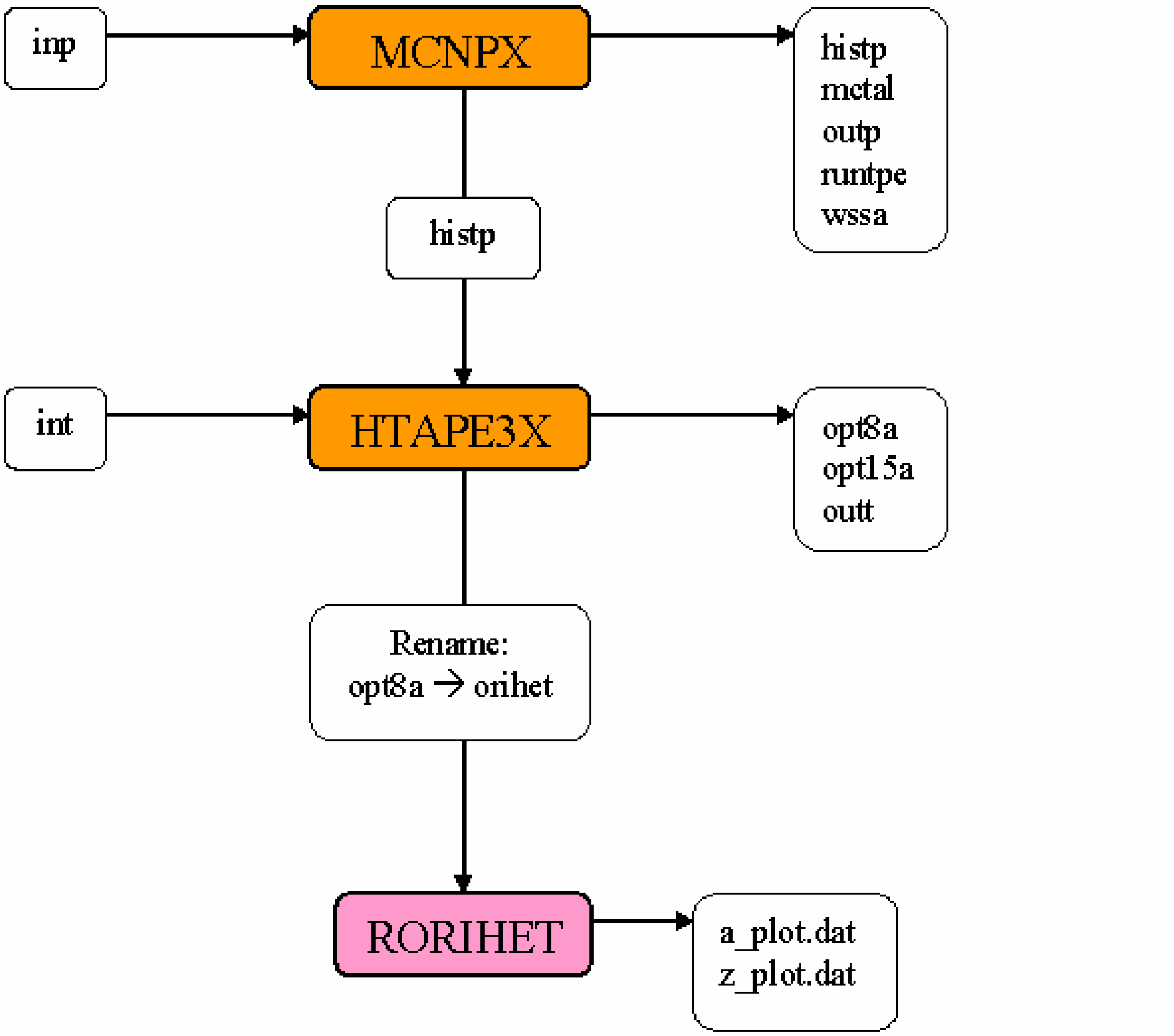

Figure 2-2: *Sequence of the programs to obtain the spallation yields as a function of the mass number A or of the charge number Z.*

2.3.2. The Cugnon code in the Stand-alone version

The file avv_zvv.out is created by a local extension of the Cugnon code in Stand-alone version at the FZK. The program RCU creates input tables as a function of the mass number (cugnon_a.dat) and of the charge number (cugnon_z.dat) for the public domain program XMGRACE.

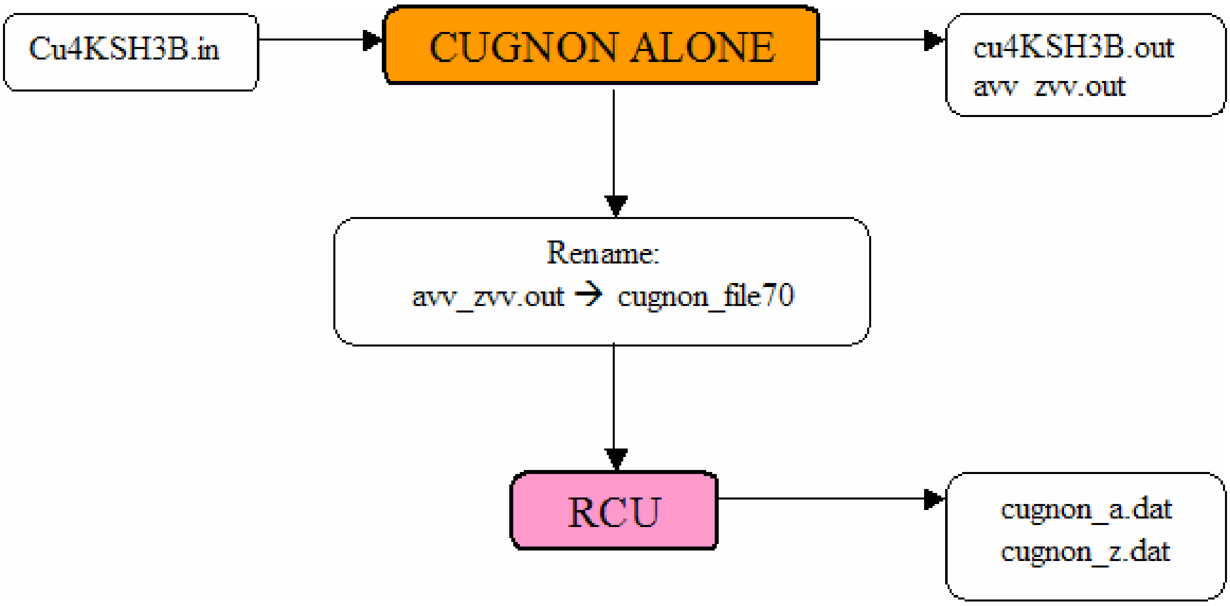

Figure 2-3: *Sequence of the programs to use the Cugnon code in Stand-alone version.*

2.3.3. Plot of isotopes

After runnig MCNPX and HTAPE3X, we use the modul of HETMIX of KAPROS to create the input table (HETMIX_1.dat) for the for the public domain program XMGRACE. It is necessary to create the adapted "plottab.dat" file to indicate the studied isotopes.

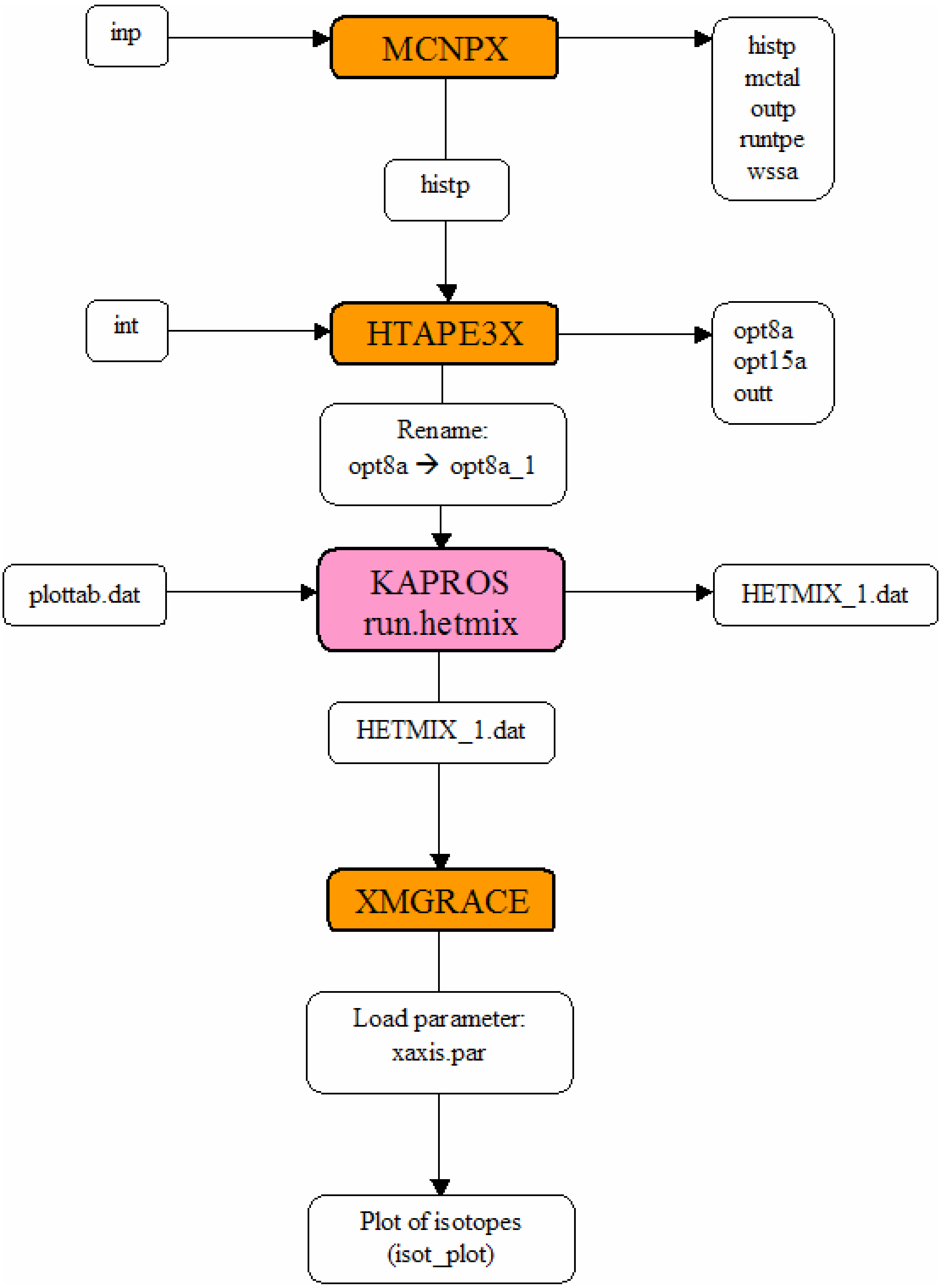

Figure 2-4: *Sequence of the programs to obtain a view of the spallation yields per isotopes.*

Chapter 3.

Comparison of MCNPX with the INCL4-ABLA model and the Cugnon-Schmidt code in the Stand-alone version

The purpose of this part is the comparison of the Cugnon-Schmidt in Stand-alone program and INCL4-ABLA implementation in MCNPX.

3.1. Comparison of the two codes

As shown on figure 3-1, MCNPX offers two methods to calculate the cross sections and the residual nuclei distributions: The first one was applied previously in [23] and evaluates the data of the binary history output file *histp* from MCNPX via the program HTAPE3X (HTAPE3X is a part of the MCNPX package) [33, 34]. The second possibility was advised to us by [37] and is to request in the input file of MCNPX evaluation tally 8, described in [35]. This option calculates and produces directly in the output file the residual nuclei production per source proton. This tally is available only since the new beta version MCNPX 2.5e.

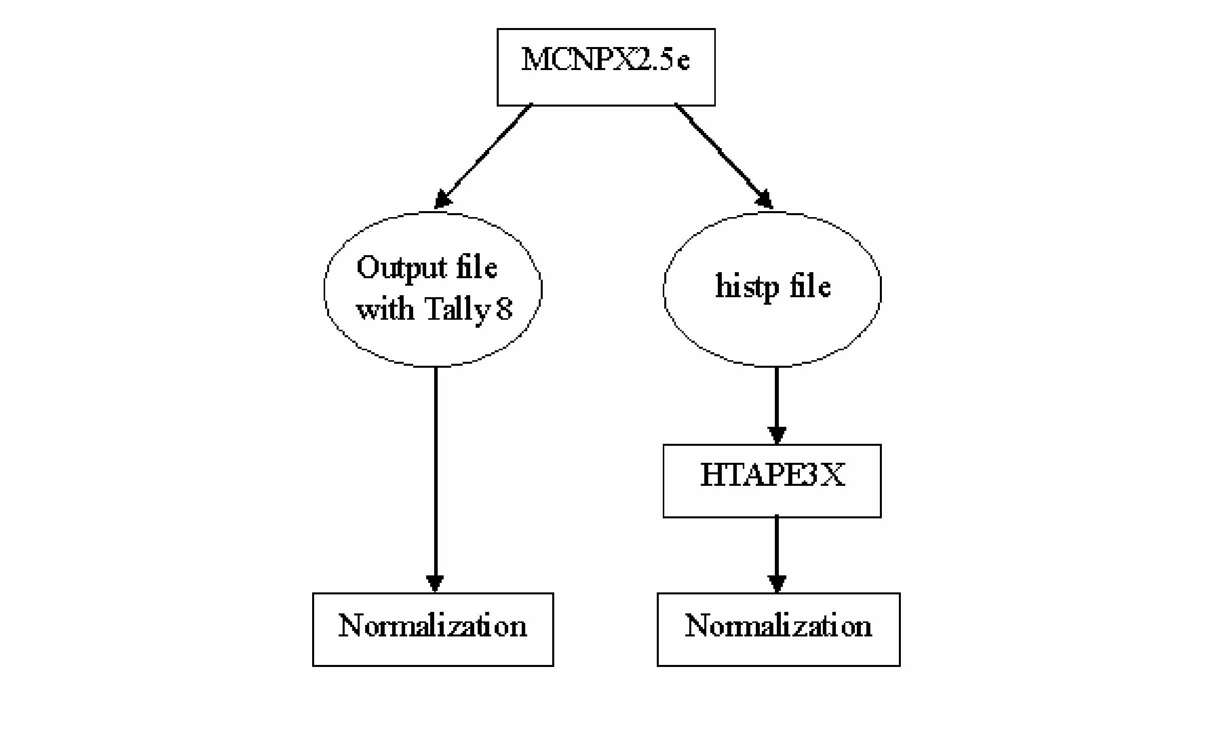

Figure 3-1: *Two different methods of treatments to obtain the spallation yields in MCNPX.*

We have checked that the two methods give exactly the same distribution before normalization. The output files of HTAPE3X and of the direct computation with tally 8 option can be consulted in annex A. These calculations were obtained by irradiation of a ^{208}Pb target at 1 GeV protons beam and by running 300.000 particles.

To obtain the spallation yields, it is necessary to normalize the distributions. We have analyzed how the normalization factor must be determined according to the type of reactions which one studies. When a proton collides with a target nucleus in a non-elastic reaction, this collision can give rise to a cascade (spallation reaction) but, in other cases, the incoming proton can pass through the target nuclei without any interaction (transparency). The input parameters allow us to choose between a forced cascade or cascade with transparencies.

There are four input cards (LCA, LCB, LEA and LEB) in MCNPX [33] which allow the user controlling the physics options. We will be interested more particularly in the LCA card. The LCA card is used to select the Bertini, ISABEL, CEM or INCL4 models, as well as to set certain parameter used in these models which are discussed thereafter.

We want to obtain the cross sections. It means that only the first interaction of the source particle is taken into account. Thus, the transport and the slowing-down are turned off. This option is controlled by the eighth parameter of the LCA card, called NOACT. There are two values of this parameter which allow obtaining the cross sections. It is -1 and -2. NOACT equal to -1 is used to compute with HTAPE3X code. The NOACT equal to -2 is used to compute double-differential cross sections and residual nuclei with the tally 8 option.

If a cascade is forced, we must use the reaction cross section to normalize the yields.

One can use as a normalization factor, either

$$\frac{s_{reaction}}{N_{particles}} \tag{3.1}$$

Or

$$\frac{s_{geo}}{N_{particles} - N_{transparencies}} \tag{3.2}$$

with

$$s_{geo} = pR^2 \qquad (3.3).$$

In section 3.2 the geometrical cross section s_{geo} is investigated in more detail.

In the Cugnon code in the stand-alone version, the reaction is not forced (there are transparencies) and thus, the use of geometrical cross section for the normalization is correct. In contrary, in MCNPX, to obtain cross sections, we must set the NOACT parameter to -1 or -2 which corresponds to a forced cascade. So, it is not possible to normalize with the geometrical cross section. The value of the reaction cross section coming from the Bertini model is *1732 mb*. This value is obtained from the LAHET output file which gives the number of transparencies and the geometrical cross section. Then:

$$s_{reaction} = \frac{N_{particles} - N_{transparencies}}{N_{particles}} s_{geo} \tag{3.4}$$

The INCL4 model gives a cross section reaction value equal to *1793 mb*. The difference is approximately of 3%. Thus we can conclude that the reaction cross section is not very different according to the model. In the calculations the reaction cross section is fixed in an early stage to *1740 mb.*

A second input parameter for MCNPX is relevant for this question. It is the first parameter of the LCA card, called IELAS. It controls if the elastic scattering for neutrons and protons are taken into account. The program XSEX3 which is a part of the MCNPX package [33] could provide the number of elastic scattering but the conditions to obtain this value are not yet completely clear, so we can not present results normalized with this method. But in the case where the number of elastic scattering is given we can normalize the yields. Indeed, it is necessary to subtract them to the number of events.

So, to summarize:

- If a cascade is forced, we must normalize with the reaction cross section.
- If a cascade is not forced (there are transparencies), we can normalize with the geometrical cross section.
- If the elastic scattering reactions are taken into account, we need their number and then we can normalize.

The calculations with NOACT equal to -2 give a number of nonzero history tallies different of the number of particles and it must be taken into account in the normalization.
As a conclusion we recommend to use no elastic scattering for protons (IELAS=0 or 1) and to force the reactions with the NOACT parameter recommended for the tally 8 option (NOACT=-2). For an example, that corresponds to the following LCA card with the INCL4 model:

lca 1 0 0 0023 1 1 0 -2 2.

The normalization factor corresponding to this card is

$$\frac{\text{Number of particles}}{\text{Number of nuclear interactions}} s_{reaction} \quad (3.5)$$

IELAS	NOACT	Normalization
1	-1	Reaction cross section
1	-2	Reaction cross section
2	-1	Geometrical cross section
2	-2	Geometrical cross section

Table 3-1: *Summary of the different combinations of LCA parameters and the normalization associated.*

Model	Bertini	Cugnon
Reaction cross section [mb]	1732	1793

Table 3-2: *Reaction cross section for the Bertini code and for the Cugnon code.*

Perspectives:

- An interesting extension would be to obtain in a reliable way the number of elastic scattering and to check the normalization.
- Then, more precise determination of the reaction cross section for the different physical models is necessary.
- Signification of using the number of nuclear nonzero history tallies different of the events.

The three following figures 3-2, 3-3, 3-4 show that the normalization with the geometrical cross section with NOACT equal to -1 or -2 is incorrect. On the three figures, the green curve represents the results of the calculations for the three models (Bertini, ISABEL and INCL4+ABLA) parameterized by IELAS=2 (with elastic scattering for protons), NOACT=-1 and normalized with the geometrical cross section. The blue one is parameterized by IELAS=2, NOACT=-1 and is normalized with the geometrical cross section. The red one represents a non-elastic reaction (IELAS=1), parameterized by NOACT=-2 and normalized with the reaction cross section. The last black one is parameterized by IELAS=1, NOACT=-1 and is normalized with the reaction cross section. The green curve corresponds to the card used in [23]. For the ISABEL model it was checked that the yields normalized with the geometrical cross section give good results with experimental data. The figure 3-2 for the ISABEL model shows that the green curve is in very good agreement on the spallation part of the curve with experimental data, but the other parameters combinations show similar agreement. Now, let we consider figure 3-3 and figure 3-4, which represent the spallation yields for the Bertini and INCL4+ABLA models respectively. They present us a difference between the curves normalized with the geometrical cross section and the others normalized with the reaction cross section. We observe a difference with the experimental data from GSI which can be up to 18% for the Bertini model and to 23% for the INCL4+ABLA one. It means that the results obtained by comparison of the ISABEL model and the experimental data were a coincidence because that is found only for this model.

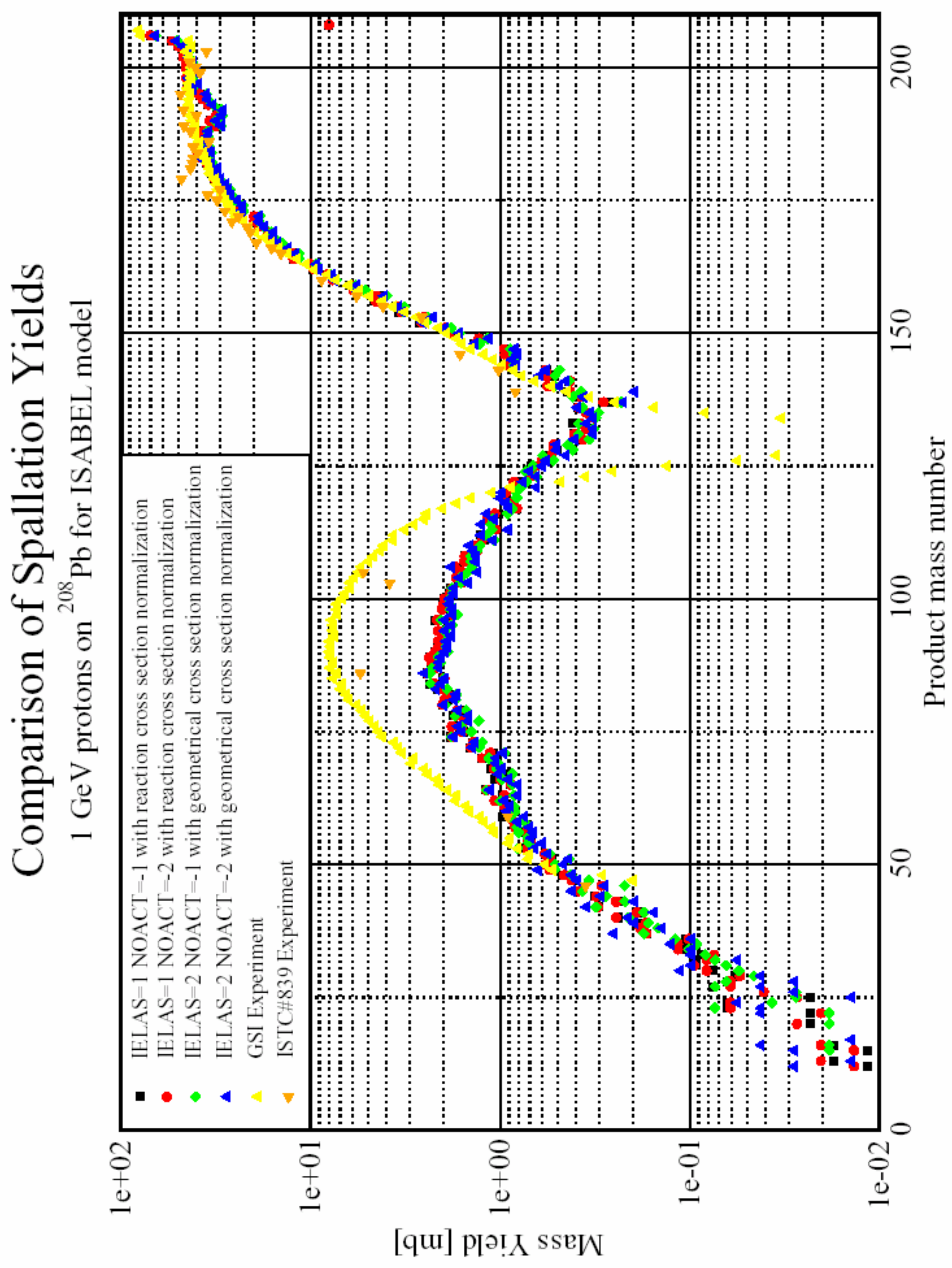

Figure 3-2: *Comparison of with MCNPX computed (ISABEL model) spallation yields obtained with different combinations of LCA parameters and experimental spallation yields (GSI, ISTC). Mass yields in millibarn [mb] as a function of the mass number A.*

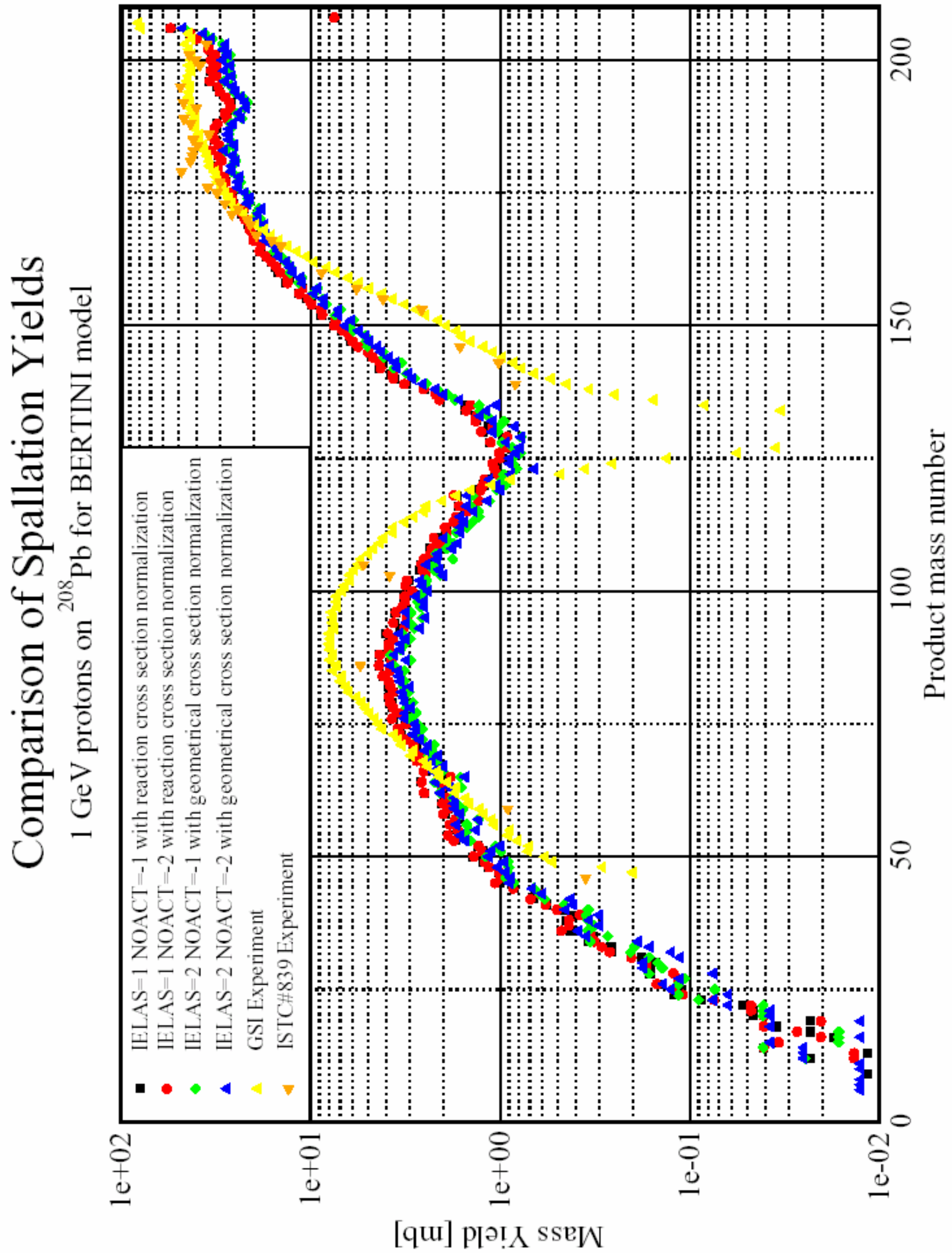

Figure 3-3: *Comparison of with MCNPX computed (BERTINI model) spallation yields obtained with different combinations of LCA parameters and experimental spallation yields (GSI, ISTC). Mass yields in millibarn [mb] as a function of the mass number A.*

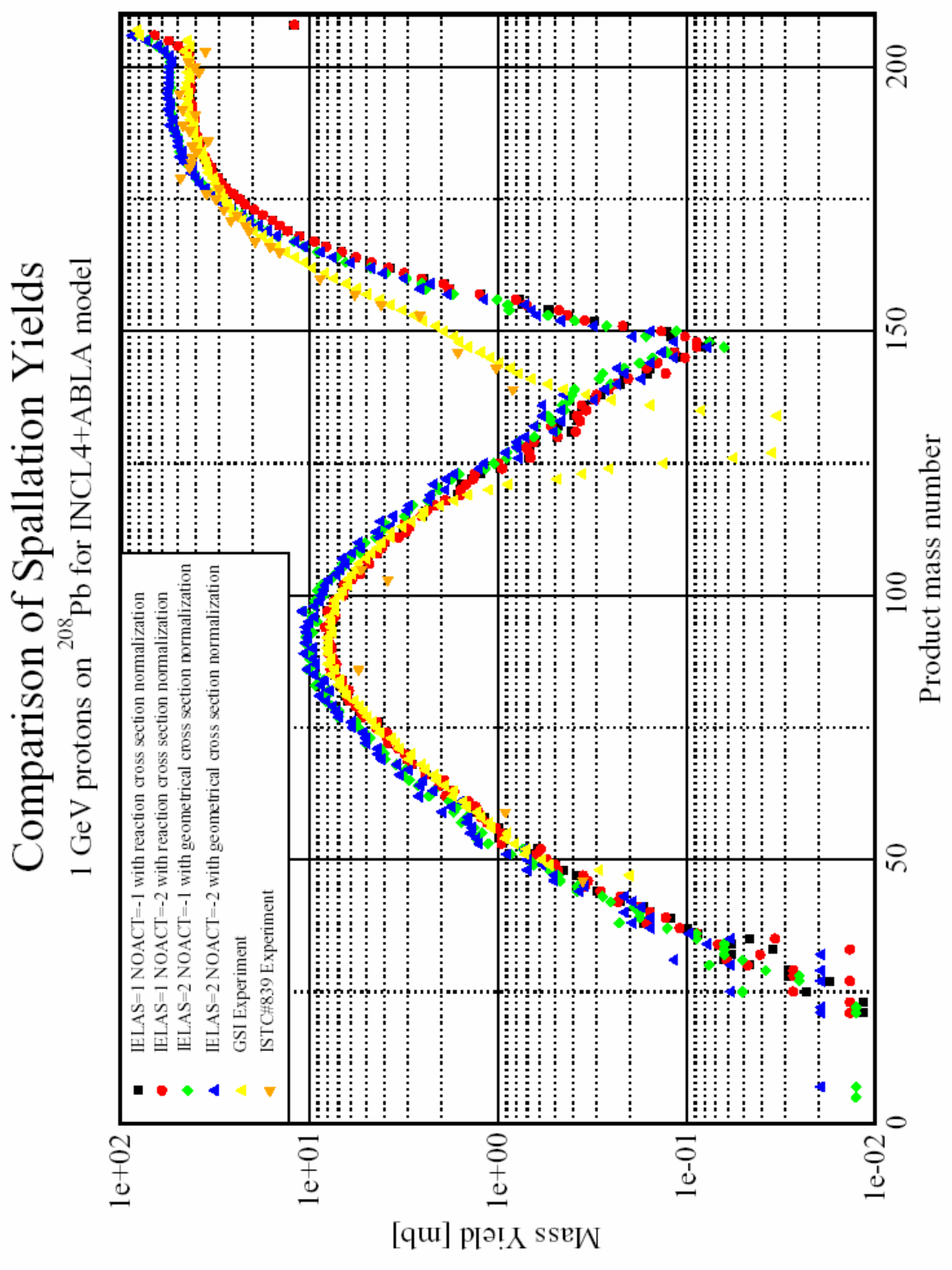

Figure 3-4: *Comparison of with MCNPX computed (INCL4+ABLA model) spallation yields obtained with different combinations of LCA parameters and experimental spallation yields (GSI, ISTC). Mass yields in millibarn [mb] as a function of the mass number A.*

3.2. Investigations related to the normalization factor

To compare the data given by the output file opt8a from the HTAPE3X program of the MCNPX package with experimental data, we need the normalization factor. The purpose of this part is the analysis of the normalization factor for spallation yields.

In order to get confidence in the results of simulation codes, validation by comparison with experimental data is necessary. The qualification of the simulation of the reaction products produced by irradiation of a target by high energetic protons is still in progress. Two types of experiments are applied for this purpose: thin or thick targets. In the thin target experiments, only primary reactions are measured, whereas in thick target reaction cascades are investigated. Both types of investigation are discussed in reference [23]. In this section, the validation is analyzed in more detail. The considered target experiments are carried out by direct proton irradiation (ISTC) or by the inverse kinematic method (GSI). The results of these experiments are cross sections for spallation products. As the simulation code MCNPX and its evaluation program HTAPE3X calculates spallation products yields per source proton, a normalization factor is required for the comparison. This normalization factor is discussed in section 3.2.1 and it is show that the geometrical cross section σ_{geo} plays an important role.

3.2.1. Formulations for the nucleus geometry

The formulation and the description of the geometry of the nucleus influence the distribution of the spallation yields. Now we analyze several formulations for the geometry of nucleus.

3.2.1.1. Range of the nucleus radius

The geometrical cross section is given by the following formula:

$$\sigma_{geo} = \pi R^2 \tag{3.6}$$

where R is the radius of the nuclei.

Thus, to obtain the geometrical cross section, it is necessary to determine the radius R of the nuclei.

It is considered, as a first approximation, that the nucleus has a spherical form and that it has an incompressible volume.The volume of the hydrogen nuclei is noted V_0:

$$V_0 = \frac{4}{3}\pi R^3 \tag{3.7}$$

If one considers that the volume of the atomic nucleus is proportional to the number of nucleons which constitute the nucleus:

$$V = AV_0 \tag{3.8}$$

The radius of a nucleus is proportional to the cubic root of the number of particles. One deduces:

$$R = r_0 A^{1/3} \tag{3.9}$$

where $r_0 = 1.2\ fm$ from [38]
$r_0 = 1.43\ fm$ from [39]

The exact value of r_0 is somewhat contentious, and different types of experiment give values of r_0 ranging from 1.07 to 1.6 [39]. As an example, Bethe has found $r_0 = 1.47 .10^{-13}\ cm$ [40], and Barkas $r_0 = 1.43 .10^{-13}\ cm$ [41]. The geometrical cross sections obtained with this different value r_0 are summarized in the table 3-4. We can observe that the best result in comparison with the Cugnon and ISABEL values is obtained with $r_0 = 1.6\ fm$.

From other experiments, nuclear radius can be found from measurements of the nuclear density. This can be shown on the figure 3-5 using a formula which is a little bit different from the simple formula, but gives essentially the same results as with $r_0 = 1.43 .10^{-13}\ cm$:

$$r = 1.07 A^{1/3} + 2.4\ fm \tag{3.10}$$

One obtains *2400 mb* for the lead.

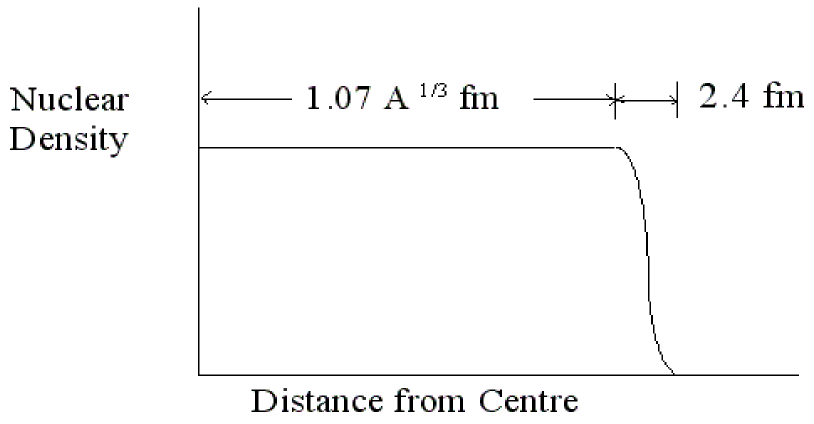

Figure 3-5: *Nuclear density as a function of the distance from the centre of nucleus which leads to the formula (3.9).*

^{208}Pb	Value from LAHET with ISABEL
Geometrical cross section [mb]	2760

Table 3-3: *Geometrical cross section from LAHET for the ISABEL model.*

^{208}Pb	Ranging of r_0				
r_0	1,07	1,21	1,27	1,43	1,6
$R=r_{0}.A^{1\backslash 3}$	6,34	7,17	7,52	8,47	9,48
Geometrical cross section [mb]	1262,68	1614,72	1778,82	2255,26	2823,35
Difference with Cugnon value	66,71%	57,43%	53,10%	40,54%	25,56%
Difference with ISABEL value	54,25%	41,50%	35,55%	18,29%	2,30%

Table 3-4: *Geometrical cross sections calculated with formulas from bibliography.*

3.2.1.2. The parameterization of J. Cugnon

The parameterization which is used in the Cugnon Stand-alone code is:

$$\begin{cases} R_0 = \left(2.745 \; .10^{-4} A_T + 1.063\right) A_T^{1/3} \; fm \\ R_{\max} = R_0 + 8a \end{cases} \tag{3.11}$$

with

$$a = 0.510 + 0.63.10^{-4} \; A_T \; fm \tag{3.12}$$

where a is the diffuseness.

This parameterization associated to the formula of the geometrical cross section (3.6) gives a value of *3793 mb* for the geometrical cross section for the Cugnon model. The input value, the intermediary calculations and the result for the geometrical cross section for the Cugnon model is shown in table 3-5 and 3-6.

^{208}Pb	
Atomic mass A	208
Atomic number Z	82
Impact parameter	8
Diffuseness a [calculated by Cugnon]	0,544

Table 3-5: *Input data for the calculation of the geometrical cross section for the Cugnon model.*

^{208}Pb	Formula from Cugnon Stand-alone code
R_{max} [fm]	10,99
R_0[fm]	6,64
Geometrical cross section [mb]	3792,90

Table 3-6: *Geometrical cross section for ^{208}Pb calculated by Cugnon according to the formula (3.11)*

3.2.1.3. Other parametrizations

There exists some others parameterizations as the one of L. Sihver [42], the similar formulas of Kox [43] and Shen [44] and the one of R. K. Tripathi [45].

The Sihver formula is independent of the energy. On the contrary, the parameterizations of Kox, Shen and Tripathi include an energy term.

The Sihver formula gives a value of *2287 mb* what represents a difference of 40% with the value from Cugnon and 17% with the value from ISABEL (see table 3-7).

^{208}Pb	Sihver formula
Geometrical cross section [mb]	2287

Difference with Cugnon value	40%
Difference with ISABEL value	17%

Table 3-7: *Geometrical cross section for ^{208}Pb calculated with the Sihver formula.*

3.2.2. Comparison of the models

MCNPX applied with the physical models Bertini, CEM and ISABEL doesn’t calculate the geometrical cross section. Only MCNPX applied with the Cugnon model gives this value in the printed output. The auxiliary program XSEX3 of the MCNPX package in principle can calculate these values, but up still now this program did not work properly in our system.

In the reference [23], the value from LAHET with the ISABEL model is used as the normalization factor. This value is equal to *2760 mb* as it is summarized in table 3-3. For a job with the Bertini model, we obtain *2462 mb*. It means that this factor depends on the physic model. That is confirmed by e-mail correspondance with A. Boudard [32]. Thus, it is necessary to take the geometric cross section of the model which is used: either *3793 mb* for the INCL4 model or *2760 mb* for the ISABEL model or *2464 mb* for the Bertini model.

The different results for the geometrical cross section are summarized in the table 3-8.

Formula from	LAHET for Bertini	LAHET for ISABEL	Cugnon Stand-alone	Bibliography R=1.6*A$^{1\backslash 3}$	Bibliography Sihver formula
Geometrical cross section [mb]	2462	2760	3793	2823	2287

Table 3-8: *Summary of the geometrical cross section of the different models (Bertini, ISABEL and INCL4 models) and of the parametrization from the bibliography.*

3.2.3. The geometrical cross section of the Lead-Bismuth-Eutectic

Currently the target material is lead-bismuth-eutectic (LBE). It is applied in the MEGAPIE project and the supporting LiSoR experiment [9].The LiSoR project will be discussed in more detail in chapter 4. These two projects work with a mix of lead and bismuth with specific proportions.The next point is to determine the normalization factor for this LBE. In the table 3-4, the last column which corresponds to $r_0 = 1.6\ fm$ has the smallest deviation in comparison of the two reference values (Cugnon and ISABEL models). Thus, we obtain a normalization factor of *2828 mb* for a lead-bismuth mix (44% Lead and 56% Bismuth):

$$s_{geo\ LBE} = 0.44 \times s_{geo\ Pb} + 0.556 \times s_{geo\ Bi} \qquad (3.13)$$

3.3. Influence of input parameters

The code of Cugnon was implemented in MCNPX. The input file is described in section 2.2. In the documentation of MCNPX [36], it is written that only the potential depth V_0 and the overall factor f_{stop} can be changed, but we can also change the Pauli blocking and the value of maximum impact parameter through *XFOISA*. They are on the LCC-Card as described in the section 2.2.

It is interesting to check the influence of the main input parameters of Cugnon and to compare the results with MCNPX.

The parameters investigated are the nuclear potential and the Pauli blocking. The influences of the *XFOISA* parameter which controls the parameter of maximum impact and the f_{stop}

parameter which controls the stopping time are not studied because these two parameters are in dependence. Indeed, if a proton comes on a sphere of radius B_{max} (defined in section 2.1), the calculation of the cascade begins when the proton touches this sphere. The stopping time is defined since this time. The *XFOISA* parameter is a function of B_{max}, as mentionned the formula (2.2). Thus, the stopping time is also a function of B_{max}. So, it is not possible to change *XFOISA* (or B_{max}) without to evaluate again the stopping time and these proportions are complex.

The figure 3-6 represents the spallation yields computed by MCNPX with INCL4+ABLA model for different values of the nuclear potential, which are calculated with the formula (2.1). The red curve is obtained with V_0=45 MeV which is the default value in MCNPX and which corresponds to the nuclides with a mass number between 70 and 210, according to [31]. The red curve is in very good agreement with the experimental data from GSI. One observes that the variation of the nuclear potential influences only the left part of the curve corresponding to the fission.

The figures 3-7 and 3-8 show the spallation yields according to the mass number obtained by irradiation of a lead target by 1 GeV proton beam computed with the Cugnon Stand-alone code and MCNPX with INCL4+ABLA for the two possibilities of Pauli blocking, namely Pauli “strict” and Pauli “statistic”. Concerning the fission part, the Pauli “strict” option underestimates slightly the results compared with experimental data from GSI. The discrepancy can be up to 3%. Then, we can observe a shift between the two Pauli options on the right part of the plot corresponding to the spallation. The Pauli “strict” curve gives results higher than the Pauli “statistic” and this difference can be up to 10%. That decreases until a mass number A<185. After this point, the Pauli “statistic” curve is in very good agreement with the experiment, in contrary to the Pauli “strict” curve which underestimates the spallation cross sections up to 4%. The seven following figures from 3-9 to 3-15 show the residual nuclei productions per isotopes obtained by irradiation of a lead target by 1 GeV proton beam too, obtained with isot_plot (described in figure 2-4). All these isotopes are situated on the spallation part of the curve. One can observe the same shift on the spallation part as on figure 3-7 and 3-8. One can also notice that this shift decreases with the augmentation of the mass number and for heavy nucleus the curve underestimates a little the spallation cross sections.

So at 1 GeV proton energy, the Pauli “statistic” option gives results in better agreement with the experimental data from GSI for the fission part than the Pauli “strict” option, the Pauli “strict” option gives the best agreement for a mass number A<185 and then, for heavy nucleus, the Pauli “statistic” is the best option.

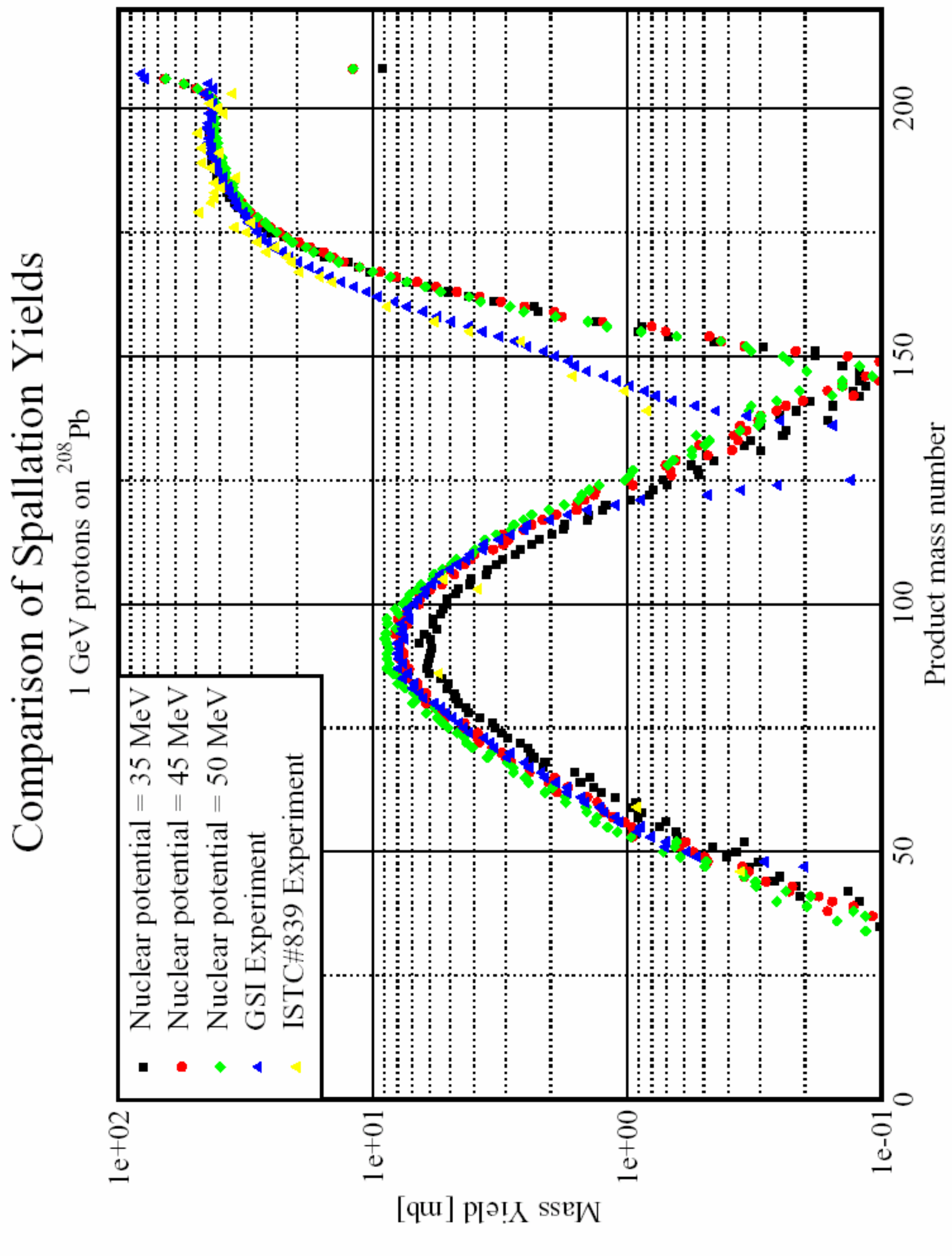

Figure 3-6: *Comparison of with MCNPX computed spallation yields (INCL4+ABLA model) for three different value of the nuclear potential and experimental spallation yields (GSI, ISTC). Mass yields in millibarn [mb] as a function of the mass number A.*

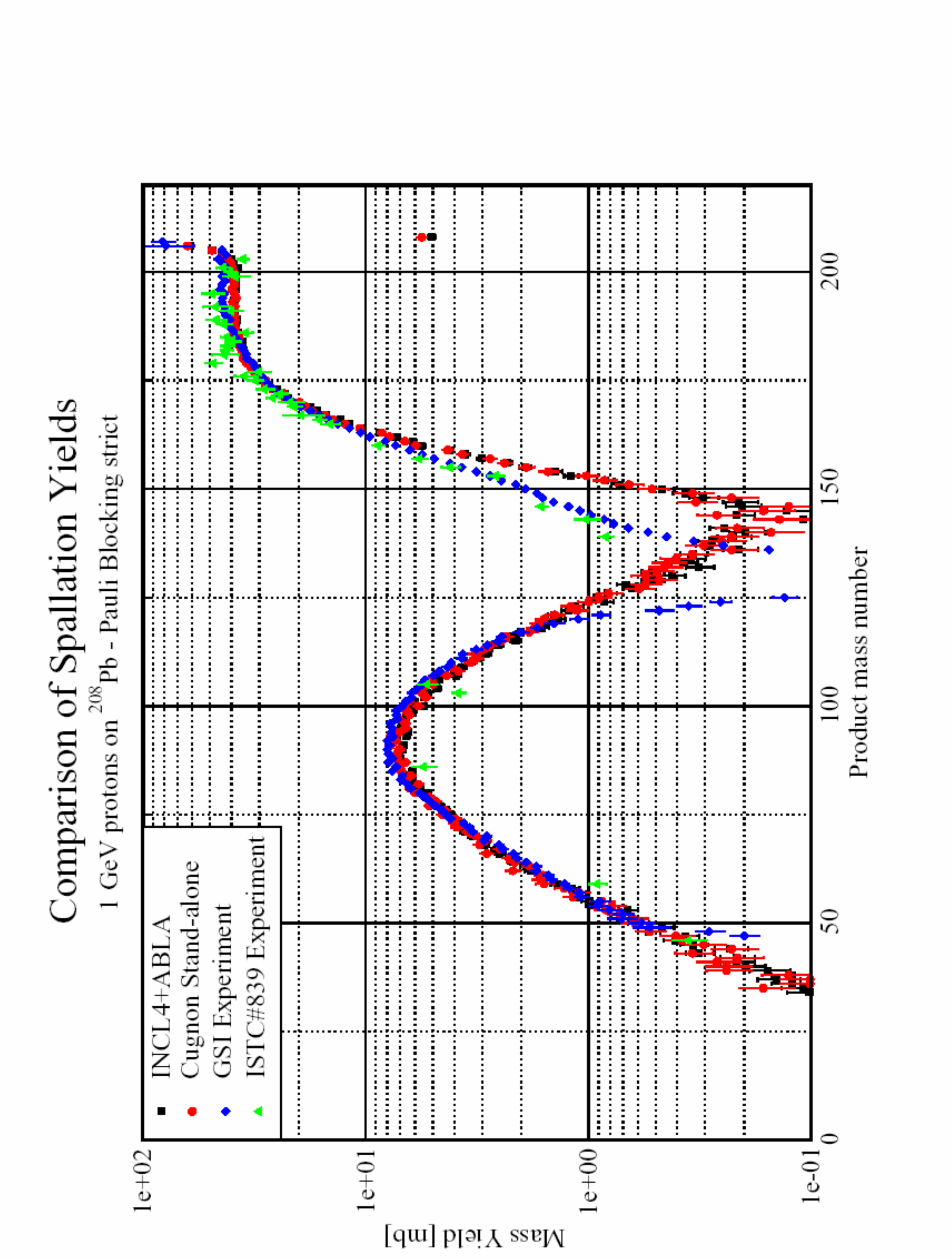

Figure 3-7*: Comparison of with MCNPX and the Cugnon code in Stand-alone version computed spallation yields (INCL4+ABLA model) with the Pauli blocking factor set to strict and experimental spallation yields (GSI, ISTC). Mass yields in millibarn [mb] as a function of the mass number A.*

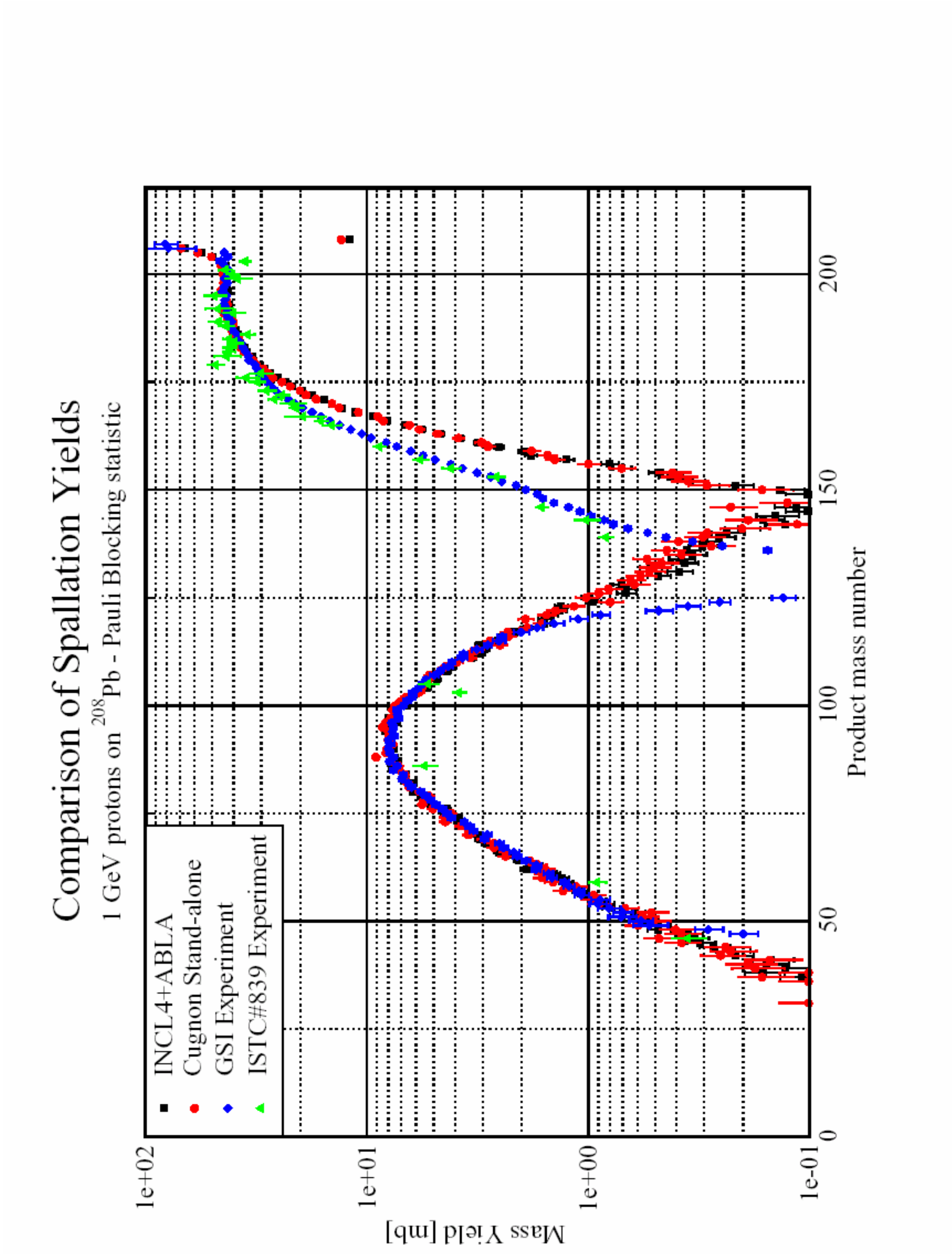

Figure 3-8: *Comparison of with MCNPX and the Cugnon code in Stand-alone version computed spallation yields (INCL4+ABLA model) with the Pauli blocking factor set to statistic and experimental spallation yields (GSI, ISTC). Mass yields in millibarn [mb] as a function of the mass number A.*

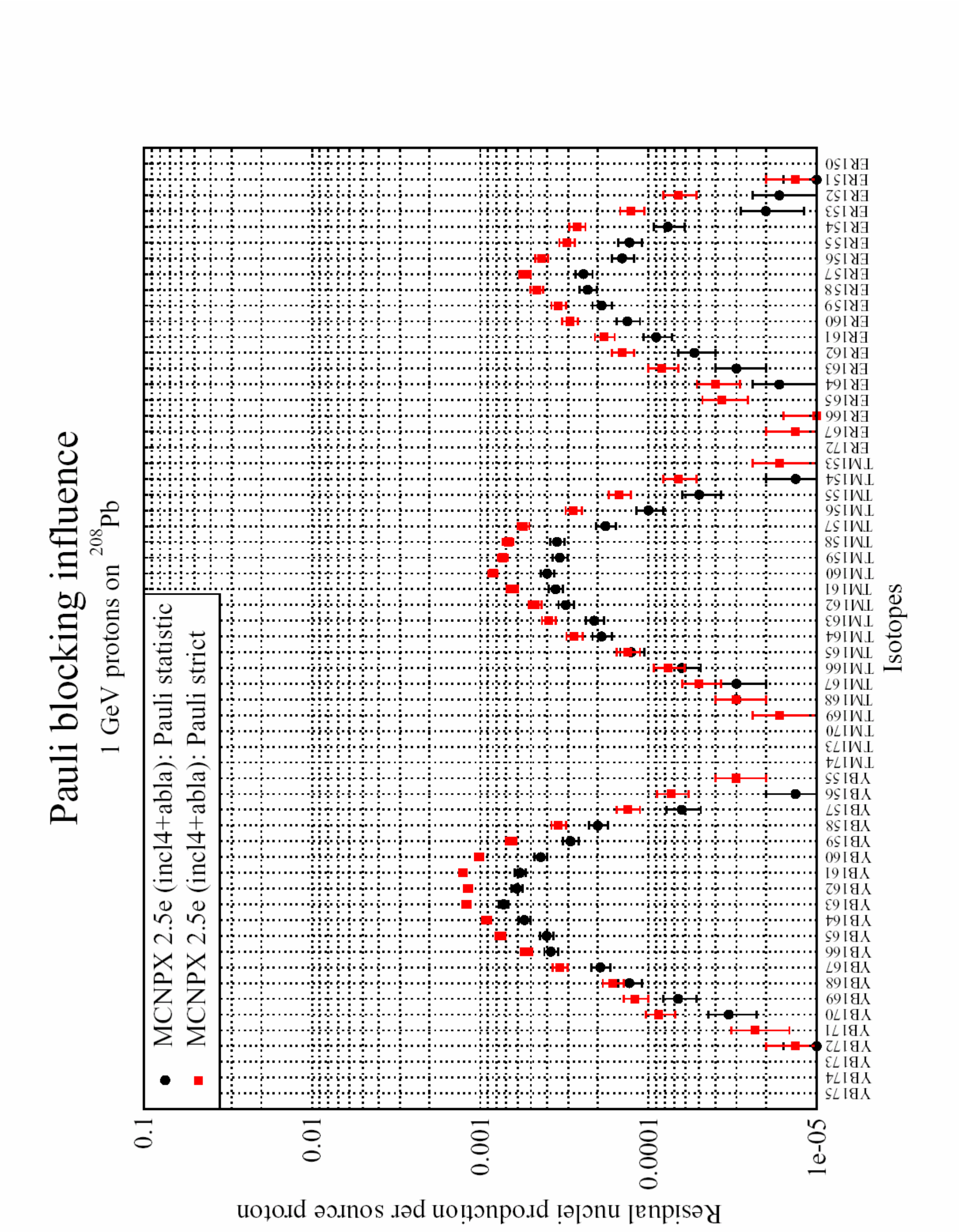

Figure 3-9: *Influence of the Pauli blocking factor on the residual nuclei production per isotopes computed with INCL4+ABLA model in MCNPX for isotopes with a charge number between 68 and 70.*

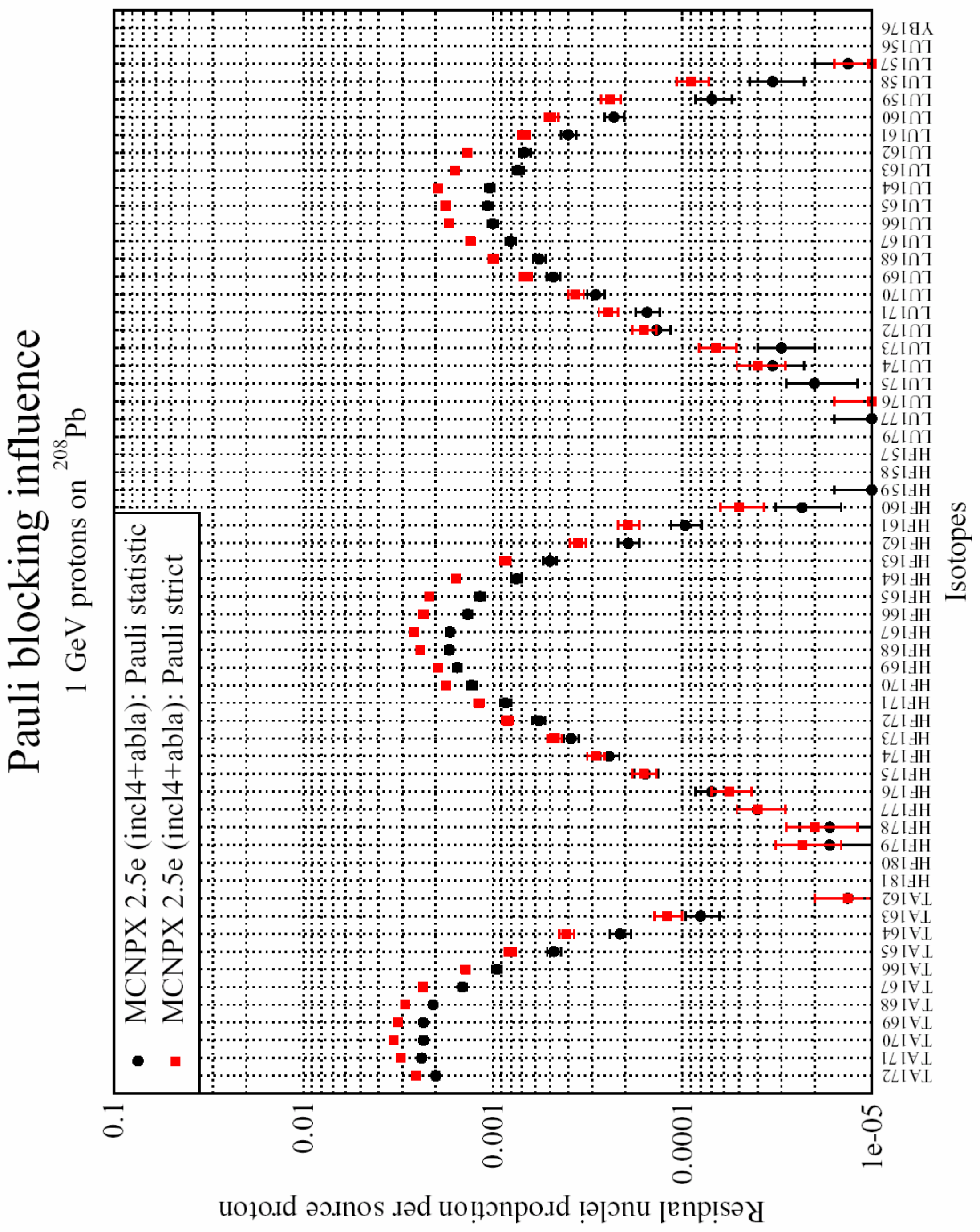

Figure 3-10: *Influence of the Pauli blocking factor on the residual nuclei production per isotopes computed with INCL4+ABLA model in MCNPX for isotopes with a charge number between 70 and 73.*

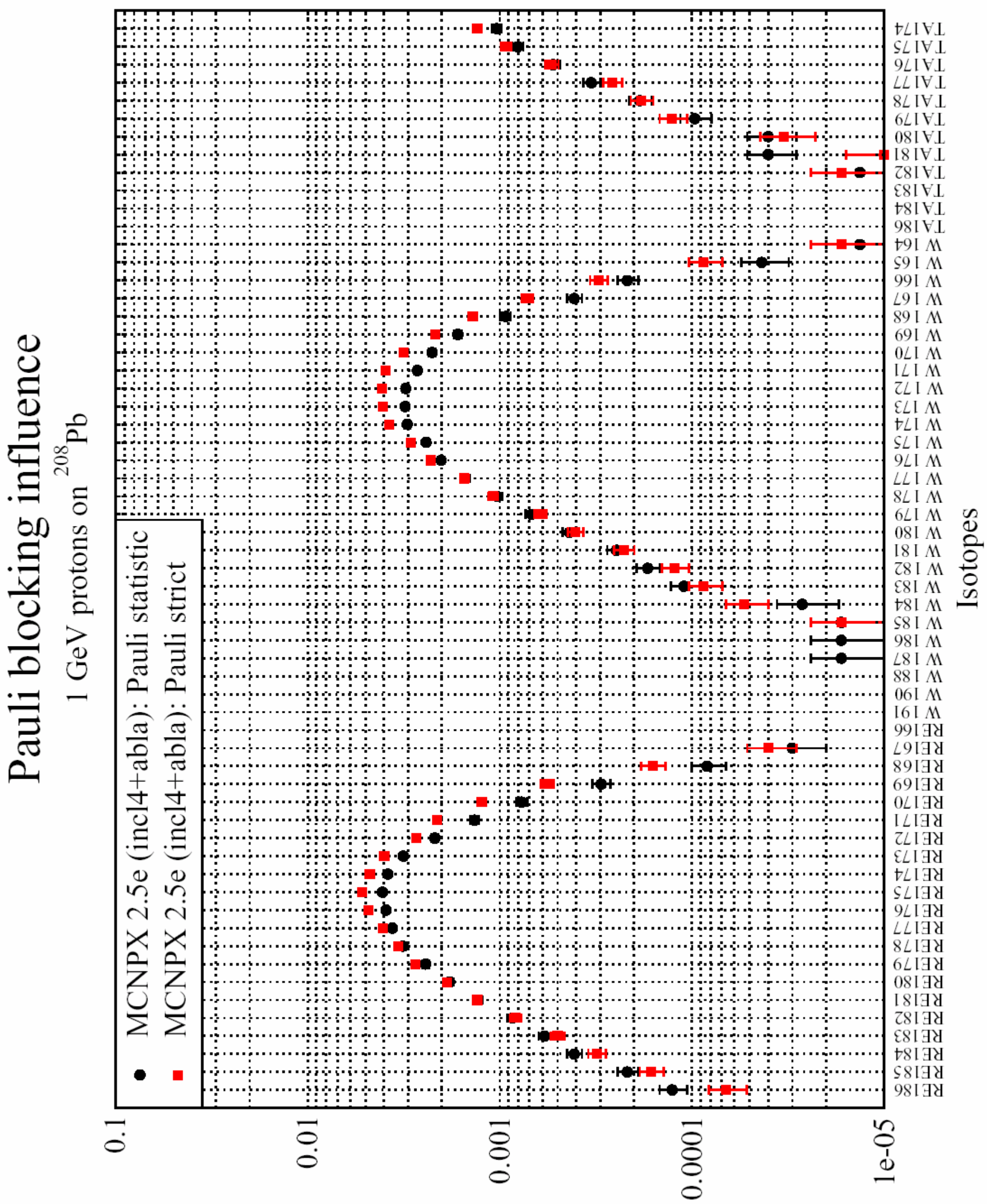

Figure 3-11: *Influence of the Pauli blocking factor on the residual nuclei production per isotopes computed with INCL4+ABLA model in MCNPX for isotopes with a charge number between 73 and 75.*

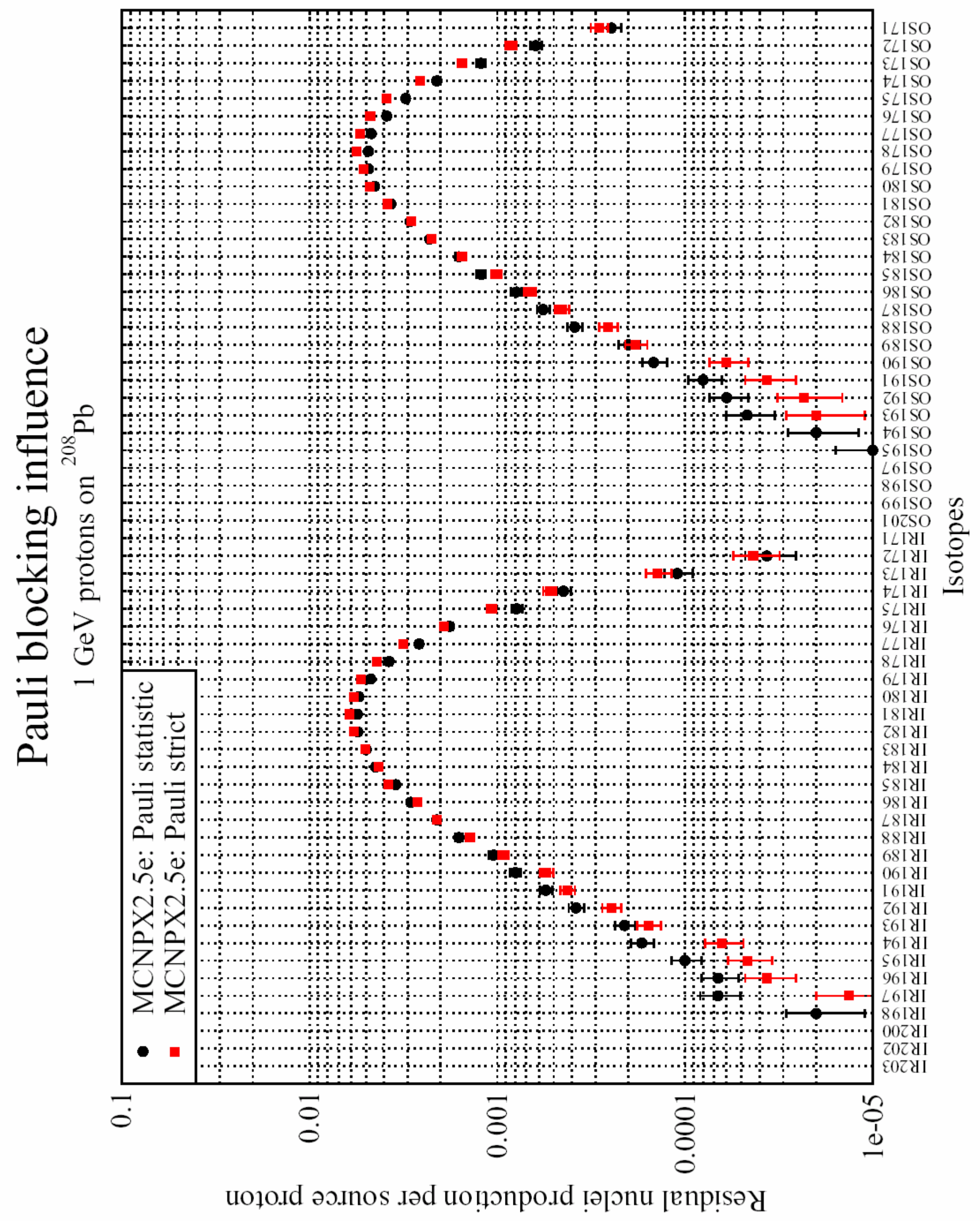

Figure 3-12: *Influence of the Pauli blocking factor on the residual nuclei production per isotopes computed with INCL4+ABLA model in MCNPX for isotopes with a charge number between 76 and 77.*

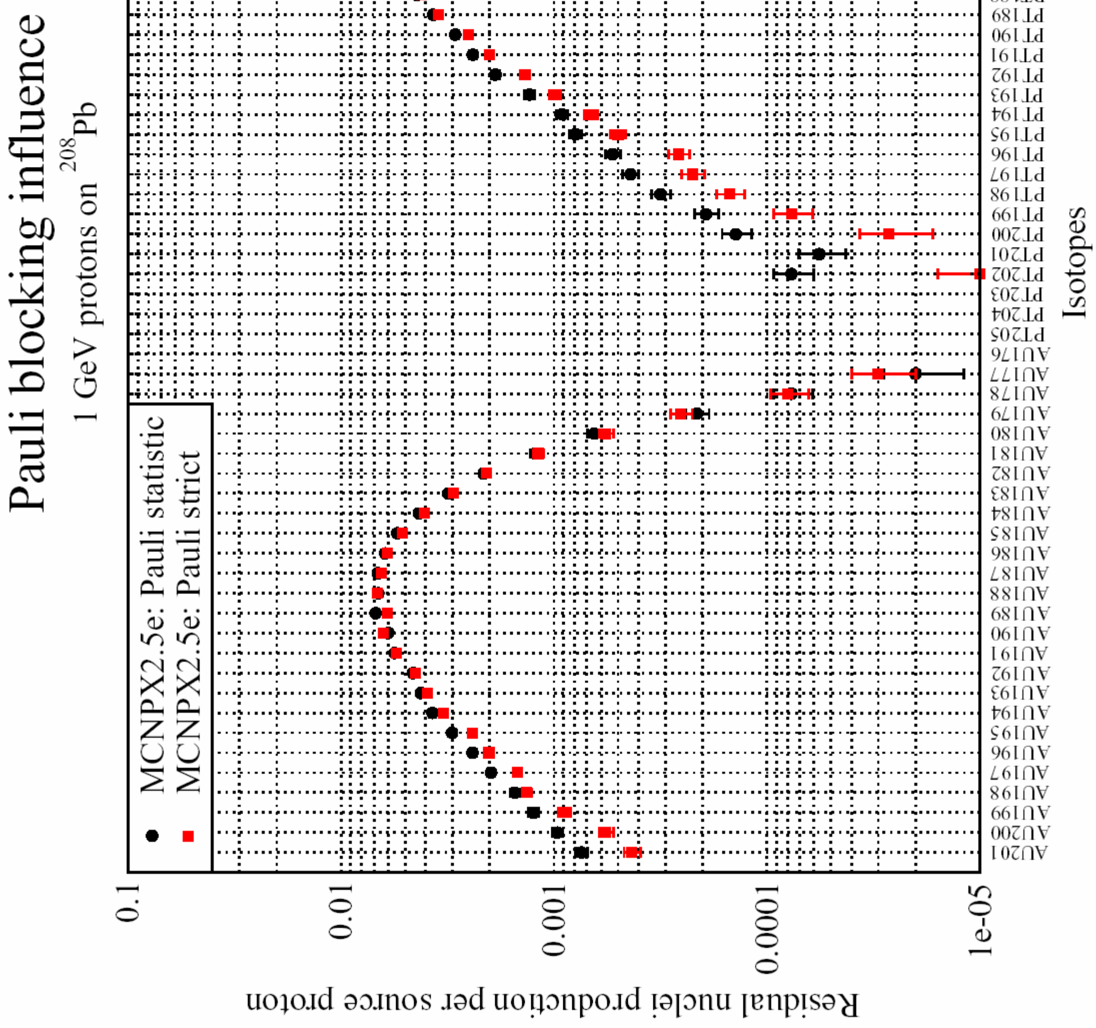

Figure 3-13: *Influence of the Pauli blocking factor on the residual nuclei production per isotopes computed with INCL4+ABLA model in MCNPX for isotopes with a charge number between 78 and 79.*

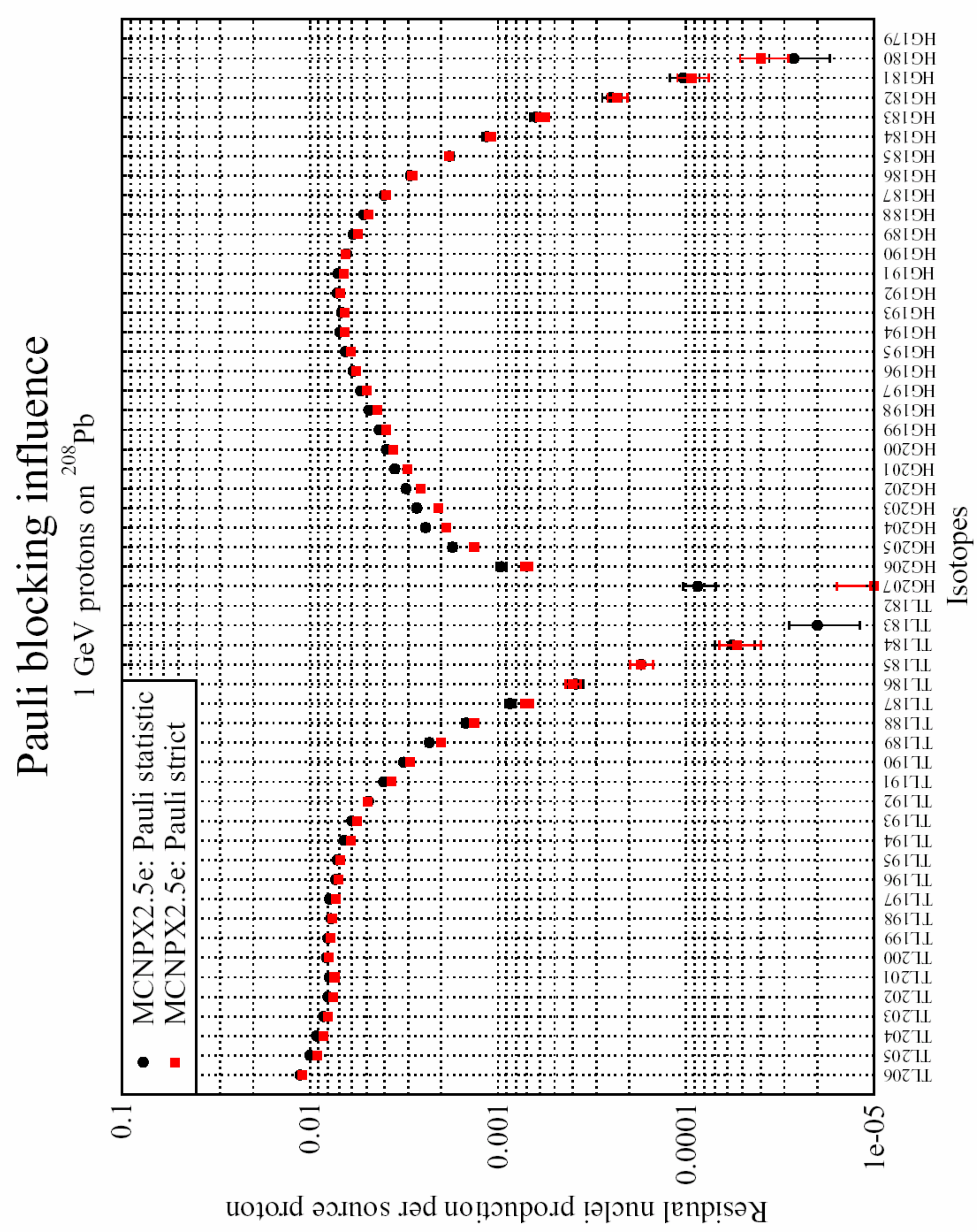

Figure 3-14: *Influence of the Pauli blocking factor on the residual nuclei production per isotopes computed with INCL4+ABLA model in MCNPX for isotopes with a charge number between 80 and 81.*

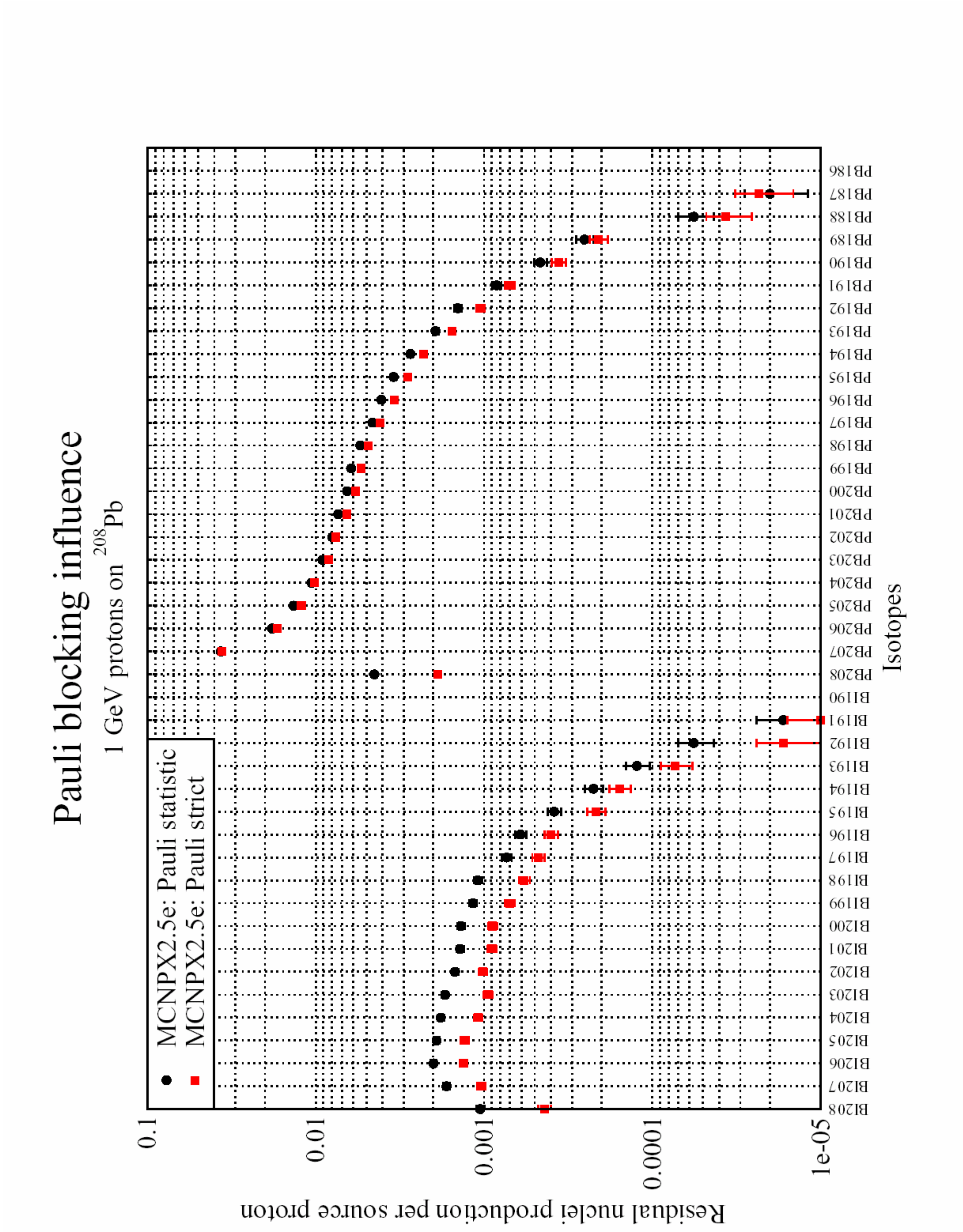

Figure 3-15: *Influence of the Pauli blocking factor on the residual nuclei production per isotopes computed with INCL4+ABLA model in MCNPX for isotopes with a charge number between 82 and 83.*

3.4. Thin target experiment at 1 GeV proton energy

3.4.1. Experimental methods

The experimental data come from two sources: ISTC [46] and GSI. All the experiments from the GSI group are available in reference [47]. There are also informations about the detector FRS, the experiment, the data and their analysis.

There are two different methods to obtain the experimental data: The inverse kinematic and direct proton irradiation.
The direct kinematic is the method used at ISTC. The principle is a target irradiated by a proton beam. The benefit of this method is the possibility to use a lot of different targets. But there are also disadvantages: First the nuclei are identified with the gamma-spectroscopy, thus only the nuclei with a half-life larger than half one hour are detected and the stable nuclei are not detected. Secondly, one obtains cumulative cross sections and the results must be analyzed.
At the GSI in Darmstadt, it is the inverse kinematics which is applied. A beam of heavy nucleus is projected on a proton target. The proton target is liquid hydrogen at 20 Kelvin. This method gives direct cross section and detects all residual nuclei. The problem is the techniques. Indeed, a high energy accelerator for heavy nucleus is a complex device.

3.4.2. Check of old measurements and validation of the different physical models

These comparisons were already done in reference [23]. This section allows us validating again the MCNPX results with the experimental data at 1 GeV proton energy. The correct method and normalization to obtain the spallation yields have been presented in the previous chapter and we can do a new validation of the different model of MCNPX Bertini, ISABEL and add the INCL4+ABLA model.
Let us consider now the figure 3-16. It shows the spallation yields of ^{208}Pb computed by MCNPX with the Bertini, ISABEL and INCL4+ABLA models compared to the experimental data at 1 GeV from GSI [48] and ISTC [46]. First of all, one observes that all the models have the same shape of curve as the experimental data. Indeed, there are two distinct parts on the curve: The left part corresponding to the fission and the second right part corresponding to the spallation. The Bertini model gives not very good estimation of the spallation cross sections. This discrepancy can be up to 50%. The ISABEL model is in very good agreement for the spallation part of the curve what corresponds to a mass number A>140 except a cavity for a mass number 186≤A≤198. However, the ISABEL model underestimates a lot the spallation

cross sections for the fission part (A<140) and the discrepancy can be up to 70%. Let us consider now the results obtained with the INCL4+ABLA model. Its agreement with the experimental data is very good, especially for the fission part (A<120) and for the spallation part since a mass number A>175. For 120≤A≤137, the INCL4+ABLA model overestimates the spallation cross sections and for 137≤A≤175, it underestimates the results.

A good solution for estimating the spallation cross sections would be to use two models:

- For a mass number A<120, we recommend to use the INCL4+ABLA model.
- For a mass number 120≤A≤140, there is a hole. All the models give results with a big difference with the experimental data, but the model which gives the smaller discrepancy is ISABEL. So we recommend it for the small contributions in this range of mass number A.
- For a mass number 140≤A≤186, we recommend to use the ISABEL model.
- For a mass number A>186, we recommend to use the INCL4+ABLA model.

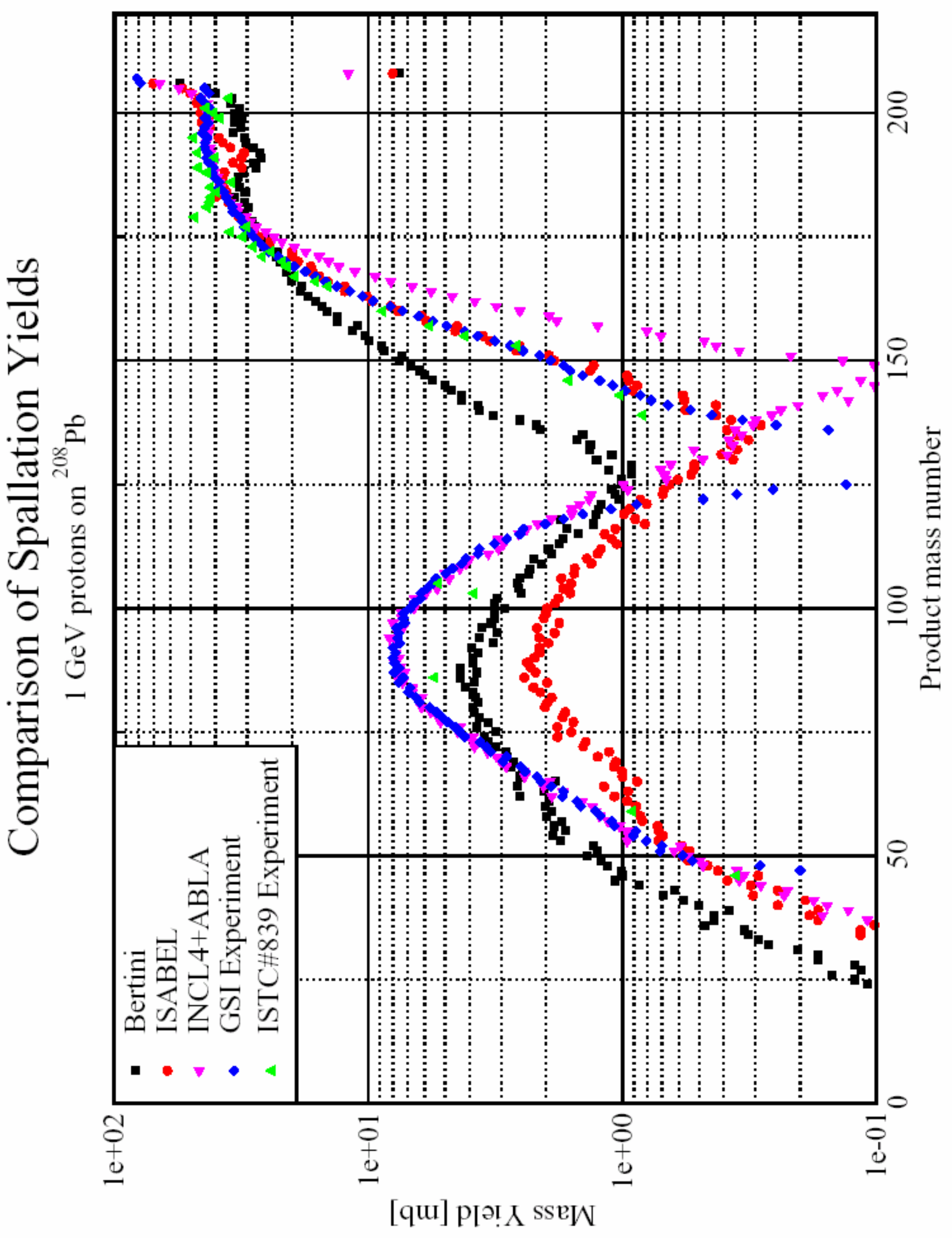

Figure 3-16: *Comparison at 1 GeV proton energy on ^{208}Pb of with MCNPX computed spallation yields (Bertini, ISABEL, INCL4+ABLA models) and experimental spallation yields (GSI [48], ISTC [46]). Mass yields in millibarn [mb] as a function of the mass number A.*

3.5. Evaluation of new experimental data

3.5.1. New available data

We have obtained preleminary experimental data at 600 MeV from Titarenko in the framework of the ISTC project #2002 [49] (See annex B). The independent yields of a reaction product with mass number A and charge number Z is the probability for the nuclide to be produced directly as a reaction proceeds. The cumulative yield is meant the probability for the nuclide to be produced in all the appropriate processes that can lead to its production. The experimental data show on the figures 3-17 and 3-18 are raw data, which has to be analyzed in more detail.

Recently results of 500 MeV experiments with inverse kinematic methods at GSI became available [27, 50]. The fission part [27] and the spallation [50] part are obtained independently.

3.5.2. Thin target experiment at 600 MeV proton energy

The figure 3-17 and 3-18 show us the new experimental data at 600 MeV from ISTC project #2002 [49] compared to the spallation cross sections obtained with MCNPX and the Cugnon code in Stand-alone version by irradiation of a ^{208}Pb target at 600 MeV protons beam energy as a function of the mass number A (see figure 3-17) and as a function of the charge number (see figure 3-18)

One can observe a significant dispersion of the experimental data, especially for the fission part. It can be explained because it is raw data. As already said in the previous section, this experimental data must be evaluated. The next step is to analyze with more detail this data. However, one can observe that the spallation part has a shape near of the shape of the curve obtaine with the simulation codes.

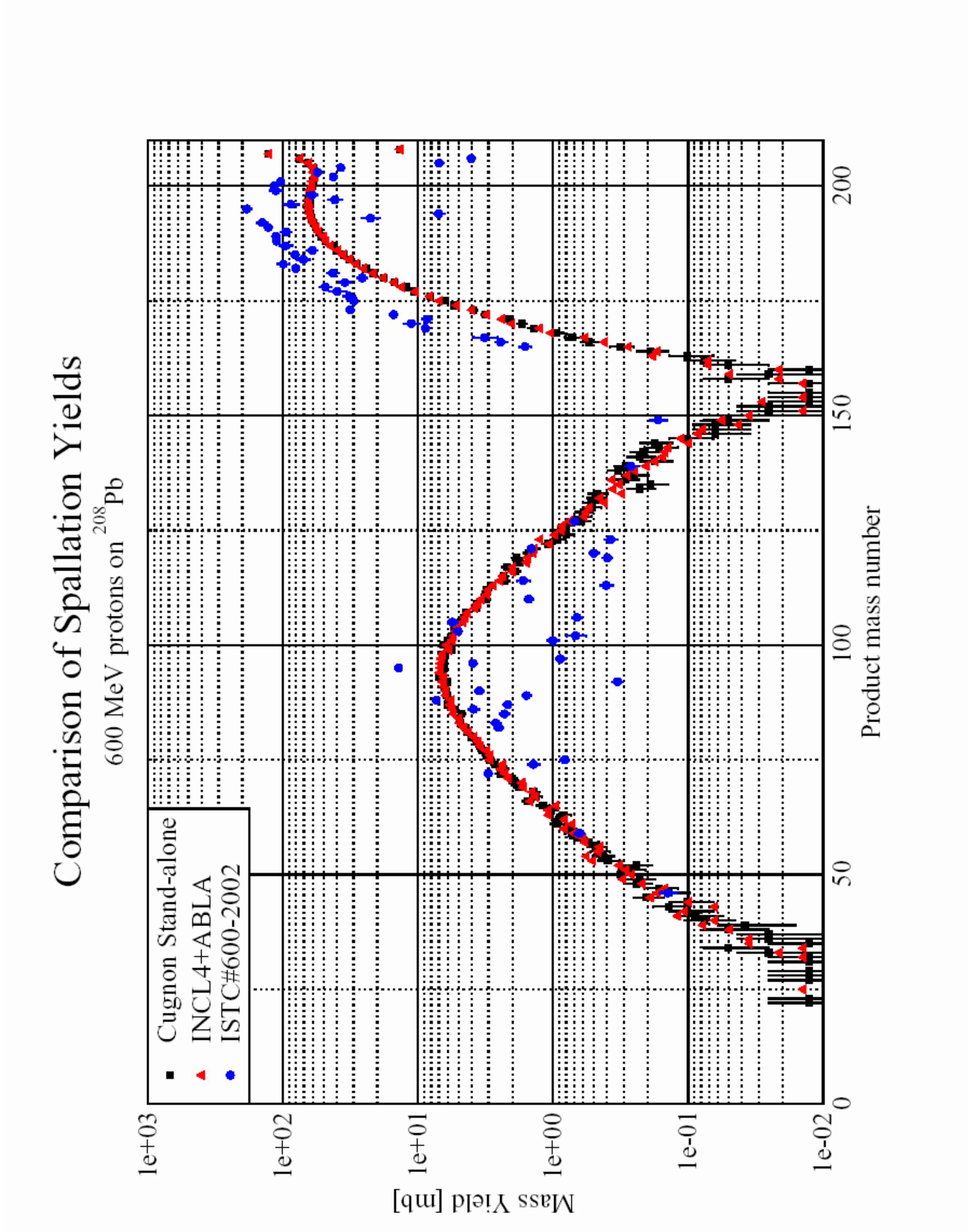

Figure 3-17: *Comparison at 600 MeV proton energy on ^{208}Pb of with MCNPX and the Cugnon code in Stand-alone version computed spallation yields (INCL4+ABLA model) and experimental spallation yields (ISTC [49]). Mass yields in millibarn [mb] as a function of the mass number A.*

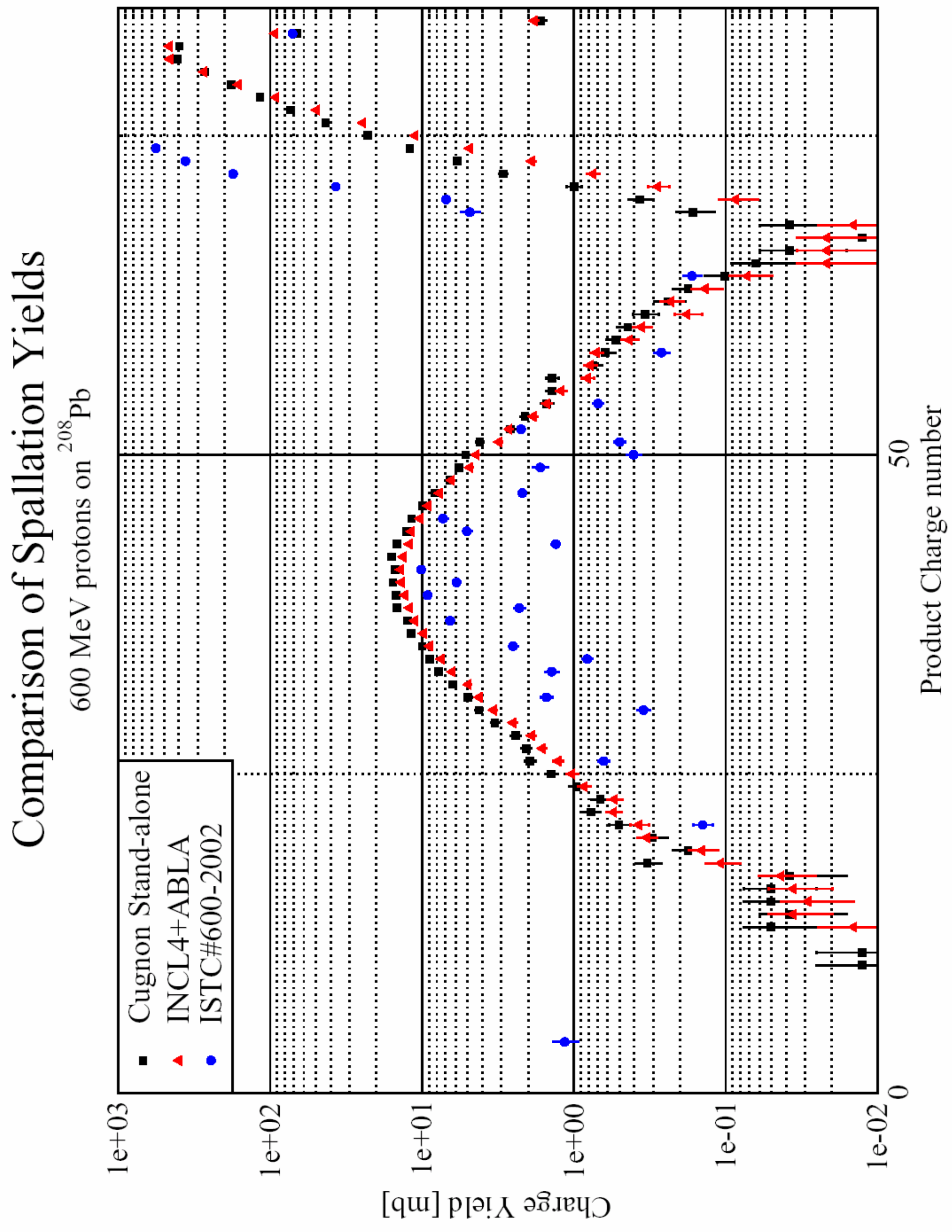

Figure 3-18: *Comparison at 600 MeV protons energy on ^{208}Pb of with MCNPX and the Cugnon code in Stand-alone version computed spallation yields (INCL4+ABLA model) and experimental spallation yields (ISTC [49]). Charge yields in millibarn [mb] as a function of the charge number Z.*

3.5.3. Thin target experiment at 500 MeV proton energy

The figure 3-19 shows us this experimental data at 500 MeV compared with the spallation yields computed at 500 MeV with MCNPX (INCL4+ABLA model) and with the Cugnon code in Stand-alone version.

- Comparison on the spallation part of the curve:

The results of the two simulation codes with the Pauli “strict” option are in very good agreement with the experiments for the spallation part. There is the same hole for a mass number A≤140 as at 1 GeV protons energy.

- Comparison on the fission part of the curve:

For the fission part, one can observe a difference between the experiment and the simulation. But in reference [27], it is explained that there is a problem with this data. Indeed, these values are higher than the experimental results at 1 GeV. In reference [27], this difference is discussed and a correction is proposed which leads to good agreement with our simulations.

The influence of the Pauli blocking at 500 MeV on the spallation yields computed with the Cugnon code in Stand-alone version compared to the experimental data at 500 MeV is shown in figure 3-20. One observes that the red triangle curve corresponding to Pauli strict is in very good agreement with the experimental data. This conclusion is in agreement with the results at 1 GeV where Pauli strict gave also the best agreement with the experimental data from GSI.

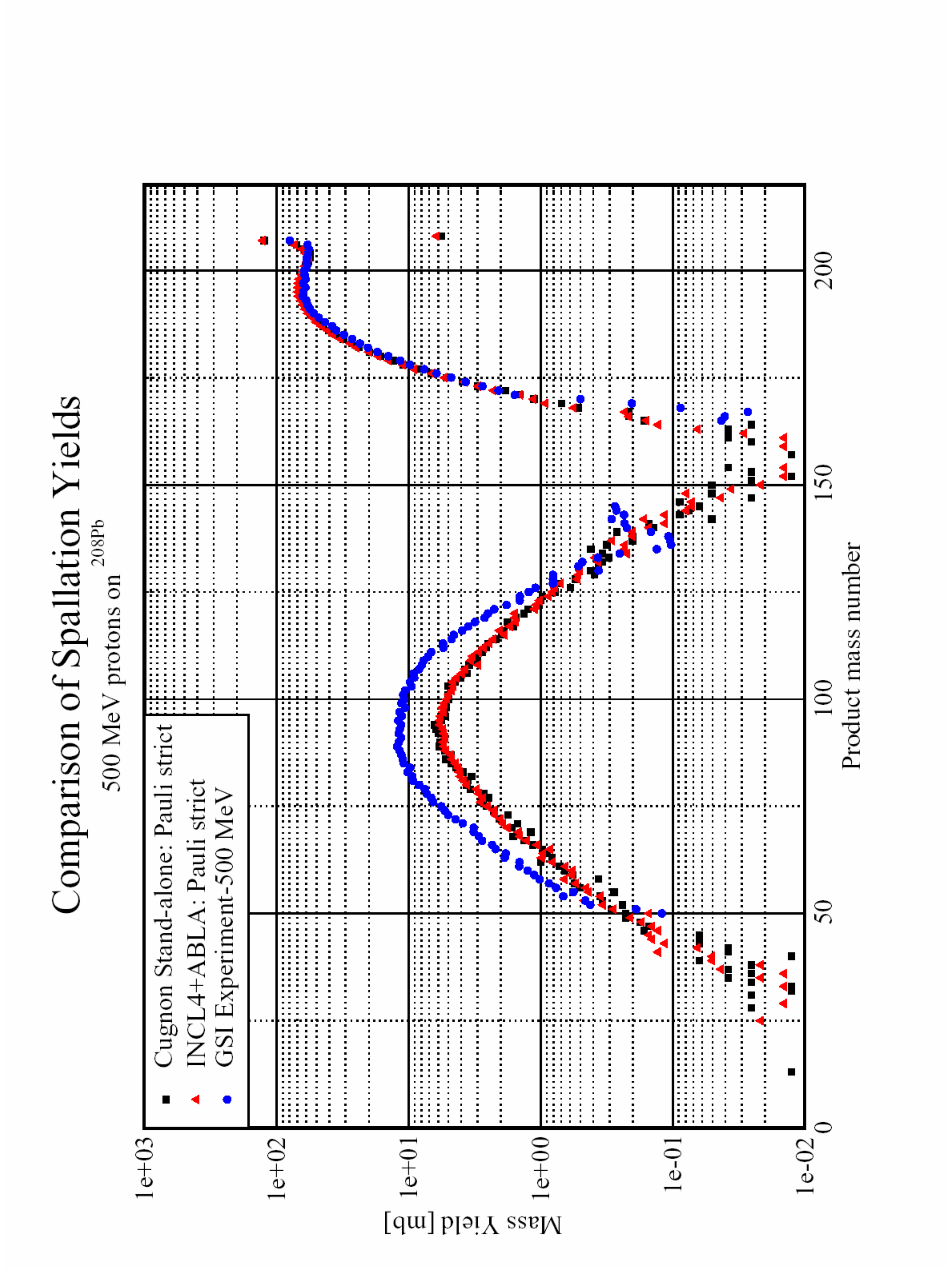

Figure 3-19: *Comparison of with MCNPX (INCL4+ABLA model) (red triangle) and the Cugnon code in Stand-alone version (black square) computed spallation yields at 500 MeV protons energy and experimental spallation yields at 500 MeV (GSI [27, 50]). Mass yields in millibarn [mb] as a function of the mass number A.*

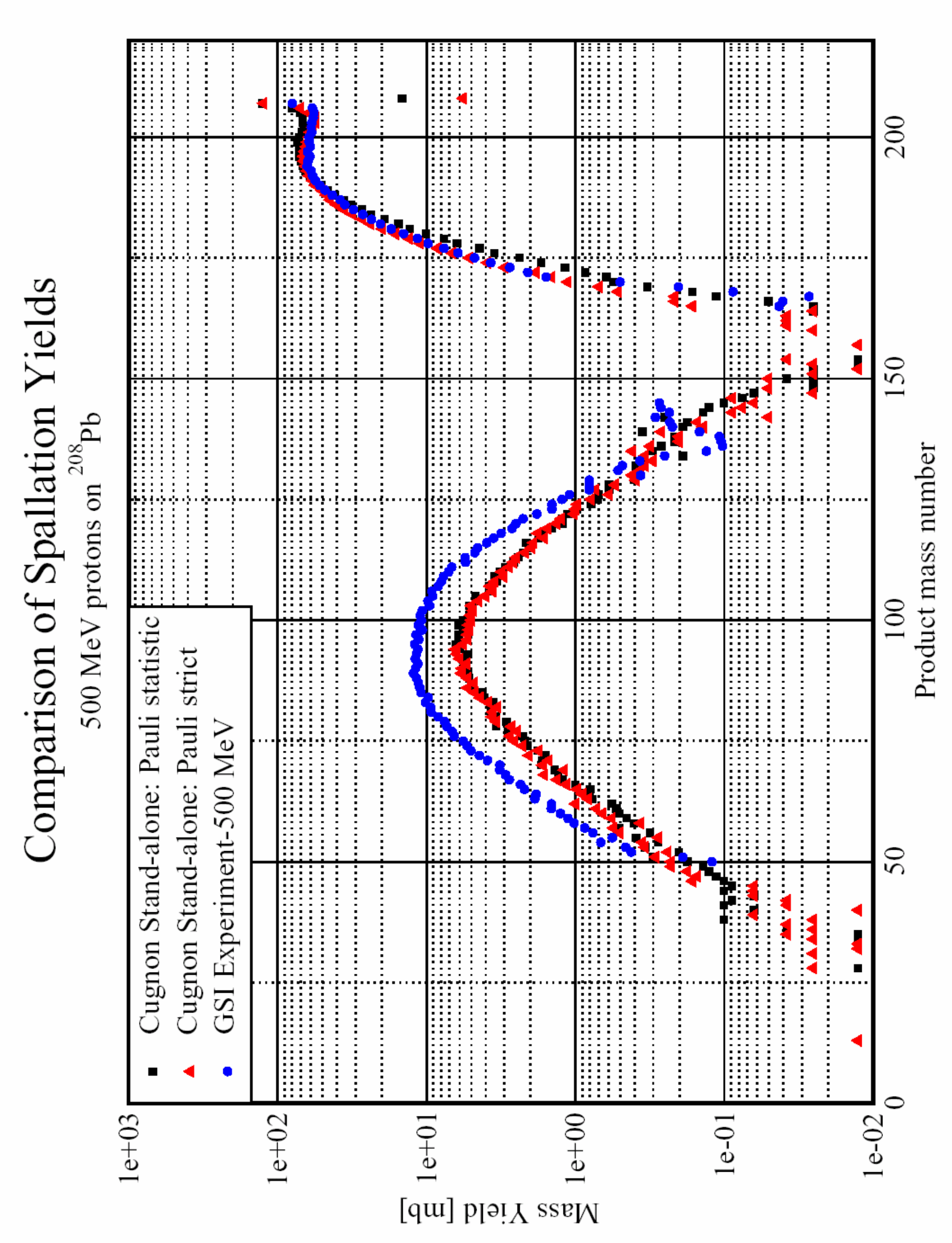

Figure 3-20: *Comparison of with the Cugnon code in Stand-alone version computed spallation yields at 500 MeV protons energy with the Pauli blocking factor set to statistic (black square) and to strict (red triangle) and experimental spallation yields at 500 MeV (GSI [27, ,50]). Mass yields in millibarn [mb] as a function of the mass number A.*

Chapter 4.

LiSoR: A supporting experiment for the MEGAPIE project

4.1. Description of the LiSoR experiment

LiSoR (Liquid metal Solid metal Reaction) is an experimental program, which is supporting the MEGAPIE (1 Megawatt Pilot Experiment) project [1, 10]. The LiSoR experiment simulates the specific MEGAPIE conditions and is a validation step for the MEGAPIE safety assessment and analysis. The purpose is the study of the window damage and the qualification of materials under irradiation and stress and in presence of a flowing molten metal mix (Pb-Bi).

Lead-Bismuth-Eutectic (LBE) is the prime candidate to be applied as target material for MEGAPIE due to the low melting point, low vapor pressure and the satisfactory neutron production efficiency. Yet, the compatibility between LBE and structural materials under irradiation and stress has to be proved.

The figure 4-1, taken from [51], shows the test tube of the LiSoR experiment.

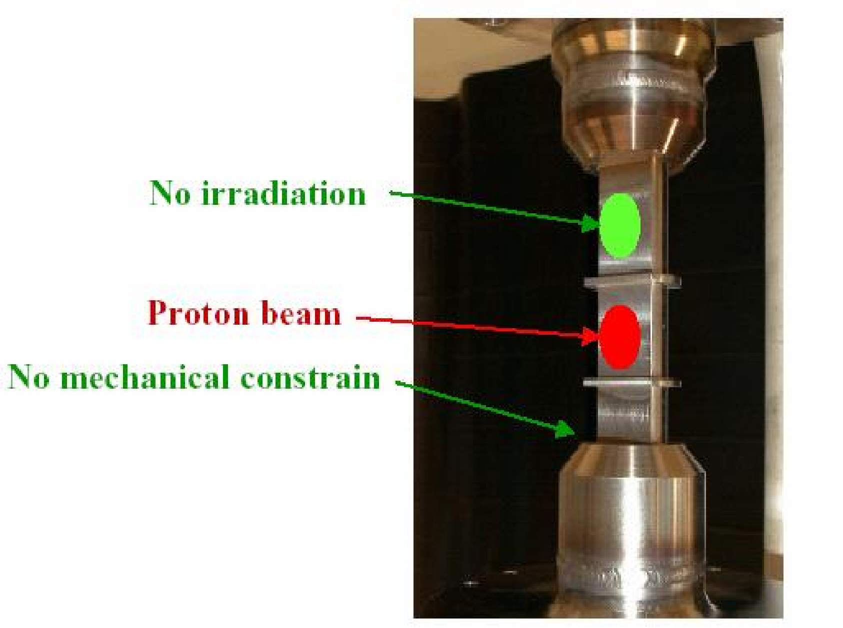

Figure 4-1: *Test tube of the LiSoR experiment.*

4.2. Simulation parameters

4.2.1. The target geometry

The figure 4-2 represents a schema of the test tube and its cross section, taken from [52]. It is the real geometry which is used for the experimental tests. The current version of MCNPX may create the geometry of the tube, but doesn't calculate the volumes of the cells. Thus, it was necessary to add to the input file a volume card ("VOL-Card") which specified our calculated volumes. The calculations of the cell volumes are summarized in annex C and the volume is in the input file for LiSoR given in table 4-1. The table 4-1 gives also the input for the geometry of the test tube and the figure 4-3 shows the visualization obtained with graphics options of MCNPX. The black numbers and the red numbers represent respectively the different surfaces and cells, defined in table 4-1.

The different cells are shown in the figure 4-3 and are defined as following:

Cell 1: The exterior of the sphere.

Cell 2: The interior of the sphere without the tube tested.

Cell 3: The segment into the tube.

Cell 4: The place for the LBE.

Cell 5: The frame of the tube.

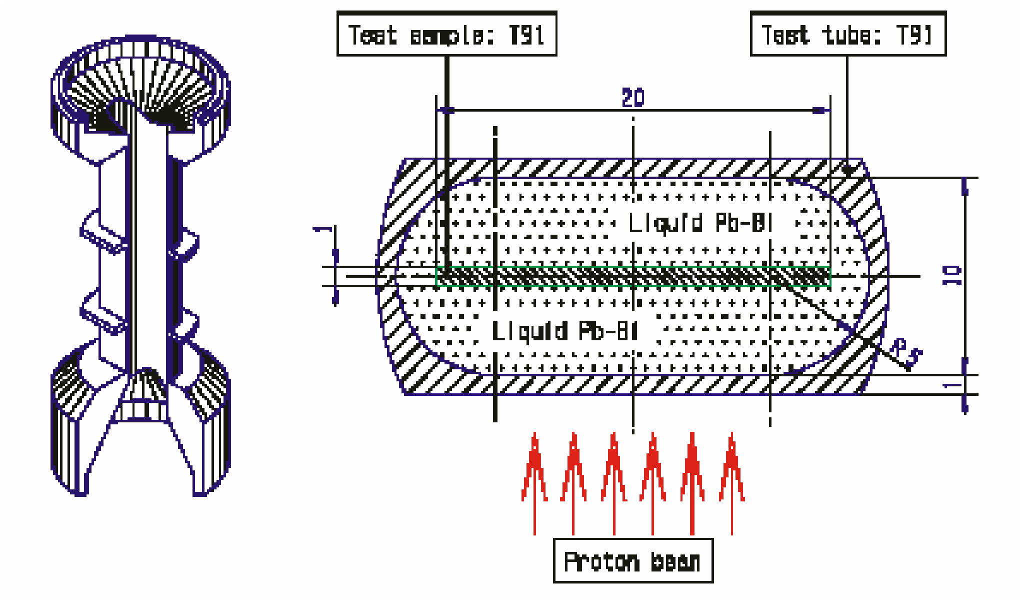

Figure 4-2: *Schema of the LiSoR test tube and its cross section.*

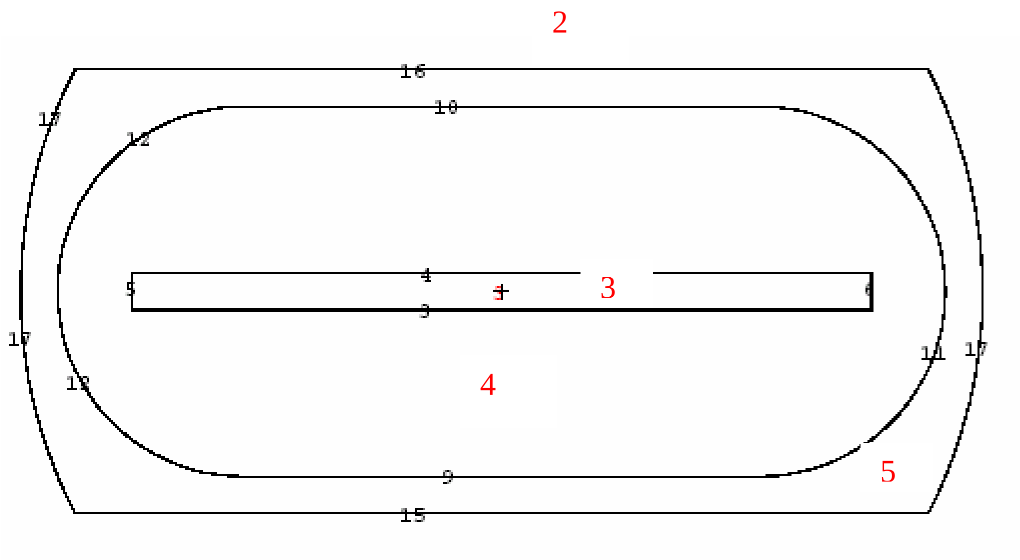

Figure 4-3: *MCNPX real geometry visualization of the LiSoR test tube cross section.*

In the references [9], [53] and [54], a simplified geometry has been developed for the simulation. The cross section is represented in figure 4-4. MCNPX can calculate the volumes of this model.

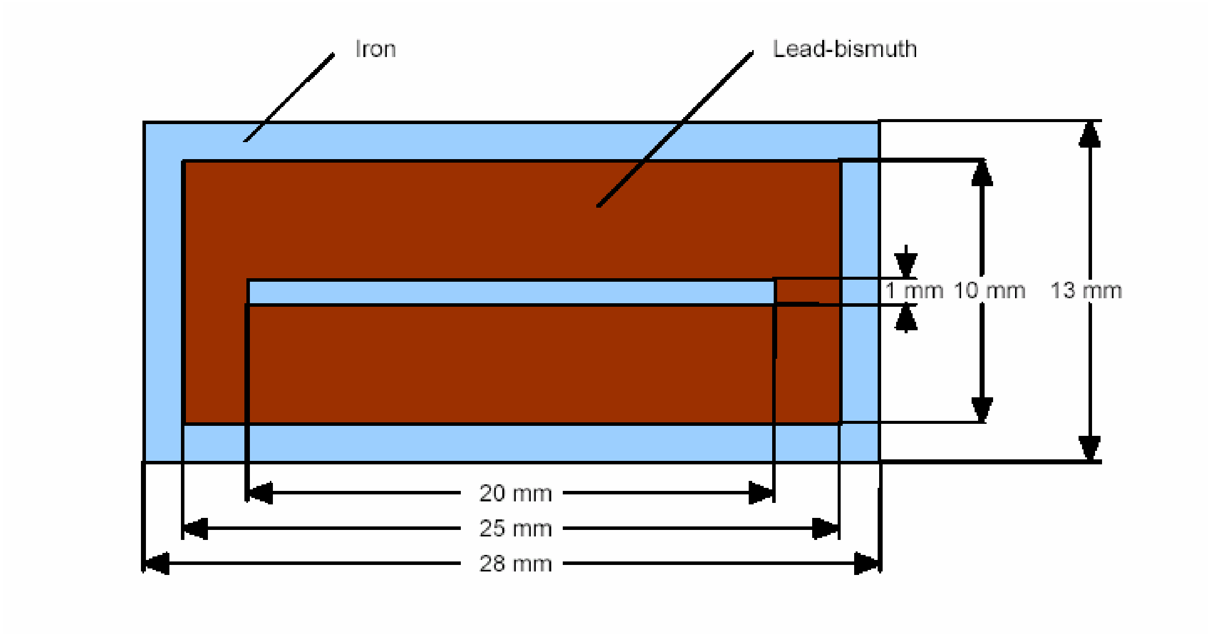

Figure 4-4: *LiSoR test tube cross section of the simplified geometry taken from [53]*.

```
 MCNPX test problem
c ---------------------------------------------------------------
c LISOR
c Production residual nuclei.
c ---------------------------------------------------------------
c Cells
c ---------------------------------------------------------------
 3 2 -7.730      -4 3 -6 5 -8 7
 4 1 -10.4776 (-8 7 -10 9 -14  13  4):
               (-8 7 -10 9 -14  13 -3):
               (-8 7 -10 9 -13 -12  4):
               (-8 7 -10 9 -13 -12 -3):
               (-8 7 -10 9 -13 -12 -4 3 -5):
               (-8 7 -10 9  14 -11  4):
               (-8 7 -10 9  14 -11 -3):
               (-8 7 -10 9  14 -11 -4 3 6)
 5 2 -7.730   (-8 7 -14 13 -16  10):
              (-8 7 -14 13  -9  15):
              (-8 7 -16 15 -13  19 12 -17):
              (-8 7 -16 15 -20  14 11 -17):
              (-8 7 -16 15 -19 -17 12):
              (-8 7 -16 15  20 -17 11)
 2 0          (-2 8):
              (-2 -7):
              (-2 -8 7 16):
              (-2 -8 7 -15):
              (-2 -8 7 -16 15 17)
 1 0          2

c ---------------------------------------------------------------
c Surfaces
c ---------------------------------------------------------------
 2  so  30
 3  pz  -0.05
 4  pz  0.05
 5  px  -1
 6  px  1
 7  py  -20
 8  py  20
 9  pz  -0.5
 10  pz  0.5
 11  c/y  0.7 0 0.5
 12  c/y  -0.7 0 0.5
 13  px  -0.6999
 14  px  0.6999
 15  pz  -0.6
 16  pz  0.6
 17  cy  1.3
 19  px  -1.2
 20  px  1.2

c ---------------------------------------------------------------
c Geometry card
c ---------------------------------------------------------------
 VOL NO 8. 79.42 59.08 112950.84 1000000.
c ---------------------------------------------------------------
```

```
c ---------------------------------------------------------------
c Materials
c ---------------------------------------------------------------
 m1   82206.60c -0.10809
      82207.60c -0.09929
      82208.60c -0.23262
      83209.60c -0.56
 m2   26056.60c -0.89414224
      24052.60c -0.08302175
       6000.60c -0.00100511
      25055.60c -0.0038194
      14000.60c -0.00432196
      42000.60c -0.00954851
      23000.60c -0.00201021
      41093.60c -0.00065332
      15031.60c -0.00017087
      28058.60c -0.00130664
c ---------------------------------------------------------------
c Source
c ---------------------------------------------------------------
 sdef x=d1 y=d2 z=-0.6 erg=72 par=9 dir=0 vec=001
 sp1 -41 0.1883856 0
 sp2 -41 0.1883856 0
c ---------------------------------------------------------------
c Options
c ---------------------------------------------------------------
 imp:n 1 1 1 1 0
 imp:h 1 1 1 1 0
 phys:n 150
 phys:h 150
 mode n h
 histp
 lca   2 1 1 23 1 1 0 1 0
c ---------------------------------------------------------------
c Tallies
c ---------------------------------------------------------------
 FC4 Neutron flux integrated over cell 4 (unit:particles/cm3)
 F4:n 4
c 69 energy group structure from 0 MeV to 10 MeV
 E4  0. 0.010e-6 0.015e-6 0.020e-6 0.025e-6 0.030e-6 0.035e-6
     0.042e-6 0.050e-6 0.058e-6 0.067e-6 0.080e-6 0.100e-6 0.140e-6
     0.180e-6 0.220e-6 0.250e-6 0.280e-6 0.300e-6 0.320e-6 0.350e-6
     0.400e-6 0.500e-6 0.625e-6 0.780e-6 0.850e-6 0.910e-6 0.950e-6
     0.972e-6 0.996e-6 1.020e-6 1.045e-6 1.071e-6 1.097e-6 1.123e-6
     1.150e-6 1.300e-6 1.500e-6 2.100e-6 2.600e-6 3.300e-6 4.000e-6
     9.877e-6 15.968e-6 27.700e-6 48.052e-6 75.5014e-6 148.728e-6
     367.262e-6 906.898e-6 1425.1e-6 2239.45e-6 3519.1e-6 5530.e-6
     0.009118 0.01503 0.02478 0.04085 0.06734
     0.111 0.183 0.3025 0.500 0.821 1.353 2.231 3.679 6.0655 150.
  FQ4 f e
c ---------------------------------------------------------------
 print 128
 nps 5000000
 prdmp 2j -1
```

Table 4-1: *MCNPX input file for LiSoR calculations with the real geometry of the test tube.*

The martensitic stainless steel T91 is envisaged as window material in the MEGAPIE project through which the proton beam impinges onto the target.

The structure is made up of a rectangular steel pipe, a steel segment at the pipe center and a loop of about 25 liters of liquid Lead-Bismuth eutectic. The steel used for the pipe and for the segment is steel T91 and the composition is summarized in table 4-2. The liquid Lead-Bismuth eutectic is composed of 44% lead and 56% bismuth by weight. The lead has itself an isotopic composition shown in table 4-3 and the bismuth is pure ^{209}Bi. According to [54] the lead is composed of following isotopes: ^{204}Pb, ^{206}Pb, ^{207}Pb and ^{208}Pb. Because MCNPX does not supply a neutron cross section library for the ^{204}Pb, the fraction of ^{204}Pb is distributed on the three other isotopes.

Fe-26	Cr-24	C-6	Mn-55	Si-14	Mo-42	V-23	Nb-41	P-15	Ni-28
89,41%	8,30%	0,10%	0,38%	0,43%	0,95%	0,20%	0,07%	0,02%	0,13%

Table 4-2: *Steel T91 composition in weight percentage, taken from [9]*.

BISMUTH	LEAD		
Bi-209	Pb-206	Pb-207	Pb-208
56,00%	10,81%	9,93%	23,26%

Table 4-3: *Coolant composition in weight percentage, taken from [54]*.

This real geometry will be noted RG thereafter, and the simpler geometry SG.

4.2.2. Beam parameters

The parameters of the proton beam are summarized in the table 4-4.

Parameter	Value
Incident beam energy on target	72 MeV
Maximal beam current	50 mA
Maximal current density	$\approx 2.5\ mA/cm^2$
Beam profile on target (Gaussian)	$s_x = s_y = 0.8\ mm$

Table 4-4: *Beam parameters for the LiSoR irradiation experiment.*

4.3. Preliminary calculations

4.3.1. The Polonium issue

The Polonium is an element produced by the capture of a neutron in a nuclei of ^{209}Bi and subsequent β-decay. The results of these investigations are important for the estimation of the radiotoxicity induced by the Polonium in the Lead-Bismuth targets of ADS systems [55].
Indeed, the ^{210}Po is an α-transmitter of fairly short half life (138 days) and is quite volatile. These two characteristics make it one of the most dangerous elements.

4.3.2. Production of Polonium isotopes in the LBE eutectic

The simulation in reference [53] was performed with the LAHET code [34] applied with the Bertini model and five million proton cascades were started. Thus, all our calculations are realized with the Bertini model and with five million proton cascades.
The Polonium production rates in lead-bismuth and the induced activity due to α-decay per coulomb are shown in Table 4-5. Polonium isotopes with atomic number between 203 and 209 were found.

4.3.2.1. Remarks on the applied units

The Gram-Atom is the quantity of an element whose weight in grams is numerically equal to the atomic weight of the element. Thus, it is proportional to the mass of the atom

corresponding and the factor of proportionality is the number of Avogadro N_A. For example, 1 Gram-Atom of Carbon 12 will be 12 Grams of pure Carbon 12.
The mole is the unit of quantity of material equivalent to the sum of the Gram-Atom of the elements composing it.
The Coulomb is a unit of electrical charge equal to the amount of charge transferred by a current of 1 ampere in 1 second
The Becquerel is the standard international unit of radioactive decay and it is represented as one disintegration per second.

The units utilised by the PSI in [9] and [52] are:

- $\left[\frac{Atoms}{Coulomb}\right]$ for the initial production rate.
- $\left[\frac{Gram.Atom}{liter}\right]$ for the intermediate production rate utilised for the calculation related to the decay of the Polonium isotopes.
- $\left[\frac{Becquerel}{Coulomb}\right]$ and $[Bq]$ for the α-activity.

The production rates come from the file opt8a generated by MCNPX and HTAPE3X. The program CRORINP changes the units and creates an adapted file for ORIHET3. For the later use of the small auxilliary program CRORINP (see figure 5-3), it is important to note that the average beam current is an intern constant in this program and that it is necessary to change it within an application for MEGAPIE or LiSoR as example.

4.3.2.2. Calculation of radioactivity

The first step will be to show how to calculate the induced α-activity at the end of the irradiation. It can be written as:

$$A_a = l \times K_a \times PR_0 \tag{4.1}$$

where A_a is the α-activity in $\left[\frac{Becquerel}{Coulomb}\right]$.

l is the decay constants in $\left[s^{-1}\right]$.

PR_0 is the initial production rate in $\left[\frac{Atoms}{Coulomb}\right]$.

K_a is the branching ratio for the α-activity in $[\%]$.

The values of this branching ratio for the α-activity are taken from [56]

The decay constants l are calculated as following:

$$l = \frac{\ln(2)}{T_{1/2}} \tag{4.2}$$

where $T_{1/2}$ is the half-life in $[s]$.
The next step is to show how to calculate the decay of the nuclei.
The time dependent evolution of the number of unstable nuclei can be written as:

$$N(t) = N_0 e^{-lt} \tag{4.3}$$

where N_0 is the number of atoms of unstable nuclei existing at the end of the irradiation.

The number of decay corresponding to the production rate is:

$$D(t) = N_0 - N(t) = N_0\left(1 - e^{-lt}\right) \tag{4.4}$$

where $D(t)$ is the number of atoms of unstable nuclei at the time t after the end of the irradiation.

The following formula allows calculating the production rate in $\left[\frac{Gram.Atom}{liter}\right]$ at different times after the end of the irradiation, taken into account the appropriate dimension conversions, to compare directly with the results of [53]:

$$PR(t) = \frac{I}{N_A \times l \times V} PR_0 \times \left(1 - e^{(-lt)}\right) \tag{4.5}$$

where $PR(t)$ is the production rate at the time t in $\left[\frac{Gram.Atom}{liter}\right]$.

PR_0 is the initial production rate in $\left[\frac{Atoms}{Coulomb}\right]$.

$I = 50\ mA = 50.10^{-6}\ A$ is the average beam current during the irradiation.

$N_A = 6.022.10^{23}\ \frac{Atoms}{Gram.Atom}$ is the Avogadro’s number.

$V = 25\ l$ is the volume of eutectic of the LiSoR experiment.

Moreover:

$$A_a(t) = PR(t) \times l \times V \times K_a \times N_A \tag{4.6}$$

Thus, with the formulas (4.5) and (4.6) we can calculate the time dependent α-activity after the end of the irradiation as a function of the initial production rates PR_0:

$$A_a(t) = K_a \times I \times PR_0 \times \left(1 - e^{(-l\,t)}\right) \tag{4.7}$$

where $A_a(t)$ is the α-activity at the time t in $[Bq]$.

To obtain the total activity, the following formula can be applied:

$$A_T = \frac{A_a}{K_a} \tag{4.8}$$

where A_T is the total activity in $[Bq]$.

4.3.2.3. Comparison of formula (4.7) with results of ORIHET3

The production rate calculation was performed with the ORIHET3 program [13]. The sequence of the operations to obtain the output files *.dec and *.bup are shown in figure 5-3. As it is explained in [13] and [23], ORIHET3 solves the Bateman equations in order to calculate the time dependent concentrations of the nuclides. The differences between the results obtained with the theoretical formula (4.6) of the previous section with those of ORIHET3 are given in table 4-5. We can observe that the differences are very small.

	α-Activity [Becq]								
	1 month			3 months			6 months		
Nuclides	Theory Formula (4.7)	ORIHET3	Difference	Theory Formula (4.7)	ORIHET3	Difference	Theory Formula (4.7)	ORIHET3	Difference
Po-203	6,95E+07	6,96E+07	0,14%	6,95E+07	6,96E+07	0,14%	6,95E+07	6,96E+07	0,14%
Po-204	4,23E+09	4,22E+09	0,22%	4,23E+09	4,22E+09	0,22%	4,23E+09	4,22E+09	0,22%
Po-205	3,81E+08	3,81E+08	0,03%	3,81E+08	3,81E+08	0,03%	3,81E+08	3,81E+08	0,03%
Po-206	4,35E+10	4,37E+10	0,26%	4,78E+10	4,77E+10	0,24%	4,79E+10	4,77E+10	0,31%
Po-207	1,68E+08	1,76E+08	4,96%	1,68E+08	1,76E+08	4,96%	1,68E+08	1,76E+08	4,96%
Po-208	1,52E+10	1,52E+10	0,12%	4,47E+10	4,48E+10	0,23%	8,67E+10	8,66E+10	0,18%
Po-209	4,30E+07	4,29E+07	0,16%	1,29E+08	1,29E+08	0,10%	2,58E+08	2,58E+08	0,02%

Table 4-5: *Alpha-activity of the polonium isotopes after continuous irradiation at 50 μA.*

The following calculations include two parts. The first part treats the study of the production rates (see tables 4-6 and 4-7) and of the α-activity directly after the irradiation and the second part is related to the decay of isotopes after one, three and six months (see table 4-9).

4.3.2.4. Polonium production rates and induced activity

		LAHET		FLUKA		MCNPX real geometry			MCNPX simpler geometry		
Nuclides	Half-lifes [seconds]	Production rate [atoms/Clb]	Production rate [gr atoms/s]	Production rate [atoms/Clb]	Production rate [gr atoms/s]	Production rate [atoms/Clb]	Production rate [gr atoms/s]	error	Production rate [atoms/Clb]	Production rate [gr atoms/s]	error
Po-203	2,088E+03	1,561E+15	1,296E-13	1,475E+15	1,225E-13	2,501E+15	2,077E-13	37,6%	1,263E+15	1,0487E-13	23,6%
Po-204	1,271E+04	1,330E+16	1,104E-12	1,203E+16	9,988E-13	1,504E+16	1,249E-12	11,6%	1,281E+16	1,0636E-12	3,8%
Po-205	6,480E+03	1,630E+16	1,353E-12	2,175E+16	1,806E-12	1,886E+16	1,566E-12	13,6%	1,905E+16	1,5817E-12	14,4%
Po-206	7,603E+05	1,146E+16	9,515E-13	1,682E+16	1,397E-12	1,783E+16	1,480E-12	35,7%	1,757E+16	1,4588E-12	34,8%
Po-207	2,010E+03	9,768E+15	8,110E-13	1,342E+16	1,114E-12	1,958E+16	1,626E-12	50,1%	1,678E+16	1,3932E-12	41,8%
Po-208	9,139E+07	8,628E+15	7,164E-13	1,458E+16	1,211E-12	1,608E+16	1,335E-12	46,3%	1,535E+16	1,2745E-12	43,8%
Po-209	3,217E+09	1,692E+15	1,405E-13	2,925E+15	2,429E-13	1,488E+15	1,235E-13	13,7%	1,522E+15	1,2637E-13	11,2%

Table 4-6: *Production rates of Polonium isotopes just after irradiation and cooling time of zero.*

			LAHET	FLUKA	MCNPX real geometry		MCNPX simpler geometry	
Nuclides	Decay constant λ	Branching ratio percent α-decays	Induced α-Activity [Becq/Clb]	Induced α-Activity [Becq/Clb]	Induced α-Activity [Becq/Clb]	error	Induced α-Activity [Becq/Clb]	error
Po-203	3,320E-04	0,11%	5,700E+08	5,386E+08	9,133E+08	37,6%	4,612E+08	23,6%
Po-204	5,454E-05	0,66%	4,787E+09	4,330E+09	5,413E+09	11,6%	4,611E+09	3,8%
Po-205	1,070E-04	0,04%	6,974E+08	9,306E+08	8,070E+08	13,6%	8,151E+08	14,4%
Po-206	9,117E-07	5,45%	5,694E+08	8,357E+08	8,859E+08	35,7%	8,730E+08	34,8%
Po-207	3,448E-04	0,02%	6,737E+08	9,256E+08	1,350E+09	50,1%	1,157E+09	41,8%
Po-208	7,584E-09	100,00%	6,544E+07	1,106E+08	1,220E+08	46,3%	1,164E+08	43,8%
Po-209	2,155E-10	99,52%	3,628E+05	6,272E+05	3,191E+05	13,7%	3,264E+05	11,2%

Table 4-7: *Alpha activities of Polonium isotopes just after irradiation and cooling time of zero.*

The branching ratios are not the same in the references [53] and [54] (see table 4-8). The branching ratios from [53] are taken from [56] and we will use this data for our calculations.

Branching ratio percent α-decays	
Taken from [53]	Taken from [54]
0,02%	0,11%
0,60%	0,66%
0,07%	0,04%
5,00%	5,45%
0,00%	0,02%
99,97%	100,00%
99,98%	99,52%

Table 4-8: *Branching ratio for the α-decays in percent used in references [53] and [54].*

4.3.2.5. Build-up of Polonium concentration and activity

The evolution in time of the concentrations in $\left[\frac{Gram.Atom}{liter}\right]$ of the Polonium isotopes was obtained assuming a continuous proton beam of $50\ mA$, and applying the formula (4.5).

The table 4-9 shows us the concentration of the different Polonium isotopes calculated with LAHET, FLUKA and MCNPX at three different times: after one, three and six months. The differences are caculated compared with the LAHET values. We show here only the results obtained for the simplified geometry because the calculations from [51] were performed with the simplified geometry and the differences are small. However, the data for the real geometry are supplied in annex D. We can observe that this difference can be up to 43.8% for the Polonium 208 and to 41.8% for the Polonium 207. But for the other isotopes, the difference is acceptable. One can notice that the differences are smaller with the simplified geometry than with the real geometry. It is in agreement with the calculation conditions of the LAHET values. We can observe that the two isotopes ^{208}Po and ^{209}Po have more important activities than the other Polonium isotopes. It is due to the longer half-lifes of the ^{208}Po and ^{209}Po.

	LAHET-1 month		FLUKA-1 month		MCNPX (Simplified geometry)-1 month		
Nuclides	α-Activity [Becq]	Production rate [gr.atoms/liter eutectic]	α-Activity [Becq]	Production rate [gr.atoms/liter eutectic]	α-Activity [Becq]	Production rate [gr.atoms/liter eutectic]	Difference
Po-203	8,586E+07	1,562E-11	8,113E+07	1,476E-11	6,947E+07	1,264E-11	23,6%
Po-204	4,389E+09	8,100E-10	3,970E+09	7,326E-10	4,227E+09	7,801E-10	3,8%
Po-205	3,260E+08	5,061E-10	4,350E+08	6,753E-10	3,810E+08	5,915E-10	14,4%
Po-206	2,840E+10	3,797E-08	4,169E+10	5,573E-08	4,355E+10	5,821E-08	34,8%
Po-207	9,768E+07	9,407E-11	1,342E+08	1,292E-10	1,678E+08	1,616E-10	41,8%
Po-208	8,537E+09	7,476E-08	1,443E+10	1,263E-07	1,519E+10	1,330E-07	43,8%
Po-209	4,779E+07	1,480E-08	8,262E+07	2,559E-08	4,299E+07	1,332E-08	11,2%

	LAHET-3 months		FLUKA-3 months		MCNPX (Simplified geometry)-3 months		
Nuclides	α-Activity [Becq]	Production rate [gr.atoms/liter eutectic]	α-Activity [Becq]	Production rate [gr.atoms/liter eutectic]	α-Activity [Becq]	Production rate [gr.atoms/liter eutectic]	Difference
Po-203	8,586E+07	1,562E-11	8,113E+07	1,476E-11	6,947E+07	1,264E-11	23,6%
Po-204	4,389E+09	8,100E-10	3,970E+09	7,326E-10	4,227E+09	7,801E-10	3,8%
Po-205	3,260E+08	5,061E-10	4,350E+08	6,753E-10	3,810E+08	5,915E-10	14,4%
Po-206	3,121E+10	4,172E-08	4,580E+10	6,123E-08	4,784E+10	6,396E-08	34,8%
Po-207	9,768E+07	9,407E-11	1,342E+08	1,292E-10	1,678E+08	1,616E-10	41,8%
Po-208	2,511E+10	2,199E-07	4,243E+10	3,716E-07	4,467E+10	3,912E-07	43,8%
Po-209	1,433E+08	4,439E-08	2,477E+08	7,673E-08	1,289E+08	3,993E-08	11,2%

	LAHET-6 months		FLUKA-6 months		MCNPX (Simplified geometry)-6 months		
Nuclides	α-Activity [Becq]	Production rate [gr.atoms/liter eutectic]	α-Activity [Becq]	Production rate [gr.atoms/liter eutectic]	α-Activity [Becq]	Production rate [gr.atoms/liter eutectic]	Difference
Po-203	8,586E+07	1,562E-11	8,113E+07	1,476E-11	6,947E+07	1,264E-11	23,6%
Po-204	4,389E+09	8,100E-10	3,970E+09	7,326E-10	4,227E+09	7,801E-10	3,8%
Po-205	3,260E+08	5,061E-10	4,350E+08	6,753E-10	3,810E+08	5,915E-10	14,4%
Po-206	3,123E+10	4,175E-08	4,583E+10	6,127E-08	4,788E+10	6,401E-08	34,8%
Po-207	9,768E+07	9,407E-11	1,342E+08	1,292E-10	1,678E+08	1,616E-10	41,8%
Po-208	4,875E+10	4,270E-07	8,238E+10	7,215E-07	8,673E+10	7,596E-07	43,8%
Po-209	2,863E+08	8,870E-08	4,950E+08	1,533E-07	2,576E+08	7,979E-08	11,2%

Table 4-9: *Concentrations and alpha-activities of Polonium isotopes after continuous irradiation.*

4.4. Calculations related to the LiSoR experimental results

The experimental data [57] are measured in the spallation neutron facility SINQ at PSI [58, 59].

	Total activity [Bq]					
Nuclides	LAHET	FLUKA Simplier geometry	FLUKA real geometry	MCNPX Simpler geometry	MCNPX real geometry	Experiment PSI
Po-203	7,805E+10	7,375E+10	2,30E+11	6,315E+10	1,251E+11	
Po-204	6,642E+11	6,007E+11	9,90E+11	6,397E+11	7,511E+11	
Po-205	8,150E+11	1,087E+12	1,10E+12	9,525E+11	9,430E+11	
Po-206	6,050E+10	8,880E+10	9,10E+10	9,276E+10	9,413E+10	1,87E+11
Po-207	4,884E+11	6,710E+11	7,90E+11	8,390E+11	9,790E+11	
Po-208	4,003E+08	6,764E+08	5,90E+08	7,122E+08	7,460E+08	9,02E+08
Po-209	2,231E+06	3,857E+06		2,007E+06	1,962E+06	
Po-206/Po-208	1,511E+02	1,313E+02	1,54E+02	1,302E+02	1,262E+02	2,07E+02

Table 4-10: *Total activity of the Polonium isotopes for several simulations codes and for the experiment.*

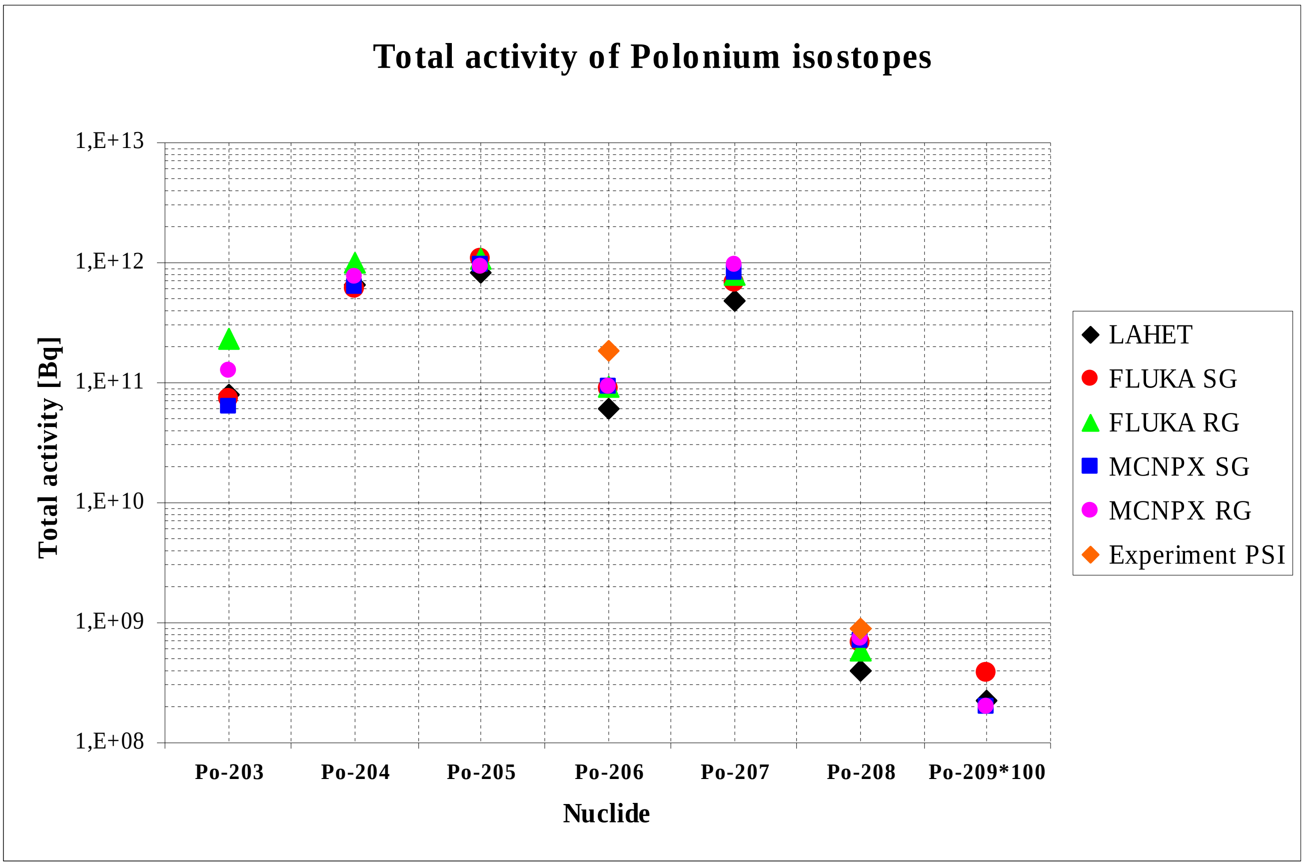

Figure 4-5: *Comparison of the total activity of the Polonium isotopes directly after 34 hours irradiation.*

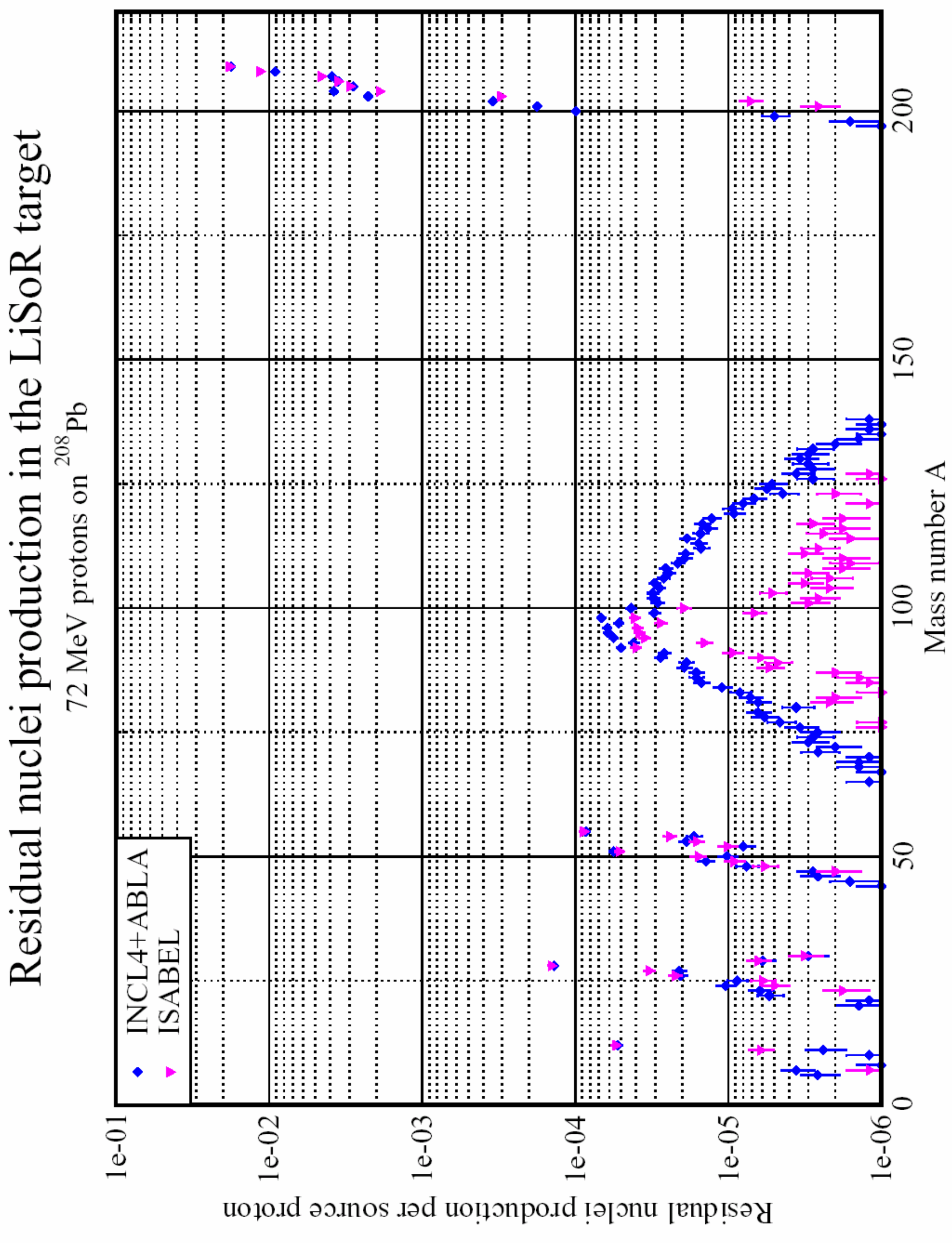

Figure 4-6: *Residual nuclei production in the LiSoR as a function of the mass number A.*

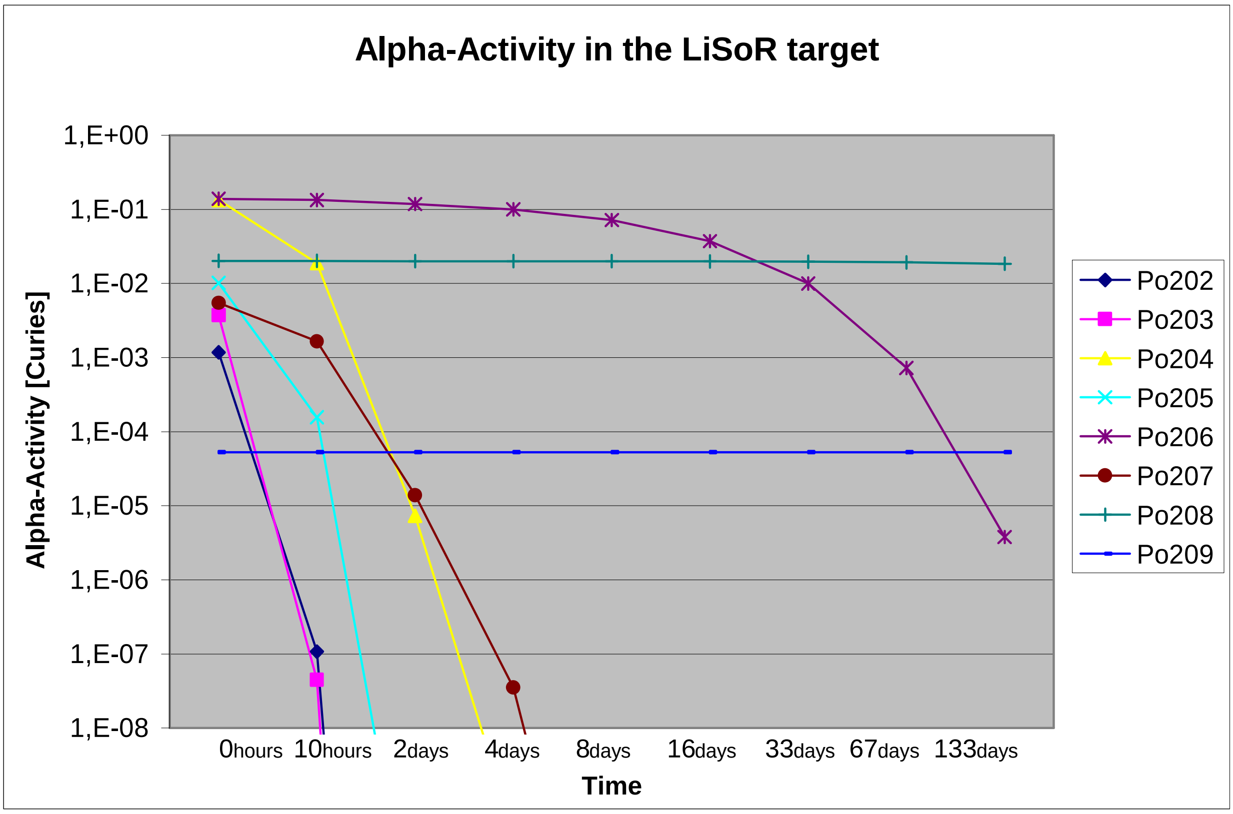

Figure 4-7: *Time dependence of the alpha-activity for the polonium isotopes. Alpha-activity in Curies [Ci] as a function of the time.*

The data of table 4-10 are shown in figure 4-5. It represents the total activity of the Polonium isotopes after 34 hours irradiation according to the conditions of the LiSoR experiment. One can observe a relativ good agreement between the different simulation codes and with the experimental data. The simulationed results underestimate the experimental data up to 42% for the ^{209} Po, 18% for the ^{208}Po and 50% for the ^{206}Po. But there are very few experimental data in order to obtain conclusive results.

The figure 4-6 shows the total residual nuclei production per source proton as a function of the mass number for the real geometry of the LiSoR test tube. One can observe that the spallation part of the curve increase to a very high point in comparison of the fission part. This difference is explained by the very low energy proton beam (72 MeV).

Figure 4-7 shows the decay of the Polonium isotopes after 34 hours irradiation at $50\ mA$. One can observe that the isotopes 202, 203, 204, 205, 206 and 207 are disappeared after a few days. The two isotopes 208 and 209 have a longer half-life and that´s why their decay is very long.

Chapter 5.

Comparison KAPROS/ORIHET3

5.1. KAPROS

5.1.1. Theory

The burn-up equations are described in [11] and are solved with the program BURNUP [12].

With the burn-up code one investigates the time dependent change of the atomic density of a nuclide N. Changes result from the depletion and the production.
The production of a nuclide may occur through the following ways:

- Decay other nuclides.
- Neutron capture (to which here also (n, 2n) - and (n, 3n) - reaction is counted) of other nuclides.
- Creation of fission products by fission.

The reduction of the isotope number density of a nuclide can take place via the following reactions:

- Decay of this nuclides.
- Neutron capture (to which here also (n, 2n) - and (n, 3n) - reactions are counted) of this nuclide.
- Fission.

The time dependence of the nuclide density described by the balance of production and loss rates for each individual nuclide is shown in the following formula:

$$\frac{dN_i}{dt} = \sum_{j=1}^{M} l_{i,j}\, l_j N_j + \overline{\Phi} \sum_{k=1}^{M} f_{i,k}\, s_k N_k - \left(l_i + \overline{\Phi} s_i \right) N_i \tag{5.1}$$

where

N_i Atom density of the isotope I, unit: [particles/cm^3].

λ_i Disintegration constant of the isotope I, unit: [1/s].

σ_i Spectrum-weighted one-group absorption cross sections of the isotope I, unit:[10^{-24}cm^2]=[barn].

$l_{i,j}$ Fraction of the decay of the isotope j, leading to I, unit: nondimensional $0< l_{i,j}<1$.

$f_{i,k}$ Fraction of the absorption of the isotope k, leading to I, unit: nondimensional $0< f_{i,j}<1$.

$\overline{\Phi}$ Mean (spatial, energy and time averaged) absolute neutron flux density, unit: [neutrons/cm^2*s].

M Number of treated isotopes.

The above equation applies to each nuclide i=1,…M. Moreover, the mean absolute neutron flux density $\overline{\Phi}$ is supposed to be constant on an considered interval of time. That´s why the equation can be treated as homogeneous differential equation system. One can write the M coupled differential equations as:

$$\left[\frac{dN}{dt}\right] = [A][N] \tag{5.3}$$

where

$\left[\frac{dN}{dt}\right]$: Vector (length M) of nuclide density.

$[A]$: (M, M)-Matrix containing the decay and production coefficient.

The program treats the following radioactive processes of decomposition:

- Emission of a positron, in which case the produced nuclide remains in the basic state and/or in with isomers a state.
- Transition isomers from the state in the basic state.
- Emission of a alpha particle, α -decay.
- Emission of negatrons, in which case the produced nuclide remains in the basic state and/or in with isomers a state, β-decay.
- Emission of delayed neutrons (only for fission products).
- Spontaneous fission (only for actinides).

The program treats the following neutron reactions:

- (n, α) reaction (light elements, actinides, fission products).
- (n, p) reaction (light elements, actinides, fission products).
- (n, γ) reaction to the initial state and to isomer state.(light elements, actinides, fission products).
- (n, 2n) reaktion to the initial state and to isomers state.(light elements, actinides).
- (n, 3n) reaktion (actinides).
- Fission (actinides).

At the time of the decomposition of actinides, the formation of the fission products is treated only for one limited number (currently the maximum is 5) of actinides in the program. It depends also on the considered reactor type (NLIBE=1,2,3,4).

The library is a reformatted KORIGEN [60] library.

The BURNUP modul is developed from the Oak Ridge Code ORIGEN [61]. That's why the method for the numerical solution is the same.

The transition matrix is built from the data of three specific libraries. The first contains the data for decay and activation for light elements, the second data for actinides and the third data for fission products

5.1.2. Flowchart for KAPROS burn up calculations

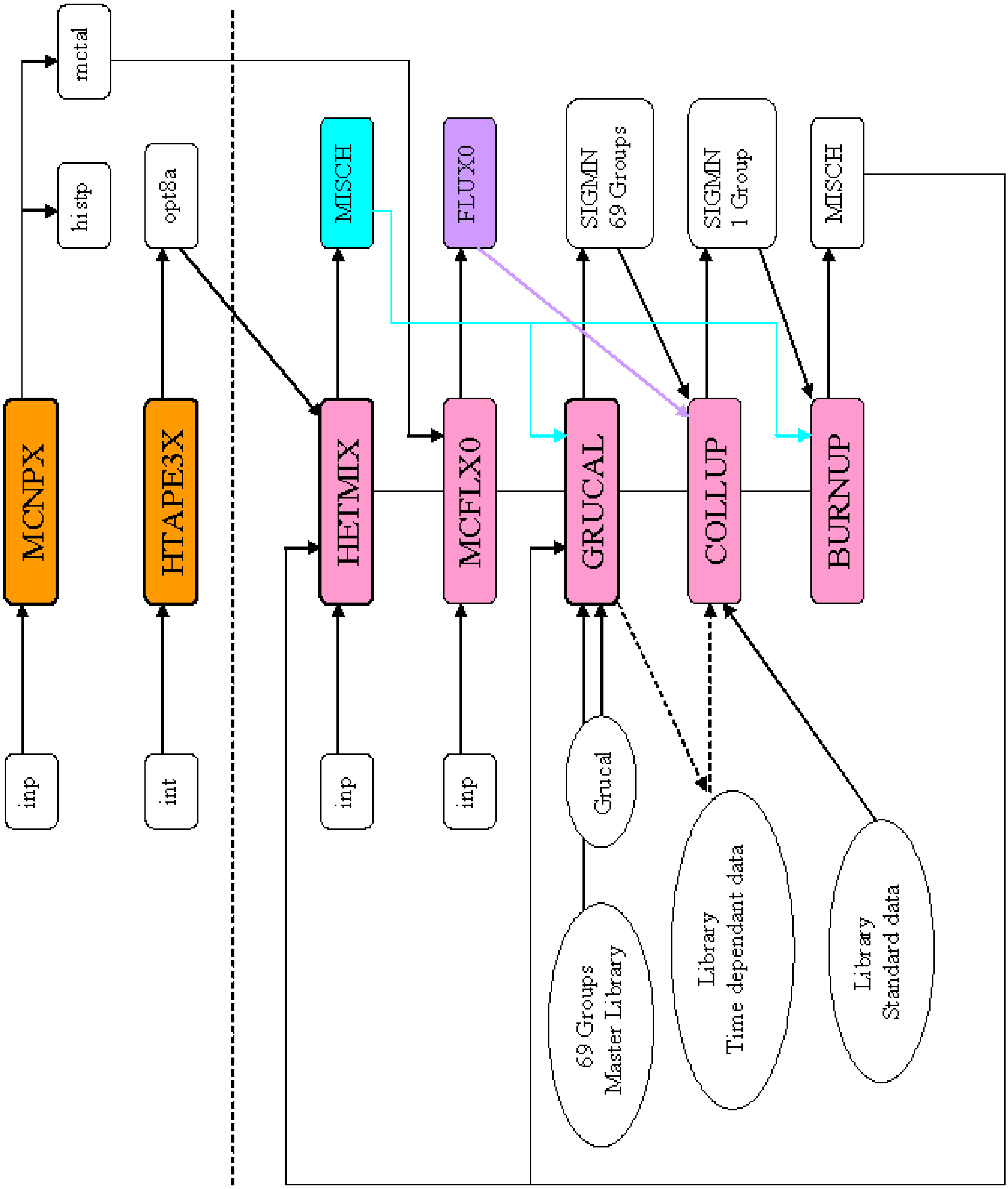

Figure 5-1: *Sequence of the programs for the use of KAPROS for time dependence calculations.*

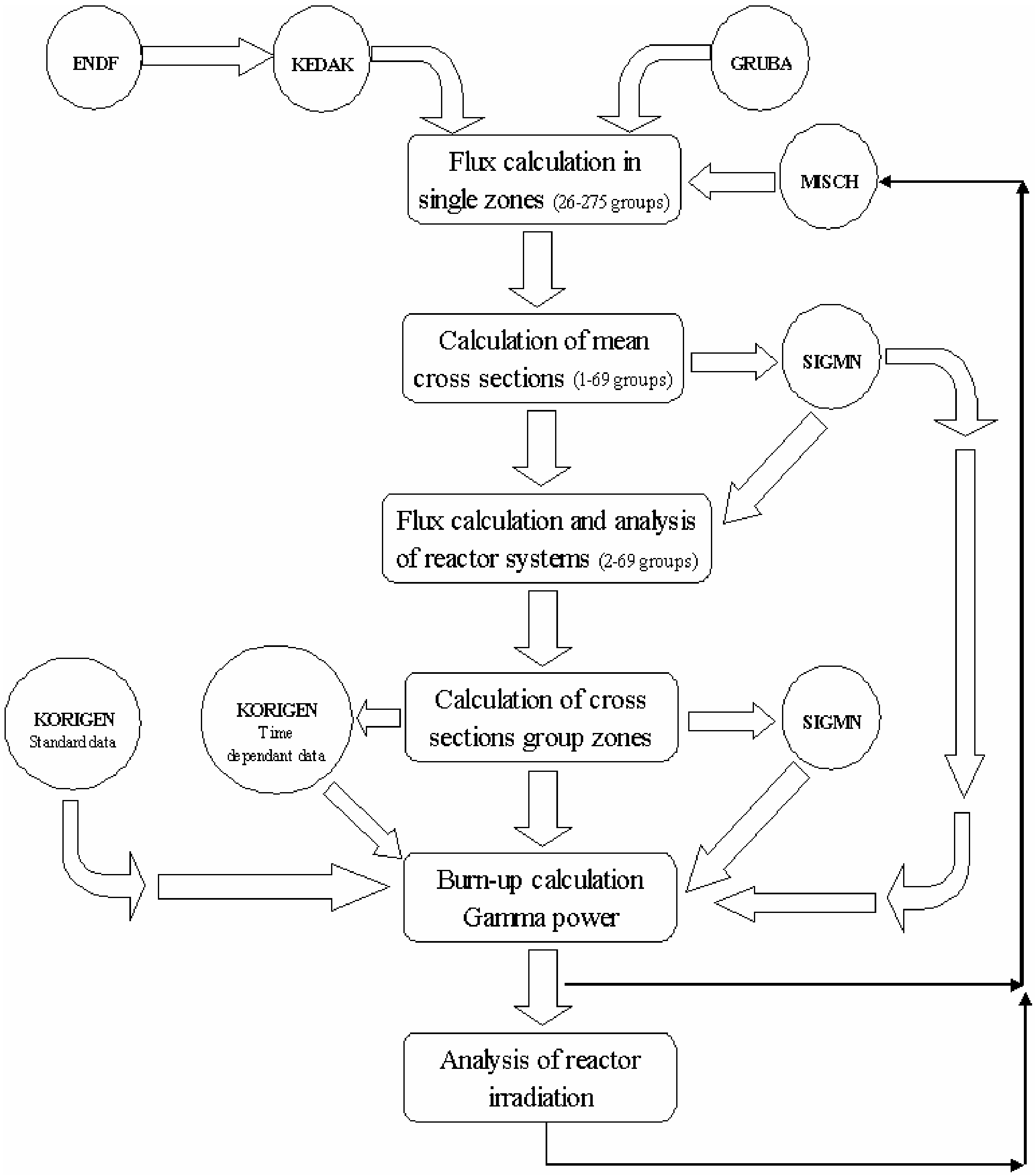

Figure 5-2: *Flowchart of the different KAPROS programs related to the figure 5-1.*

Figure 5-1 describes the sequence of the involved modules in KAPROS and explains the main principles of its operation. Figure 5-2 show the flowchart of the different programs called in the KAPROS burn up calculations.
The dotted line on figure 5-1 delimits the MCNPX job, above and the KAPROS job, below.
The mctal file contains 69 groups flux.
The MISCH block from HETMIX includes the density of particles
The MCFLX0 module extracts the flux stored on the mctal file.
GRUCAL calculates the cross sections for 69 energy groups. The results are stored in SIGMN block.
The task of COLLUP is to condense the 69 groups of cross section in only one group. It uses the formula:

$$\sum_{1group} = \frac{\int_i \Phi_i \sum_i}{\int_i \Phi_i} \tag{5.4}$$

We obtain a new SIGMN block with one group cross section. It may contain up to 800 isotopes.
The particularity of the KAPROS is the possibility to make a loop with the MISCH block obtained with BURNUP.
The BURNUP module allows solving the burn-up equations. The grouping of the programs GRUCAL, COLLUP and BURNUP is performed in the KAPROS procedure BURN0D. The table 5-1 presents an input (input batablocks) file for a KAPROS job. One can distinguish different parts of the input file which begin with the command line is "*KSIOX DBN=*datablock*". Datablock is used in corresponding modules.

The application of these code systems was prepared more detailed for investigations of the LiSoR problem. However, because of unexpected problems with the analysis of the normalization of the results of the MCNPX calculation as described in chapter 3, it was decided to perform these investigations in a later stage of investigations.

5.1.3. The input file

```
// Jobkarte (REGION=1024K)
// EXEC KSG
//K.FT20F001 DD DISP=SHR,DSN=INR415.KORFI(NDLITE)
//K.FT21F001 DD DISP=SHR,DSN=INR415.KORFI(NDACT)
//K.FT22F001 DD DISP=SHR,DSN=INR415.KORFI(NDFPS)
//K.FT03F001 DD SYSOUT=A,DCB=*.FT06F001
//K.SYSIN DD *
*KSIOX DBN=GRUCAL,TYP=CARD,PMN=PRGRUC
'GRUCAL  '
'KFKINR  ' '       ' '       '
'MISCH   '
'NOTGRMAT'
'DATBLOCK'
'AUSWERT '
'ZUSATZ  ' 2
'SFISS  ' '       ' 1 0
'SCAPT  ' '       ' 1 0
'GRUCEND '
*$*$

*KSIOX DBN=INPUT DIXCON,TYP=CARD,PMN=PDXCON
'CNTR' 'PRGR' 'GRST' 1 'GRNR' 1
*$*$

*KSIOX DBN=INPUT
BURNUP,IND=1,TYP=CARD,PMN=PBURNI
'NUDA' 'REAC' 3 1.0 0.0 0.0
'BUTB' 2 'FE  ' 'O  16  '
'FPWS' 3 'XE  ' 0.0 'KR  ' 0.0 'SR  ' 0.4
*$*$

*KSIOX DBN=FLUXIN,TYP=CARD,PMN=PBURNF,IND=1
1
1 100.0
2.0 3.0 5.1E+15
*$*$

*KSIOX DBN=MISCH,TYP=CARD,PMN=PDXCON,IND=1
1
 7 '      ' 'U 235  ' 'PU239  ' *$ MIXTURE 1
   'U 235  '   1500.0  5.0000E-05
   'U 238  '   1500.0  7.0000E-03
   'PU239  '   1500.0  1.5000E-03
   'FE     '   1500.0  1.5000E-02
   'SI     '   1500.0  1.5000E-02
   'O  16  '   1500.0  1.5000E-02
   'SPP 9  '   1500.0  1.0000E-11
*$*$
*KSIOX DBN=INPUT
RENAME,IND=1,TYP=CARD,PMN=PRREN
'SIGMNO        ' 1 'SIGMN1        ' 1 0
*$*$

*GO SM=DIXCON
*GO SM=RENDB,MPARM=1
*GO SM=BURNUP,MPARM=1
```

Table 5-1: *Input file for a KAPROS job.*

5.2. ORIHET3

5.2.1. Utilization of the program

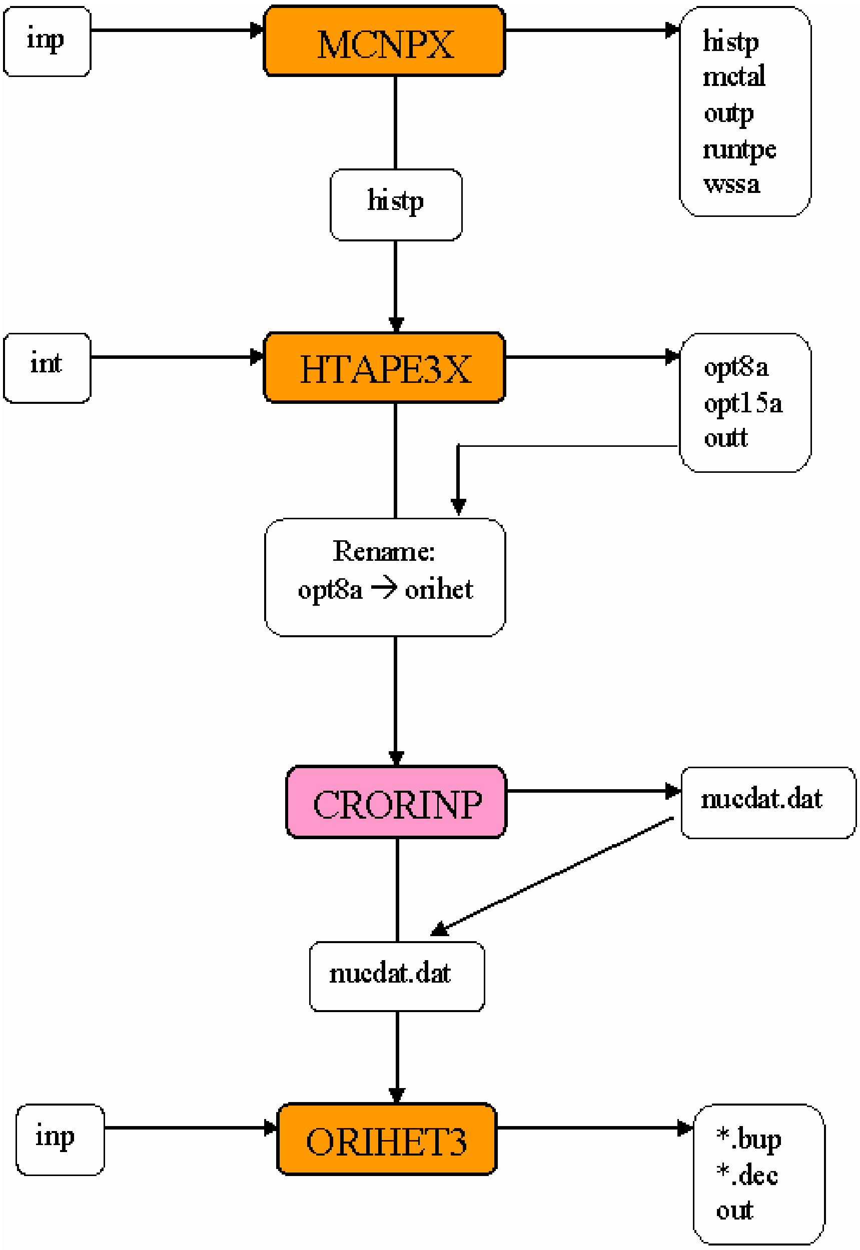

Figure 5-3: *Sequence of the programs to the use of ORIHET3 for time dependence calculations.*

5.2.2. The input file for ORIHET3

%time_step 1. 4. 8. 12. 16. 20. 24. 28. 32. 34. unit=h;	Calculation of the activity build up during the irradiation at different
%title SINQ Target activity build up [with fission];	time step indicated in hours.
%basis In total target mass for 0.05 mA;	
%nuclide_library nubasex ;	Use of the NUBASEX nuclides library
%output none grammes/thresh=1.0e-13 activity/nucl /thresh=1.0e-13;	The program doesn´t take into account the activity under the indicated threshold
%output unit = ci neutr/nucl alpha/nucl;	Output: Activity in Curies [Ci]
%conc zero;	
%prod file="nucdat.dat";	Input file named nucdat.dat
%calculate logfile = x.bup ;	Output file named x.bup
%time_step 10. 20. 40. 100. 200. 400. 800. 1200. 2400. 4800. unit=h;	Calculation of the decay of the residual nuclei after 34 hours irradiation
%output check=1 ;	at different time step indicated in hours.
%title SINQ Target activity decay following 34 hours irradiation;	
%prod zero;	
%concen time_step=10 ;	
%calculate logfile = y.dec ;	Output file named y.dec
%end ;	

Table 5-2: *Input file for an ORIHET3 job and meaning of somes terms.*

Conclusion

Within the Beta-Testing of MCNPX, investigations to study the Accelerator Driven Systems are performed at the Institut for Reactor Safety (IRS).

The first chapters were dedicated to the description of the spallation reaction, to give the charasteristics necessary for a good understanding of the results of this reaction and to the presentation of the models which had been used in this work.

The main work of this study was the validation of the implementation of the INCL4+ABLA code in the new beta version 2.5e of MCNPX after the code of the Cugnon group was integrated in MCNPX. First the normalized MCNPX results were compared with the corresponding results obtained with Cugnon Stand-alone and they were in very good agreement for the fission part and for the spallation part too. Particularly, this study shows how to define the input parameters and the corresponding normalization to obtain the spallation yields. An important part was devoted to the detailed understanding of the calculations of the geometrical cross section. The MCNPX results were compared with the experimental data at different energy level. At 1 GeV proton energy, MCNPX results with recommended input parameters were in good agreement with the data from the GSI (Darmstadt) and the data from ISTC (Moscow). A dispersion of the raw data from ISTC was found at 600 MeV proton energy. The data from GSI for 500 MeV were in very good agreement for the spallation part, but a difference of 40% was observed for the fission part which would be disappear after the discussed correction of the experimental data.

After the validation of MCNPX, we investigated to the LiSoR experiment. This experiment has the role to prepare the MEGAPIE project by simulating the MEGAPIE conditions (under irradiation, under strain and in the presence of Lead-Bismuth-Eutectic). We focused this study on predictions for the Polonium generation. Indeed, the Polonium is an important problem of MEGAPIE because it may cause contamination of the target. The main isotopes ^{208}Po and ^{209}Po were particularly considered due to their α-activity. An interesting question is to study the ^{210}Po which is produced by activation and the program ORIHET3 used for the decay calculations doesn’t take into account activation.

The last chapter of this work presented two codes for depletion calculation: ORIHET3 developed at PSI and KAPROS developed at FZK. Their characteristics and their uses were explained. The next step is the comparison of calculations to evaluate the two codes and especially to study the ^{210}Po generation by activation.

Annex A
Distribution of spallation yields before normalization calculated by MCNPX and obtained by HTAPE3X and with the tally 8 option

These results are performed with the INCL4+ABLA model for 300.000 cascades histories by irradiation of a ^{208}Pb target by 1 GeV proton beam. The LCA input card is the one defined in section 3.1.

The first table is the result from HTAPE3X. This is the direct output file opt8a except the column with the mass number A. Indeed, it is easier to have the same value in order to compare with the output file obtained with tally 8.

The data are given only for the spallation corresponding to charge munber ranging between 65 and 85.

Z	N	A	Yields	Error
65	80	145	3,33E-06	1
65	84	149	3,33E-06	1
65	85	150	6,67E-06	0,7071
65	88	153	6,67E-06	0,7071
65	89	154	3,33E-06	1
65	90	155	3,33E-06	1
66	85	151	3,33E-06	1
67	86	153	3,33E-06	1
68	89	157	3,33E-06	1
68	90	158	6,67E-06	0,7071
68	91	159	3,33E-06	1
68	92	160	6,67E-06	0,7071
68	95	163	6,67E-06	0,7071
68	96	164	3,33E-06	1
68	99	167	3,33E-06	1
69	88	157	3,33E-06	1
69	90	159	1,33E-05	0,5
69	92	161	6,67E-06	0,7071
69	93	162	1,67E-05	0,4472
69	94	163	1,00E-05	0,5773
69	95	164	3,33E-06	1
69	96	165	3,33E-06	1
69	97	166	3,33E-06	1
69	98	167	6,67E-06	0,7071
69	100	169	6,67E-06	0,7071
70	89	159	3,33E-06	1
70	90	160	3,33E-06	1
70	91	161	2,33E-05	0,378
70	92	162	1,00E-05	0,5773
70	93	163	3,00E-05	0,3333
70	94	164	1,33E-05	0,5
70	95	165	1,67E-05	0,4472
70	96	166	2,33E-05	0,378
70	97	167	2,00E-05	0,4082
70	98	168	1,00E-05	0,5773
70	99	169	3,33E-06	1
70	100	170	3,33E-06	1
70	101	171	3,33E-06	1
70	103	173	3,33E-06	1
70	107	177	3,33E-06	1
71	88	159	3,33E-06	1
71	90	161	3,33E-06	1
71	91	162	6,67E-06	0,7071
71	92	163	2,00E-05	0,4082
71	93	164	4,33E-05	0,2773
71	94	165	3,67E-05	0,3015
71	95	166	6,67E-05	0,2236
71	96	167	7,33E-05	0,2132
71	97	168	7,00E-05	0,2182
71	98	169	4,67E-05	0,2673
71	99	170	4,33E-05	0,2773
71	100	171	2,67E-05	0,3535
71	101	172	1,33E-05	0,5
71	102	173	3,33E-06	1
71	103	174	6,67E-06	0,7071
71	104	175	1,33E-05	0,5
71	106	177	6,67E-06	0,7071
72	91	163	1,67E-05	0,4472
72	92	164	1,67E-05	0,4472
72	93	165	6,00E-05	0,2357
72	94	166	6,33E-05	0,2294
72	95	167	1,07E-04	0,1768
72	96	168	1,70E-04	0,14
72	97	169	2,03E-04	0,128
72	98	170	1,97E-04	0,1302
72	99	171	1,43E-04	0,1525
72	100	172	1,17E-04	0,169
72	101	173	9,33E-05	0,189
72	102	174	6,67E-05	0,2236
72	103	175	3,00E-05	0,3333
72	104	176	1,33E-05	0,5
72	105	177	6,67E-06	0,7071
72	106	178	6,67E-06	0,7071
73	92	165	1,33E-05	0,5
73	93	166	2,67E-05	0,3535
73	94	167	5,67E-05	0,2425
73	95	168	1,87E-04	0,1336
73	96	169	1,83E-04	0,1348
73	97	170	3,47E-04	0,098
73	98	171	3,30E-04	0,1005
73	99	172	3,47E-04	0,098
73	100	173	2,87E-04	0,1078
73	101	174	3,13E-04	0,1031
73	102	175	2,03E-04	0,128
73	103	176	1,60E-04	0,1443
73	104	177	1,00E-04	0,1826
73	105	178	8,67E-05	0,1961
73	106	179	3,33E-05	0,3162
73	107	180	1,67E-05	0,4472
73	108	181	1,67E-05	0,4472
73	109	182	1,00E-05	0,5773
73	110	183	6,67E-06	0,7071
73	114	187	3,33E-06	1
74	92	166	1,33E-05	0,5
74	93	167	3,33E-06	1
74	94	168	3,33E-05	0,3162
74	95	169	1,20E-04	0,1667
74	96	170	2,57E-04	0,1139
74	97	171	4,00E-04	0,0913
74	98	172	5,53E-04	0,0776
74	99	173	6,57E-04	0,0712
74	100	174	7,47E-04	0,0668
74	101	175	7,50E-04	0,0666
74	102	176	6,17E-04	0,0735
74	103	177	4,80E-04	0,0833
74	104	178	4,00E-04	0,0913
74	105	179	2,73E-04	0,1104
74	106	180	1,83E-04	0,1348
74	107	181	1,07E-04	0,1768
74	108	182	7,00E-05	0,2182
74	109	183	3,00E-05	0,3333
74	110	184	3,33E-05	0,3162
74	111	185	1,00E-05	0,5773
74	112	186	1,00E-05	0,5773
75	92	167	3,33E-06	1
75	93	168	3,33E-06	1
75	94	169	1,67E-05	0,4472
75	95	170	9,33E-05	0,189
75	96	171	2,00E-04	0,1291
75	97	172	3,40E-04	0,099
75	98	173	5,67E-04	0,0767
75	99	174	8,77E-04	0,0616
75	100	175	1,24E-03	0,0518
75	101	176	1,32E-03	0,0503
75	102	177	1,32E-03	0,0502
75	103	178	1,39E-03	0,0489
75	104	179	1,20E-03	0,0527
75	105	180	8,63E-04	0,0621
75	106	181	6,60E-04	0,071
75	107	182	4,87E-04	0,0827
75	108	183	3,60E-04	0,0962
75	109	184	1,90E-04	0,1324
75	110	185	1,03E-04	0,1796
75	111	186	6,00E-05	0,2357
75	112	187	4,67E-05	0,2673
75	113	188	1,33E-05	0,5
75	114	189	1,67E-05	0,4472
75	115	190	1,00E-05	0,5773
75	116	191	3,33E-06	1
75	118	193	3,33E-06	1
76	93	169	6,67E-06	0,7071
76	94	170	6,67E-06	0,7071
76	95	171	2,33E-05	0,378
76	96	172	9,00E-05	0,1924
76	97	173	2,53E-04	0,1147
76	98	174	3,57E-04	0,0967
76	99	175	7,93E-04	0,0648
76	100	176	1,25E-03	0,0515
76	101	177	1,79E-03	0,0432
76	102	178	2,28E-03	0,0382
76	103	179	2,28E-03	0,0382
76	104	180	2,32E-03	0,0379
76	105	181	2,14E-03	0,0395
76	106	182	1,93E-03	0,0415
76	107	183	1,47E-03	0,0476
76	108	184	1,15E-03	0,0539
76	109	185	7,93E-04	0,0648
76	110	186	5,63E-04	0,0769
76	111	187	3,47E-04	0,098
76	112	188	2,13E-04	0,125
76	113	189	1,37E-04	0,1562
76	114	190	6,00E-05	0,2357
76	115	191	4,33E-05	0,2773
76	116	192	2,00E-05	0,4082
76	117	193	1,00E-05	0,5773
76	118	194	1,33E-05	0,5
76	119	195	6,67E-06	0,7071
76	120	196	3,33E-06	1
77	96	173	1,33E-05	0,5
77	97	174	7,67E-05	0,2085
77	98	175	2,00E-04	0,1291
77	99	176	4,33E-04	0,0877
77	100	177	9,67E-04	0,0587
77	101	178	1,57E-03	0,046
77	102	179	2,23E-03	0,0386
77	103	180	3,04E-03	0,0331
77	104	181	3,53E-03	0,0307
77	105	182	3,77E-03	0,0297
77	106	183	3,71E-03	0,0299
77	107	184	3,47E-03	0,0309
77	108	185	2,91E-03	0,0338
77	109	186	2,20E-03	0,0389
77	110	187	1,73E-03	0,0439

Z	N	A	Yields	Error
77	111	188	1,22E-03	0,0522
77	112	189	9,43E-04	0,0594
77	113	190	6,60E-04	0,071
77	114	191	3,80E-04	0,0936
77	115	192	3,03E-04	0,1048
77	116	193	1,47E-04	0,1507
77	117	194	9,33E-05	0,189
77	118	195	9,00E-05	0,1924
77	119	196	6,00E-05	0,2357
77	120	197	3,33E-05	0,3162
77	121	198	2,00E-05	0,4082
77	122	199	1,67E-05	0,4472
77	123	200	6,67E-06	0,7071
77	124	201	3,33E-06	1
77	125	202	6,67E-06	0,7071
77	126	203	3,33E-06	1
78	96	174	3,33E-06	1
78	97	175	3,33E-06	1
78	98	176	5,33E-05	0,25
78	99	177	1,67E-04	0,1414
78	100	178	4,83E-04	0,083
78	101	179	9,37E-04	0,0596
78	102	180	1,76E-03	0,0435
78	103	181	2,91E-03	0,0338
78	104	182	3,91E-03	0,0291
78	105	183	4,83E-03	0,0262
78	106	184	5,42E-03	0,0247
78	107	185	5,75E-03	0,024
78	108	186	5,49E-03	0,0246
78	109	187	5,27E-03	0,0251
78	110	188	4,34E-03	0,0277
78	111	189	3,80E-03	0,0296
78	112	190	3,13E-03	0,0326
78	113	191	2,25E-03	0,0384
78	114	192	1,80E-03	0,043
78	115	193	1,32E-03	0,0503
78	116	194	1,00E-03	0,0577
78	117	195	6,80E-04	0,07
78	118	196	4,27E-04	0,0884
78	119	197	3,43E-04	0,0985
78	120	198	2,90E-04	0,1072
78	121	199	1,87E-04	0,1336
78	122	200	1,43E-04	0,1525
78	123	201	8,33E-05	0,2
78	124	202	4,00E-05	0,2887
78	125	203	6,67E-06	0,7071
78	126	204	1,00E-05	0,5773
79	99	178	3,00E-05	0,3333
79	100	179	1,37E-04	0,1562
79	101	180	3,30E-04	0,1005
79	102	181	7,23E-04	0,0679
79	103	182	1,57E-03	0,0461
79	104	183	2,68E-03	0,0352
79	105	184	3,88E-03	0,0293
79	106	185	5,17E-03	0,0253
79	107	186	6,33E-03	0,0229
79	108	187	7,32E-03	0,0213
79	109	188	7,86E-03	0,0205
79	110	189	7,79E-03	0,0206
79	111	190	7,23E-03	0,0214
79	112	191	6,49E-03	0,0226

Z	N	A	Yields	Error
79	113	192	5,68E-03	0,0242
79	114	193	4,94E-03	0,0259
79	115	194	4,04E-03	0,0287
79	116	195	3,18E-03	0,0323
79	117	196	2,65E-03	0,0354
79	118	197	1,90E-03	0,0418
79	119	198	1,60E-03	0,0457
79	120	199	1,25E-03	0,0517
79	121	200	9,50E-04	0,0592
79	122	201	7,70E-04	0,0658
79	123	202	5,17E-04	0,0803
79	124	203	3,63E-04	0,0958
79	125	204	2,03E-04	0,128
79	126	205	9,33E-05	0,189
79	127	206	1,33E-05	0,5
80	100	180	1,00E-05	0,5773
80	101	181	7,00E-05	0,2182
80	102	182	2,20E-04	0,1231
80	103	183	4,60E-04	0,0851
80	104	184	1,00E-03	0,0577
80	105	185	2,08E-03	0,04
80	106	186	3,36E-03	0,0315
80	107	187	5,02E-03	0,0257
80	108	188	6,56E-03	0,0225
80	109	189	7,47E-03	0,021
80	110	190	8,89E-03	0,0193
80	111	191	9,47E-03	0,0187
80	112	192	9,77E-03	0,0184
80	113	193	9,43E-03	0,0187
80	114	194	9,48E-03	0,0187
80	115	195	8,38E-03	0,0199
80	116	196	7,88E-03	0,0205
80	117	197	7,11E-03	0,0216
80	118	198	5,90E-03	0,0237
80	119	199	5,26E-03	0,0251
80	120	200	4,64E-03	0,0267
80	121	201	3,95E-03	0,029
80	122	202	3,17E-03	0,0324
80	123	203	2,90E-03	0,0338
80	124	204	2,26E-03	0,0384
80	125	205	1,81E-03	0,0429
80	126	206	9,37E-04	0,0596
80	127	207	5,67E-05	0,2425
81	101	182	3,33E-06	1
81	102	183	1,33E-05	0,5
81	103	184	9,00E-05	0,1924
81	104	185	1,63E-04	0,1428
81	105	186	5,33E-04	0,079
81	106	187	1,28E-03	0,051
81	107	188	2,21E-03	0,0388
81	108	189	3,24E-03	0,032
81	109	190	4,94E-03	0,0259
81	110	191	6,63E-03	0,0224
81	111	192	7,85E-03	0,0205
81	112	193	9,43E-03	0,0187
81	113	194	9,92E-03	0,0182
81	114	195	1,12E-02	0,0172
81	115	196	1,14E-02	0,017
81	116	197	1,13E-02	0,0171
81	117	198	1,14E-02	0,017
81	118	199	1,13E-02	0,0171

Z	N	A	Yields	Error
81	119	200	1,07E-02	0,0175
81	120	201	1,06E-02	0,0176
81	121	202	1,01E-02	0,0181
81	122	203	9,84E-03	0,0183
81	123	204	9,91E-03	0,0183
81	124	205	1,04E-02	0,0178
81	125	206	1,11E-02	0,0173
81	126	207	2,05E-02	0,0126
81	127	208	1,93E-04	0,1313
82	104	186	3,33E-06	1
82	105	187	4,33E-05	0,2773
82	106	188	1,57E-04	0,1459
82	107	189	3,13E-04	0,1031
82	108	190	8,40E-04	0,063
82	109	191	1,43E-03	0,0482
82	110	192	2,56E-03	0,036
82	111	193	3,60E-03	0,0304
82	112	194	4,85E-03	0,0262
82	113	195	5,85E-03	0,0238
82	114	196	7,20E-03	0,0214
82	115	197	8,11E-03	0,0202
82	116	198	8,68E-03	0,0195
82	117	199	9,42E-03	0,0187
82	118	200	1,00E-02	0,0182
82	119	201	1,07E-02	0,0176
82	120	202	1,10E-02	0,0173
82	121	203	1,22E-02	0,0164
82	122	204	1,29E-02	0,016
82	123	205	1,55E-02	0,0146
82	124	206	2,03E-02	0,0127
82	125	207	3,72E-02	0,0093
82	126	208	4,75E-03	0,0264
83	107	190	3,33E-06	1
83	108	191	5,00E-05	0,2582
83	109	192	1,17E-04	0,169
83	110	193	3,17E-04	0,1026
83	111	194	6,03E-04	0,0743
83	112	195	8,00E-04	0,0645
83	113	196	1,23E-03	0,0521
83	114	197	1,53E-03	0,0466
83	115	198	1,82E-03	0,0427
83	116	199	2,21E-03	0,0388
83	117	200	2,23E-03	0,0386
83	118	201	2,63E-03	0,0355
83	119	202	2,55E-03	0,0361
83	120	203	2,74E-03	0,0348
83	121	204	2,97E-03	0,0334
83	122	205	2,91E-03	0,0338
83	123	206	3,01E-03	0,0332
83	124	207	2,29E-03	0,0381
83	125	208	1,49E-03	0,0472
84	110	194	6,67E-06	0,7071
84	111	195	1,67E-05	0,4472
84	112	196	2,00E-05	0,4082
84	113	197	1,67E-05	0,4472
84	114	198	7,00E-05	0,2182
84	115	199	3,67E-05	0,3015
84	116	200	8,67E-05	0,1961
84	117	201	1,07E-04	0,1768
84	118	202	1,53E-04	0,1474
84	119	203	9,00E-05	0,1924

Z	N	A	Yields	Error
84	120	204	9,00E-05	0,1924
84	121	205	7,00E-05	0,2182
84	122	206	6,00E-05	0,2357
84	123	207	3,00E-05	0,3333
84	124	208	3,33E-06	1
85	120	205	3,33E-06	1

Z/A	Yields	Error
65144	0,00E+00	0
65145	3,33E-06	1
65146	0,00E+00	0
65147	0,00E+00	0
65148	0,00E+00	0
65149	3,33E-06	1
65150	6,67E-06	0,7071
65151	0,00E+00	0
65152	0,00E+00	0
65153	6,67E-06	0,7071
65154	3,33E-06	1
65155	3,33E-06	1
65156	0,00E+00	0
65157	0,00E+00	0
65158	0,00E+00	0
65159	0,00E+00	0
65160	0,00E+00	0
65161	0,00E+00	0
65162	0,00E+00	0
65163	0,00E+00	0
65164	0,00E+00	0
65165	0,00E+00	0
66145	0,00E+00	0
66146	0,00E+00	0
66147	0,00E+00	0
66148	0,00E+00	0
66149	0,00E+00	0
66150	0,00E+00	0
66151	3,33E-06	1
66152	0,00E+00	0
66153	0,00E+00	0
66154	0,00E+00	0
66155	0,00E+00	0
66156	0,00E+00	0
66157	0,00E+00	0
66158	0,00E+00	0
66159	0,00E+00	0
66160	0,00E+00	0
66161	0,00E+00	0
66162	0,00E+00	0
66163	0,00E+00	0
66164	0,00E+00	0
66165	0,00E+00	0
66166	0,00E+00	0
66167	0,00E+00	0
66168	0,00E+00	0
67147	0,00E+00	0
67148	0,00E+00	0
67149	0,00E+00	0
67150	0,00E+00	0
67151	0,00E+00	0
67152	0,00E+00	0
67153	3,33E-06	1
67154	0,00E+00	0
67155	0,00E+00	0
67156	0,00E+00	0
67157	0,00E+00	0
67158	0,00E+00	0
67159	0,00E+00	0
67160	0,00E+00	0
67161	0,00E+00	0
67162	0,00E+00	0
67163	0,00E+00	0
67164	0,00E+00	0
67165	0,00E+00	0
67166	0,00E+00	0
67167	0,00E+00	0
67168	0,00E+00	0
67169	0,00E+00	0
67170	0,00E+00	0
68147	0,00E+00	0
68148	0,00E+00	0
68149	0,00E+00	0
68150	0,00E+00	0
68151	0,00E+00	0
68152	0,00E+00	0
68153	0,00E+00	0
68154	0,00E+00	0
68155	0,00E+00	0
68156	0,00E+00	0
68157	3,33E-06	1
68158	6,67E-06	0,7071
68159	3,33E-06	1
68160	6,67E-06	0,7071
68161	0,00E+00	0
68162	0,00E+00	0
68163	6,67E-06	0,7071
68164	3,33E-06	1
68165	0,00E+00	0
68166	0,00E+00	0
68167	3,33E-06	1
68168	0,00E+00	0
68169	0,00E+00	0
68170	0,00E+00	0
68171	0,00E+00	0
68172	0,00E+00	0
68173	0,00E+00	0
69151	0,00E+00	0
69152	0,00E+00	0
69153	0,00E+00	0
69154	0,00E+00	0
69155	0,00E+00	0
69156	0,00E+00	0
69157	3,33E-06	1
69158	0,00E+00	0
69159	1,33E-05	0,5
69160	0,00E+00	0
69161	6,67E-06	0,7071
69162	1,67E-05	0,4472
69163	1,00E-05	0,5773
69164	3,33E-06	1
69165	3,33E-06	1
69166	3,33E-06	1
69167	6,67E-06	0,7071
69168	0,00E+00	0
69169	6,67E-06	0,7071
69170	0,00E+00	0
69171	0,00E+00	0
69172	0,00E+00	0
69173	0,00E+00	0
69174	0,00E+00	0
69175	0,00E+00	0
69176	0,00E+00	0
70153	0,00E+00	0
70154	0,00E+00	0
70155	0,00E+00	0
70156	0,00E+00	0
70157	0,00E+00	0
70158	0,00E+00	0
70159	3,33E-06	1
70160	3,33E-06	1
70161	2,33E-05	0,378
70162	1,00E-05	0,5773
70163	3,00E-05	0,3333
70164	1,33E-05	0,5
70165	1,67E-05	0,4472
70166	2,33E-05	0,378
70167	2,00E-05	0,4082
70168	1,00E-05	0,5773
70169	3,33E-06	1
70170	3,33E-06	1
70171	3,33E-06	1
70172	0,00E+00	0
70173	3,33E-06	1
70174	0,00E+00	0
70175	0,00E+00	0
70176	0,00E+00	0
70177	3,33E-06	1
70178	0,00E+00	0
70179	0,00E+00	0
71151	0,00E+00	0
71152	0,00E+00	0
71153	0,00E+00	0
71154	0,00E+00	0
71155	0,00E+00	0
71156	0,00E+00	0
71157	0,00E+00	0
71158	0,00E+00	0
71159	3,33E-06	1
71160	0,00E+00	0
71161	3,33E-06	1
71162	6,67E-06	0,7071
71163	2,00E-05	0,4082
71164	4,33E-05	0,2773
71165	3,67E-05	0,3015
71166	6,67E-05	0,2236
71167	7,33E-05	0,2132
71168	7,00E-05	0,2182
71169	4,67E-05	0,2673
71170	4,33E-05	0,2773
71171	2,67E-05	0,3535
71172	1,33E-05	0,5
71173	3,33E-06	1
71174	6,67E-06	0,7071
71175	1,33E-05	0,5
71176	0,00E+00	0
71177	6,67E-06	0,7071
71178	0,00E+00	0
71179	0,00E+00	0
71180	0,00E+00	0
71181	0,00E+00	0
71182	0,00E+00	0
71183	0,00E+00	0
72154	0,00E+00	0
72155	0,00E+00	0
72156	0,00E+00	0
72157	0,00E+00	0
72158	0,00E+00	0
72159	0,00E+00	0
72160	0,00E+00	0
72161	0,00E+00	0
72162	0,00E+00	0
72163	1,67E-05	0,4472
72164	1,67E-05	0,4472
72165	6,00E-05	0,2357
72166	6,33E-05	0,2294
72167	1,07E-04	0,1768
72168	1,70E-04	0,14
72169	2,03E-04	0,128
72170	1,97E-04	0,1302
72171	1,43E-04	0,1525
72172	1,17E-04	0,169
72173	9,33E-05	0,189
72174	6,67E-05	0,2236
72175	3,00E-05	0,3333
72176	1,33E-05	0,5
72177	6,67E-06	0,7071
72178	6,67E-06	0,7071
72179	0,00E+00	0
72180	0,00E+00	0
72181	0,00E+00	0
72182	0,00E+00	0
72183	0,00E+00	0
72184	0,00E+00	0
73157	0,00E+00	0
73158	0,00E+00	0

Z/A	Yields	Error
73159	0,00E+00	0
73160	0,00E+00	0
73161	0,00E+00	0
73162	0,00E+00	0
73163	0,00E+00	0
73164	0,00E+00	0
73165	1,33E-05	0,5
73166	2,67E-05	0,3535
73167	5,67E-05	0,2425
73168	1,87E-04	0,1336
73169	1,83E-04	0,1348
73170	3,47E-04	0,098
73171	3,30E-04	0,1005
73172	3,47E-04	0,098
73173	2,87E-04	0,1078
73174	3,13E-04	0,1031
73175	2,03E-04	0,128
73176	1,60E-04	0,1443
73177	1,00E-04	0,1826
73178	8,67E-05	0,1961
73179	3,33E-05	0,3162
73180	1,67E-05	0,4472
73181	1,67E-05	0,4472
73182	1,00E-05	0,5773
73183	6,67E-06	0,7071
73184	0,00E+00	0
73185	0,00E+00	0
73186	0,00E+00	0
74158	3,33E-06	1
74159	0,00E+00	0
74160	0,00E+00	0
74161	0,00E+00	0
74162	0,00E+00	0
74163	0,00E+00	0
74164	0,00E+00	0
74165	0,00E+00	0
74166	1,33E-05	0,5
74167	3,33E-06	1
74168	3,33E-05	0,3162
74169	1,20E-04	0,1667
74170	2,57E-04	0,1139
74171	4,00E-04	0,0913
74172	5,53E-04	0,0776
74173	6,57E-04	0,0712
74174	7,47E-04	0,0668
74175	7,50E-04	0,0666
74176	6,17E-04	0,0735
74177	4,80E-04	0,0833
74178	4,00E-04	0,0913
74179	2,73E-04	0,1104
74180	1,83E-04	0,1348
74181	1,07E-04	0,1768
74182	7,00E-05	0,2182
74183	3,00E-05	0,3333
74184	3,33E-05	0,3162
74185	1,00E-05	0,5773
74186	1,00E-05	0,5773
74187	0,00E+00	0
74188	0,00E+00	0
74189	0,00E+00	0
74190	0,00E+00	0
75161	0,00E+00	0
75162	0,00E+00	0
75163	0,00E+00	0
75164	0,00E+00	0
75165	0,00E+00	0
75166	0,00E+00	0
75167	3,33E-06	1
75168	3,33E-06	1
75169	1,67E-05	0,4472
75170	9,33E-05	0,189
75171	2,00E-04	0,1291
75172	3,40E-04	0,099
75173	5,67E-04	0,0767
75174	8,77E-04	0,0616
75175	1,24E-03	0,0518
75176	1,32E-03	0,0503
75177	1,32E-03	0,0502
75178	1,39E-03	0,0489
75179	1,20E-03	0,0527
75180	8,63E-04	0,0621
75181	6,60E-04	0,071
75182	4,87E-04	0,0827
75183	3,60E-04	0,0962
75184	1,90E-04	0,1324
75185	1,03E-04	0,1796
75186	6,00E-05	0,2357
75187	4,67E-05	0,2673
75188	1,33E-05	0,5
75189	1,67E-05	0,4472
75190	1,00E-05	0,5773
75191	3,33E-06	1
75192	0,00E+00	0
76163	3,33E-06	1
76164	0,00E+00	0
76165	0,00E+00	0
76166	0,00E+00	0
76167	0,00E+00	0
76168	0,00E+00	0
76169	6,67E-06	0,7071
76170	6,67E-06	0,7071
76171	2,33E-05	0,378
76172	9,00E-05	0,1924
76173	2,53E-04	0,1147
76174	3,57E-04	0,0967
76175	7,93E-04	0,0648
76176	1,25E-03	0,0515
76177	1,79E-03	0,0432
76178	2,28E-03	0,0382
76179	2,28E-03	0,0382
76180	2,32E-03	0,0379
76181	2,14E-03	0,0395
76182	1,93E-03	0,0415
76183	1,47E-03	0,0476
76184	1,15E-03	0,0539
76185	7,93E-04	0,0648
76186	5,63E-04	0,0769
76187	3,47E-04	0,098
76188	2,13E-04	0,125
76189	1,37E-04	0,1562
76190	6,00E-05	0,2357
76191	4,33E-05	0,2773
76192	2,00E-05	0,4082
76193	1,00E-05	0,5773
76194	1,33E-05	0,5
76195	6,67E-06	0,7071
76196	3,33E-06	1
77166	0,00E+00	0
77167	0,00E+00	0
77168	0,00E+00	0
77169	0,00E+00	0
77170	0,00E+00	0
77171	0,00E+00	0
77172	0,00E+00	0
77173	1,33E-05	0,5
77174	7,67E-05	0,2085
77175	2,00E-04	0,1291
77176	4,33E-04	0,0877
77177	9,67E-04	0,0587
77178	1,57E-03	0,046
77179	2,23E-03	0,0386
77180	3,04E-03	0,0331
77181	3,53E-03	0,0307
77182	3,77E-03	0,0297
77183	3,71E-03	0,0299
77184	3,47E-03	0,0309
77185	2,91E-03	0,0338
77186	2,20E-03	0,0389
77187	1,73E-03	0,0439
77188	1,22E-03	0,0522
77189	9,43E-04	0,0594
77190	6,60E-04	0,071
77191	3,80E-04	0,0936
77192	3,03E-04	0,1048
77193	1,47E-04	0,1507
77194	9,33E-05	0,189
77195	9,00E-05	0,1924
77196	6,00E-05	0,2357
77197	3,33E-05	0,3162
77198	2,00E-05	0,4082
78168	1,67E-05	0,4472
78169	6,67E-06	0,7071
78170	3,33E-06	1
78171	6,67E-06	0,7071
78172	3,33E-06	1
78173	0,00E+00	0
78174	3,33E-06	1
78175	3,33E-06	1
78176	5,33E-05	0,25
78177	1,67E-04	0,1414
78178	4,83E-04	0,083
78179	9,37E-04	0,0596
78180	1,76E-03	0,0435
78181	2,91E-03	0,0338
78182	3,91E-03	0,0291
78183	4,83E-03	0,0262
78184	5,42E-03	0,0247
78185	5,75E-03	0,024
78186	5,49E-03	0,0246
78187	5,27E-03	0,0251
78188	4,34E-03	0,0277
78189	3,80E-03	0,0296
78190	3,13E-03	0,0326
78191	2,25E-03	0,0384
78192	1,80E-03	0,043
78193	1,32E-03	0,0503
78194	1,00E-03	0,0577
78195	6,80E-04	0,07
78196	4,27E-04	0,0884
78197	3,43E-04	0,0985
78198	2,90E-04	0,1072
78199	1,87E-04	0,1336
78200	1,43E-04	0,1525
78201	8,33E-05	0,2
79175	4,00E-05	0,2887
79176	6,67E-06	0,7071
79177	1,00E-05	0,5773
79178	3,00E-05	0,3333
79179	1,37E-04	0,1562
79180	3,30E-04	0,1005
79181	7,23E-04	0,0679
79182	1,57E-03	0,0461
79183	2,68E-03	0,0352
79184	3,88E-03	0,0293
79185	5,17E-03	0,0253
79186	6,33E-03	0,0229
79187	7,32E-03	0,0213
79188	7,86E-03	0,0205
79189	7,79E-03	0,0206
79190	7,23E-03	0,0214
79191	6,49E-03	0,0226
79192	5,68E-03	0,0242
79193	4,94E-03	0,0259
79194	4,04E-03	0,0287
79195	3,18E-03	0,0323
79196	2,65E-03	0,0354

Z/A	Yields	Error
79197	1,90E-03	0,0418
79198	1,60E-03	0,0457
79199	1,25E-03	0,0517
79200	9,50E-04	0,0592
79201	7,70E-04	0,0658
79202	5,17E-04	0,0803
79203	3,63E-04	0,0958
79204	2,03E-04	0,128
80177	9,33E-05	0,189
80178	1,33E-05	0,5
80179	0,00E+00	0
80180	1,00E-05	0,5773
80181	7,00E-05	0,2182
80182	2,20E-04	0,1231
80183	4,60E-04	0,0851
80184	1,00E-03	0,0577
80185	2,08E-03	0,04
80186	3,36E-03	0,0315
80187	5,02E-03	0,0257
80188	6,56E-03	0,0225
80189	7,47E-03	0,021
80190	8,89E-03	0,0193
80191	9,47E-03	0,0187
80192	9,77E-03	0,0184
80193	9,43E-03	0,0187
80194	9,48E-03	0,0187
80195	8,38E-03	0,0199
80196	7,88E-03	0,0205
80197	7,11E-03	0,0216
80198	5,90E-03	0,0237
80199	5,26E-03	0,0251
80200	4,64E-03	0,0267
80201	3,95E-03	0,029
80202	3,17E-03	0,0324
80203	2,90E-03	0,0338
80204	2,26E-03	0,0384
80205	1,81E-03	0,0429
80206	9,50E-04	0,0592
81184	1,47E-04	0,1507
81185	1,63E-04	0,1428
81186	5,33E-04	0,079
81187	1,28E-03	0,051
81188	2,21E-03	0,0388
81189	3,24E-03	0,032
81190	4,94E-03	0,0259
81191	6,63E-03	0,0224
81192	7,85E-03	0,0205
81193	9,43E-03	0,0187
81194	9,92E-03	0,0182
81195	1,12E-02	0,0172
81196	1,14E-02	0,017
81197	1,13E-02	0,0171
81198	1,14E-02	0,017
81199	1,13E-02	0,0171

Z/A	Yields	Error
81200	1,07E-02	0,0175
81201	1,06E-02	0,0176
81202	1,01E-02	0,0181
81203	9,84E-03	0,0183
81204	9,91E-03	0,0183
81205	1,04E-02	0,0178
81206	1,11E-02	0,0173
81207	2,05E-02	0,0126
81208	1,93E-04	0,1313
81209	0,00E+00	0
81210	0,00E+00	0
82183	0,00E+00	0
82184	0,00E+00	0
82185	0,00E+00	0
82186	3,33E-06	1
82187	4,33E-05	0,2773
82188	1,57E-04	0,1459
82189	3,13E-04	0,1031
82190	8,40E-04	0,063
82191	1,43E-03	0,0482
82192	2,56E-03	0,036
82193	3,60E-03	0,0304
82194	4,85E-03	0,0262
82195	5,85E-03	0,0238
82196	7,20E-03	0,0214
82197	8,11E-03	0,0202
82198	8,68E-03	0,0195
82199	9,42E-03	0,0187
82200	1,00E-02	0,0182
82201	1,07E-02	0,0176
82202	1,10E-02	0,0173
82203	1,22E-02	0,0164
82204	1,29E-02	0,016
82205	1,55E-02	0,0146
82206	2,03E-02	0,0127
82207	3,72E-02	0,0093
82208	4,75E-03	0,0264
82209	0,00E+00	0
82210	0,00E+00	0
82211	0,00E+00	0
82212	0,00E+00	0
82213	0,00E+00	0
82214	0,00E+00	0
83188	0,00E+00	0
83189	0,00E+00	0
83190	3,33E-06	1
83191	5,00E-05	0,2582
83192	1,17E-04	0,169
83193	3,17E-04	0,1026
83194	6,03E-04	0,0743
83195	8,00E-04	0,0645
83196	1,23E-03	0,0521
83197	1,53E-03	0,0466
83198	1,82E-03	0,0427

Z/A	Yields	Error
83199	2,21E-03	0,0388
83200	2,23E-03	0,0386
83201	2,63E-03	0,0355
83202	2,55E-03	0,0361
83203	2,74E-03	0,0348
83204	2,97E-03	0,0334
83205	2,91E-03	0,0338
83206	3,01E-03	0,0332
83207	2,29E-03	0,0381
83208	1,49E-03	0,0472
83209	0,00E+00	0
83210	0,00E+00	0
83211	0,00E+00	0
83212	0,00E+00	0
83213	0,00E+00	0
83214	0,00E+00	0
83215	0,00E+00	0
84192	0,00E+00	0
84193	0,00E+00	0
84194	6,67E-06	0,7071
84195	1,67E-05	0,4472
84196	2,00E-05	0,4082
84197	1,67E-05	0,4472
84198	7,00E-05	0,2182
84199	3,67E-05	0,3015
84200	8,67E-05	0,1961
84201	1,07E-04	0,1768
84202	1,53E-04	0,1474
84203	9,00E-05	0,1924
84204	9,00E-05	0,1924
84205	7,00E-05	0,2182
84206	6,00E-05	0,2357
84207	3,00E-05	0,3333
84208	3,33E-06	1
84209	0,00E+00	0
84210	0,00E+00	0
84211	0,00E+00	0
84212	0,00E+00	0
84213	0,00E+00	0
84214	0,00E+00	0
84215	0,00E+00	0
84216	0,00E+00	0
84217	0,00E+00	0
84218	0,00E+00	0
85196	0,00E+00	0
85197	0,00E+00	0
85198	0,00E+00	0
85199	0,00E+00	0
85200	0,00E+00	0
85201	0,00E+00	0
85202	0,00E+00	0
85203	0,00E+00	0
85204	0,00E+00	0
85205	3,33E-06	1

Annex B
Experimental data at 600 MeV for ^{208}Pb

These experimental data are preliminary data from ISTC#2002 [49].

Z	Nucl.	A	$T^{1/2}$	Yields typ	Yields	Error
83	Bi	206	6.243D	i	5,393	0,362
83	Bi	205	15.31D	i	8,001	0,533
83	Bi	204	11.22H	i	6,974	0,465
83	Bi	203	11.76H	i(m+g)	6,895	0,703
83	Bi	202	1.72H	i	6,084	0,710
82	Pb	204m	67.2M	i(m)	14,398	0,972
82	Pb	204m	67.2M	c	15,437	1,036
82	Pb	203	51.873H	c	40,834	2,913
82	Pb	202m	3.53H	i(m)	14,104	1,209
82	Pb	201	9.33H	c*	35,243	3,233
82	Pb	200	21.5H	c	27,642	1,873
82	Pb	199	90M	c*	54,758	9,722
82	Pb	197m	43M	c*	26,648	4,506
82	Pb	196	37M	c*	25,520	3,488
82	Pb	195m	15.0M	i(m)	14,656	2,974
81	Tl	202	12.23D	c	21,681	1,480
81	Tl	201	72.912H	c	61,035	4,519
81	Tl	200	26.1H	i	29,103	2,172
81	Tl	200	26.1H	c	56,684	3,780
81	Tl	199	7.42H	c	56,146	5,961
81	Tl	198m	1.87H	i(m)	25,269	3,449
81	Tl	196m	1.41H	i(m)	48,822	8,969
80	Hg	203	46.612D	c	4,141	0,284
80	Hg	197m	23.8H	i(m)	13,090	0,953
80	Hg	195	9.9H	c	56,448	6,959
80	Hg	195m	41.6H	i(m)	17,175	1,681
80	Hg	193m	11.8H	i(m)	22,237	3,559
80	Hg	192	4.85H	c	51,073	5,643
80	Hg	190	20.0M	c*	38,783	6,342
79	Au	198m	2.27D	i(m)	0,769	0,058
79	Au	198	2.69517D	i	1,623	0,121
79	Au	198	2.69517D	i(m+g)	2,399	0,162
79	Au	196	6.183D	i(m1+m2+g)	4,372	0,319
79	Au	195	186.098D	c	68,858	7,804
79	Au	194	38.02H	i(m1+m2+g)	7,770	0,676
79	Au	192	4.94H	i(m+g)	10,520	1,533
79	Au	192	4.94H	c	74,571	10,293
79	Au	191	3.18H	c*	68,531	5,060
79	Au	190	42.8M	c	53,194	5,081
78	Pt	191	2.802D	c	54,852	4,582
78	Pt	189	10.87H	c*	57,905	4,004
78	Pt	188	10.2D	c	51,755	3,595
78	Pt	187	2.35H	c	40,255	8,907
78	Pt	186	2.08H	c	39,237	8,819
78	Pt	184	17.3M	c	30,645	5,882
77	Ir	192	73.827D	i(m1+g)	0,163	0,017
77	Ir	190	11.78D	i(m1+g)	0,476	0,072
77	Ir	189	13.2D	c	52,590	5,498
77	Ir	188	41.5H	i	2,947	0,295
77	Ir	188	41.5H	c	54,672	4,076
77	Ir	187	10.5H	c*	49,886	4,015
77	Ir	186	16.64H	i	22,274	1,610
77	Ir	185	14.4H	c*	32,130	4,282
77	Ir	184	3.09H	c	34,892	3,026
77	Ir	183	57M	c	33,273	8,171
76	Os	185	93.6D	c	44,654	3,097
76	Os	183m	9.9H	c	20,252	2,008
76	Os	182	22.10H	c	38,665	2,944
76	Os	181	105M	c	11,187	1,525
76	Os	180	21.5M	c*	24,495	1,934
75	Re	183	70.0D	c	38,332	2,845

Z	Nucl.	A	$T^{1/2}$	Yields typ	Yields	Error
75	Re	182m	12.7H	c	37,451	2,976
75	Re	181	19.9H	c	27,071	3,900
75	Re	179	19.5M	c*	29,111	2,555
75	Re	178	13.2M	c*	27,447	3,774
74	W	178	21.6D	c	18,712	3,049
74	W	177	135M	c*	15,474	1,943
74	W	176	2.5H	c	8,799	2,154
73	Ta	177	56.56H	c	18,047	4,516
73	Ta	176	8.09H	i	7,165	2,625
73	Ta	176	8.09H	c	15,964	1,756
73	Ta	175	10.5H	c*	13,301	1,029
73	Ta	173	3.14H	c	11,086	1,550
72	Hf	175	70D	c	12,738	0,963
72	Hf	173	23.6H	c	8,063	0,856
72	Hf	172	1.87Y	c	6,430	0,463
72	Hf	170	16.01H	c	5,189	1,241
71	Lu	173	1.37Y	c	8,681	0,693
71	Lu	172	6.70D	c	6,665	0,496
71	Lu	171	8.24D	c*	6,340	0,453
71	Lu	170	2.012D	c	3,485	0,906
71	Lu	169	34.06H	c	3,742	0,302
70	Yb	169	32.026D	c	3,728	0,311
70	Yb	166	56.7H	c	1,765	0,167
69	Tm	167	9.25D	c	2,554	0,519
69	Tm	165	30.06H	c	1,152	0,114
64	Gd	149	9.28D	c	0,141	0,023
58	Ce	139	137.640D	c	0,254	0,028
54	Xe	127	36.4D	c	0,626	0,049
52	Te	123m	119.7D	i(m)	0,429	0,043
52	Te	121m	154D	i(m)	0,465	0,037
52	Te	121	19.16D	c	0,820	0,065
52	Te	119m	4.70D	i(m)	0,260	0,024
51	Sb	120m	5.76D	i(m)	0,471	0,035
50	Sn	113	115.09D	c	0,377	0,042
49	In	114m	49.51D	i(m)	1,522	0,140
47	Ag	110m	249.76D	i(m)	1,443	0,115
47	Ag	106m	8.28D	i(m)	0,507	0,043
45	Rh	105	35.36H	c	5,329	0,404
45	Rh	102	207D	i	0,682	0,106
45	Rh	101m	4.34D	c	0,801	0,081
44	Ru	103	39.26D	c	4,925	0,340
43	Tc	96	4.28D	i(m+g)	0,760	0,056
43	Tc	95	20.0H	c*	0,337	0,052
41	Nb	96	23.35H	i	3,079	0,294
41	Nb	95	34.975D	i(m+g)	3,422	0,231
41	Nb	95	34.975D	c	6,378	0,426
41	Nb	92m	10.15D	i(m)	0,335	0,027
40	Zr	97	16.744H	c	0,880	0,065
40	Zr	95	64.02D	c	2,945	0,197
40	Zr	89	78.41H	c	1,180	0,080
40	Zr	88	83.4D	c	0,478	0,038
39	Y	90m	3.19H	i(m)	3,362	0,244
39	Y	88	106.65D	i	2,531	0,169
39	Y	88	106.65D	c	2,946	0,200
39	Y	87	79.8H	c	1,869	0,210
38	Sr	85	64.84D	c	1,857	0,148
37	Rb	86	18.631D	i(m+g)	4,196	0,358
37	Rb	83	86.2D	c	2,173	0,177
35	Br	82	35.30H	i(m+g)	2,304	0,158
34	Se	75	119.779D	c	0,610	0,045
33	As	74	17.77D	i	1,147	0,113

Z	Nucl.	A	$T^{1/2}$	Yields typ	Yields	Error
31	Ga	72	14.10H	i	1,097	0,209
31	Ga	72	14.10H	c	1,475	0,201
30	Zn	72	46.5H	c	0,378	0,045
26	Fe	59	44.472D	c	0,528	0,045
21	Sc	46	83.79D	i(m+g)	0,112	0,016
4	Be	7	53.29D	i	1,141	0,214

Annex C
Calculations of volumes of the LiSoR test tube cells

The geometry is presented on figure C-1 and the parameters are recapitulated in table C-1.

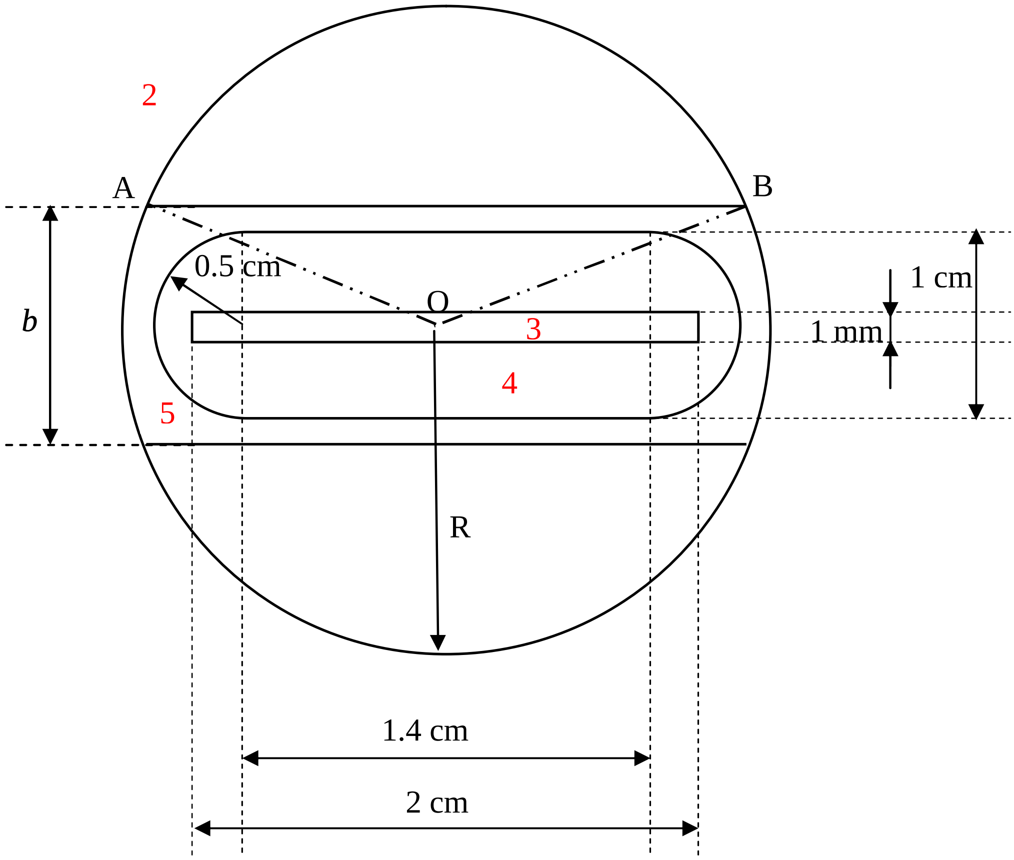

Figure C-1: *Geometrical representation of the LiSoR test tube to volume calculation.*

The principal difficulty lies in the calculation of the cell 5 volume.
First, the following formula allows calculating the angle a :

$$b = 2R\cos\left(\frac{a}{2}\right) \tag{C.1}$$

where b is the distance between the surfaces 15 and 16 defined in the MCNPX input file shown table 4-1, R is the radius of the circle and a is the angle $A\hat{O}B$ is defined in figure C-1.

Then, we obtain the formula to calculate the area of the cell 5:

$$A = R^2\left(p - a + \sin(a)\right) \tag{C.2}$$

L [cm]	40,00
b [cm]	1,20
R [cm]	1,30

Table C-1: *Summary of the main geometrical value of the LiSoR test tube.*

This allows calculating the volumes of the cell 5. The other areas are only rectangles and circles and they represent no difficulties. The results are summarized in table C-2:

cells	1	2	3	4	5
volume [cm3]	infinity	112977,12	8	79,42	32,80

Table C-2: *Cells volume of the LiSoR test tube geometry.*

Annex D

Concentrations and alpha-activities of Polonium isotopes after 34 hours continuous irradiation in the real geometry target

Nuclides	LAHET-1 month		FLUKA-1 month		MCNPX (Real geometry)-1 month		
	α-Activity [Becq]	Production rate [gr.atoms/liter eutectic]	α-Activity [Becq]	Production rate [gr.atoms/liter eutectic]	α-Activity [Becq]	Production rate [gr.atoms/liter eutectic]	error
Po-203	8,586E+07	1,562E-11	8,113E+07	1,476E-11	1,376E+08	2,502E-11	37,6%
Po-204	4,389E+09	8,100E-10	3,970E+09	7,326E-10	4,963E+09	9,159E-10	11,6%
Po-205	3,260E+08	5,061E-10	4,350E+08	6,753E-10	3,772E+08	5,856E-10	13,6%
Po-206	2,840E+10	3,797E-08	4,169E+10	5,573E-08	4,419E+10	5,908E-08	35,7%
Po-207	9,768E+07	9,407E-11	1,342E+08	1,292E-10	1,958E+08	1,886E-10	50,1%
Po-208	8,537E+09	7,476E-08	1,443E+10	1,263E-07	1,591E+10	1,393E-07	46,3%
Po-209	4,779E+07	1,480E-08	8,262E+07	2,559E-08	4,203E+07	1,302E-08	13,7%

Nuclides	LAHET-3 months		FLUKA-3 months		MCNPX (Real geometry)-3 months		
	α-Activity [Becq]	Production rate [gr.atoms/liter eutectic]	α-Activity [Becq]	Production rate [gr.atoms/liter eutectic]	α-Activity [Becq]	Production rate [gr.atoms/liter eutectic]	error
Po-203	8,586E+07	1,562E-11	8,113E+07	1,476E-11	1,376E+08	2,502E-11	37,6%
Po-204	4,389E+09	8,100E-10	3,970E+09	7,326E-10	4,963E+09	9,159E-10	11,6%
Po-205	3,260E+08	5,061E-10	4,350E+08	6,753E-10	3,772E+08	5,856E-10	13,6%
Po-206	3,121E+10	4,172E-08	4,580E+10	6,123E-08	4,855E+10	6,490E-08	35,7%
Po-207	9,768E+07	9,407E-11	1,342E+08	1,292E-10	1,958E+08	1,886E-10	50,1%
Po-208	2,511E+10	2,199E-07	4,243E+10	3,716E-07	4,679E+10	4,098E-07	46,3%
Po-209	1,433E+08	4,439E-08	2,477E+08	7,673E-08	1,260E+08	3,904E-08	13,7%

Nuclides	LAHET-6 months		FLUKA-6 months		MCNPX (Real geometry)-6 months		
	α-Activity [Becq]	Production rate [gr.atoms/liter eutectic]	α-Activity [Becq]	Production rate [gr.atoms/liter eutectic]	α-Activity [Becq]	Production rate [gr.atoms/liter eutectic]	error
Po-203	8,586E+07	1,562E-11	8,113E+07	1,476E-11	1,376E+08	2,502E-11	37,6%
Po-204	4,389E+09	8,100E-10	3,970E+09	7,326E-10	4,963E+09	9,159E-10	11,6%
Po-205	3,260E+08	5,061E-10	4,350E+08	6,753E-10	3,772E+08	5,856E-10	13,6%
Po-206	3,123E+10	4,175E-08	4,583E+10	6,127E-08	4,859E+10	6,495E-08	35,7%
Po-207	9,768E+07	9,407E-11	1,342E+08	1,292E-10	1,958E+08	1,886E-10	50,1%
Po-208	4,875E+10	4,270E-07	8,238E+10	7,215E-07	9,086E+10	7,957E-07	46,3%
Po-209	2,863E+08	8,870E-08	4,950E+08	1,533E-07	2,518E+08	7,800E-08	13,7%

Bibliography

[1] The European Technical Working Group on ADS, *A European Roadmap for Developing Accelerator Driven Systems (ADS) for Nuclear Waste Incineration*, April 2001.

[2] C. Rubbia *et al*., *Conceptual design of a fast neutron operated high power energy amplifier*, CERN/AT/95-44 (ET), 1995.

[3] http://aaa.lanl.gov/

[4] http://www.pnl.gov/atw/

[5] http://www.europhysicsnews.com/full/06/article8/article8.html

[6] J. Cugnon *et al.*, *Nucl. Phys. A*, **620**, 475 (1997).

[7] K. H. Schmidt *et al.*, *Nucl. Phys. A*, **665**, 221 (2000).

[8] J.-J. Gaimard, K.-H.Schmidt; *Nucl. Physics* A, **531**, 709 (1991).

[9] T. Auger, Y. Bortoli, A. Cadiou, T. Kirchner, J.S. Stutzman (Subatech), Y. Dai, S. Dementjev, K. Geismann, F. Gröschel, F. Heinrich, K. Kohlik, G. von Holzen, Ch. Perret, D. Viol (PSI), H. Glasbrenner (FZK), *Design Report for the LiSoR project*, 2001.

[10] http://inrwww.fzk.de/~inr487/public_html/megapie.pdf

[11] C.H.M. Broeders, PhD thesis, *Entwicklungsarbeiten für die neutronenphysikalische Auslegung von Fortschrittlichen Druckwasserreaktoren (FDWR) mit kompakten Dreiecksgittern in hexagonalen Brennelementen*, Forschungszentrum Karlsruhe, 1992.

[12] E. Stein, E. Wiegner, C. Broeders, *Kurzbeschreibung des KAPROS-Moduls BURNUP*, interne KAPROS-Notiz, 1982.

[13] F. Atchinson, H. Schaal, *ORIHET3, Version1.12, A guide for users*, May 2002.

[14] W. M. Brobeck, E. O. Lawrence *et al.*, *Phys. Rev.*, **71** (number 7), 449 (1947).

[15] J. Taieb, PhD thesis, *Etude de la production de noyaux résiduels d´évaporation issus de la réaction de spallation de l´uranium-238 par des protons á 1 GeV*, Université de Paris Sud, INP-CNRS Orsay, October 2000.

[16] http://www.cea.fr/fr/Publications/Clefs46/clefs46fr/clefs46_35.html

[17] A. Boudard, J. Cugnon, S. Leray, C. Volant, *Intranuclear Cascade for a comprehensive description of spallation reaction data*, December 3, 2001.

[18] R. Serber, *Phys. Rev.*, **72**, 1114 (1947).

[19] http://lpsc.in2p3.fr/reacteurs-hybrides/atelier_gedeon/Cugnon/Cugnon02.html

[20] H.W. Bertini, *Phys.Rev.*,**88**,1711 (1969).

[21] H.W. Bertini, *Phys.Rev.*, **31**,1801 (1963).

[22] V. S. Barashenkov *et al.*,. *Sov. Phys.*, **Usp 16**, 31 (1973).

[23] V. Baylac-Domengetroy, Diplomarbeit, *Investigations Related to the Generation of Reaction Products in the Target of Accelerator Driven Systems for Nuclear Waste Incineration*, Forschungszentrum Karlsruhe, FZKA 6908, 2003.

[24] A. Boudard *et al.*, *Phys. Rev. C*, **66**, 044615 (2002).

[25] I. Broeders, *Private communication*.

[26] C. Villagrasa-Cantón, PhD thesis, *Etude de la production de noyaux résiduels dans la réaction de spallation Fe+p à 5 énergies (300-1500 MeV/A) et applications au calcul de dommages sur une fenêtre de système hybride*, Université Paris XI Orsay, December 2003.

[27] B. Fernandez-Dominguez, PhD thesis, *Etude de la production des fragments de fission de la réaction ^{208}Pb+p à 500 AMeV*, Université de Caen, March 2003.

[28] V. F. Weisskopf, *Phys.Rev.*, **52**, 295 (1937).

[29] V.F. Weisskopf, D. H. Ewing, *Phys.Rev.*, **57**, 472 (1939).

[30] A. R. Junghans *et al.*, *Nucl. Phys. A*, **629**, 635 (1998).

[31] E. Vogt, Single neutrons halos in the valley of stability, Vancouver, May 2002.

[32] A. Boudard, *Private communication*.

[33] L. S. Waters, *MCNPX user´s manual, Version 2.4.0*, September 2002.

[34] R. E. Prael, H. Lichtenstein, *User Guide to LCS: The LAHET Code System*, LANL, September 1989.

[35] J. S. Hendricks, G. W. McKinney, L. S. Waters *et al.*, *MCNPX extensions, Version 2.5.0*, February 2004.

[36] J. S. Hendricks, G. W. McKinney, L. S. Waters *et al.*, *MCNPX extensions, Version 2.5.d*, August 2003.

[37] E-mail exchange with the SPhN (Service de Physique Nucléaire) at the CEA of Saclay.

[38] http://dpnc.unige.ch/atlas/xin/noyaux/pdf/chapitre-2.pdf

[39] http://www.carleton.ca/~dwiles/CRNL/section_one.htm

[40] H. A. Bethe, *Phys. Rev.*, **54**, 436 (1938).

[41] W. H. Barkas, *Phys. Rev.*, **55**, 961 (1939).

[42] L. Sihver *et al.*, *Phys. Rev. C*, **47**, 1225 (1993).

[43] S. Kox *et al. Phys. Rev. C*, **35**, 1678 (1987).

[44] Shen *et al. Nucl. Phys. A*, **491**, 130 (1989).

[45] R. K. Tripathi *et al.*, *NASA Technical Paper*, **3621** (1997).

[46] Y. E. Titarenko, *Experimental and theorical study of the yields od residual product nuclei produced in thin targets irradiated by 100-2600 MeV protons*, ISTC, February 2001.

[47] http://www-wnt.gsi.de/kschmidt

[48] T. Enqvist *et al.*, *Nucl.Phys.A*, **686**, 481 (2001).

[49] Y. E. Titarenko, *private communication.*

[50] L. Audouin, PhD thesis, *Dépendence en énergie des spectres isotopiques de résidus de spallation*, Université de Paris 6, September 2003.

[51] http://www.ganil.fr/eurisol/TOWN_MEETING_ABANO/ThomasKirchener.pdf

[52] H. Glasbrenner *et al.*, *First irradiation experiment at the LiSoR loop*, PSI.

[53] Y. Foucher (Subatech), M. Pepin (PSI), M. Embib (Ciemat), *Nuclear Assessment of the LiSoR project*, 2000.

[54] M. Pepin, *Production of α-Radioactivity by 72 MeV protons on lead-bismuth eutectic and subsequent radiotoxic risk by evaporation of Pb-Po from open liquid surfaces*, PSI.

[55] P. Trabuc, the problem of polonium contamination in the MEGAPIE spallation target, CEA, 2001.

[56] http://atom.kaeri.re.kr/ton/

[57] H. Glasbrenner, J. Eikenberg, F. Gröschel, L. Zanini, *Irradiated Pb-55.5 Bi*, PSI, 2003.

[58] http://asq.web.psi.ch/ASQ/facilities/SINQSYSTEMS.html

[59] http://sinq.web.psi.ch/

[60] U. Fischer, H. W. Wiese, *Verbesserte konsistente Berechnung des nuklearen Inventars abgebrannter DWR-Brennstoffe auf der Basis von Zell-Abbrabd-Verfahren mit KORIGEN*, KfK 3014 (1983).

[61] M. J. Bell, *ORIGEN- The ORNL Isotope Generation and Depletion Code*, ORNL-4628 UC-32 (1973).

Validation of Calculation Tools for the Estimation of Reaction Products in the Target of Accelerator Driven Systems

Summary

The spallation reactions have recently gained considerable interest due to their importance in technical applications. The spallation reactions generate a lot of neutrons and they can, for example, be used as spallation neutron sources. This property can be utilized in an Accelerator Driven System (ADS) which is composed of a neutron source, a spallation target and a sub-critical reactor. Thanks to the external neutron source, this application will allow to produce energy with higher safety and to incinerate nuclear waste. Actually several experimental research programs are running in order to realized the final construction of a hybrid system prototype: MUSE, TRADE, MYRRHA, MEGAPIE.

A working tool to simulate the spallation reaction is provided to us. The MCNPX code (Monte Carlo with N Particles eXtended), is developed at the LANL and it is used actually at the IRS within the framework of the beta-testing. First we analyzed the new models INCL4 and ABLA recently integrated in the new version 2.5e of MCNPX in comparison with the original codes of J. Cugnon and K. H. Schmidt. It allows us to recommend the input parameters defining the pysical models and the corresponding normalizations. Moreover the influences of different input parameters on the spallation cross sections are quantified. We investigated the agreement of this code options with the experimental data from the GSI and ISTC groups at 1 GeV, with new data from the ISTC group at 600 MeV and with recently available data at 500 MeV from the GSI group. Further we studied the decay of isotopes in a LiSoR target experiment (Liquid metal Solid metal Reaction) in order to estimate the activity of residual spallation products which are radiotoxic as the Polonium 209. The last part of this work is devoted to the study of two codes which calculate the decay of isotopes: The modul BURN0D of the KAPROS system and the ORIHET3 code. The physical principles and theire use are discussed.

Validierung von Rechen-Programmen zur Abschätzung von Reaktionsprodukten im Target von Beschleuniger-Getriebenen Systemen

Zusammenfassung

Vor kurzem haben Spallations-Reaktionen beträchtliches Interesse wegen ihrer Bedeutung für technische Anwendungen gewonnen. Die Spallations-Reaktionen erzeugen viele Neutronen und sie können zum Beispiel als Spallations-Neutronenquellen verwendet werden. Diese Eigenschaft kann in einem Beschleuniger-gesteuerten unterkritischen System (ADS) benutzt werden, welches aus einer Neutronenquelle, einem Spallations-Target und einem unterkritischen Reaktor besteht. Diese Anwendung ermöglicht, wegen der externen Neutronenquelle, Energie mit höherer Sicherheit zu produzieren und nukleare Abfälle zu verbrennen. Zur Zeit laufen mehrere experimentelle Forschungs Programme, um zum Aufbau eines Prototyps für ein hybrides Systems zu führen: MUSE, TRADE, MYRRHA, MEGAPIE.

Ein Arbeitswerkzeug steht uns zur Verfügung, um die Spallation Reaktion zu simulieren. Dieser Code, genannt MCNPX (Monte-Carlo mit N Partikeln eXtended), wird am LANL entwickelt und er wird am IRS im Rahmen des Beta-Tests verwendet. Zuerst haben wir die neuen Modelle INCL4 und ABLA, die vor kurzem in der neuen Version 2.5e von MCNPX integriert wurden, im Vergleich mit den Ursprungscodes von J. Cugnon and K. H. Schmidt analysiert. Das hat uns ermöglicht, die geeigneten Eingabe Parameter und Normalisierungen zu bestimmen. Außerdem sind die Einflüsse der unterschiedlichen Eingangs-Parameter auf die Spallations Querschnitte quantitativ bestimmt. Weiter haben wir die Übereinstimmung der Ergebnisse dieser Codes mit den experimentellen Daten von den gruppen GSI und ISTC bei 1 GeV, mit die neuen Daten von der Gruppe ISTC bei 600 MeV und mit ganz neu verfügbaren Daten von GSI bei 500 MeV untersucht. Dann haben wir den Zerfall der Isotope im Rahmen des LiSoR Projekts (Liquid metal Solid metal Reaction) studiert um die Aktivitäten der Spallationprodukte abzuschätzen, die wie zum Beispiel Polonium 209 radiotoxisch sein können. Der letzte Teil dieser Arbeit befasst sich mit zwei Codes, die den Zerfall von Isotopen berechnen. Der Modul BURN0D aus dem KAPROS System und der ORIHET3 Code. Die physikalische Grundlagen und die Benutzung dieser Programme sind dort erläutert.

Validation des Outils de Calcul pour l'Estimation des Produits de Réaction dans la Cible d'un Système Sous-Critique Piloté par Accélérateur

Résumé

Les réactions de spallation ont récemment connu un regain d'intérêt considérable grâce à leur importance dans les applications techniques. Les réactions de spallation sont en effet très neutrogènes et elles peuvent, par exemple, être employées en tant que sources de neutrons de spallation. Cette propriété peut être utilisée dans un système sous-critique piloté par accélérateur (Accelerator Driven System, ADS) qui est composé d'une source de neutron, d'une cible de spallation et d'un réacteur sous-critique. Grâce à cette source extérieure de neutrons, cette application permet de produire de l'énergie avec une augmentation de la sûreté et d'incinérer des déchets nucléaires. Actuellement plusieurs programmes expérimentaux de recherche sont en cours afin d'arriver à la construction finale d'un démonstrateur de système hybride : MUSE, TRADE, MYRRHA, MEGAPIE.

Nous avons à notre disposition un outil de travail pour simuler la réaction de spallation. Ce code, appelé MCNPX (Monte Carlo avec N Particules eXtended), est développé au LANL et il est employé actuellement à l'IRS dans le cadre du beta-testing. D'abord nous avons analysé les nouveaux modèles INCL4 et ABLA récemment intégrés dans la nouvelle version 2.5e de MCNPX en comparaison avec les codes d'origine de J. Cugnon et K. H. Schmidt. Cela nous a permis de comprendre et déterminer les paramètres d'entrée définissant les modèles physiques ainsi que les normalisations correspondantes. De plus, l'influence de certains paramètres d'entrée sur les distributions de spallation a été évaluée. Ensuite nous avons étudié la concordance de ces codes avec les données expérimentales des groupes GSI et ISTC à 1 GeV tout d'abord, puis avec les nouvelles du groupe ISTC à 600 MeV et enfin avec des données du groupe GSI à 500 MeV obtenues très récemment. Ensuite nous avons étudié la décomposition des isotopes dans une cible définit par le projet LiSoR (Liquid metal Solid metal Reaction) afin d'estimer l'activité des produits résiduels de spallation qui peuvent être radiotoxiques comme le Polonium 209, par exemple. La dernière partie de ce travail est dédiée à l'étude de deux codes calculant la décomposition des isotopes : Le module BURN0D du système KAPROS et le code ORIHET3. Les principes physiques de leur fonctionnement ainsi que leur utilisation y sont développés.